NUMERICAL ANALYSIS OF COMBINED BENDING AND TORSION OF A PRISMATIC BAR USING RIGID-PLASTIC AND WORK-HARDENING PLASTICITY THEORIES

Thesis for the Degree of Ph. D.

MICHIGAN STATE UNIVERSITY

Patrick M. Miller

1966

ABSTRACT

NUMERICAL ANALYSIS OF COMBINED BENDING AND TORSION OF A PRISMATIC BAR USING RIGID-PLASTIC AND WORK-HARDENING PLASTICITY THEORIES

by Patrick M. Miller

The problem formulation assumes an incompressible plastic material, a prismatic bar having at least one cross-sectional axis of symmetry, and the stresses to be independent of the longitudinal coordinate.

The objectives achieved in the study are threefold:

1) to better establish the torque-moment interaction curve for the perfectly-plastic material,
2) to provide a solution to the combined bending and torsion problem for both the work-hardening generalized J_2 deformation theory and the counterpart generalized J_2 flow theory, and
3) to compare the predictions of these work-hardening theories for different loading parameters.

The rigid-perfectly plastic numerical analysis is confined to a solution to an equation derived by S. Piechnik, a non-linear second-order partial differential equation. Using a finite-difference approach, the discrete analogue of this equation is solved by the

Gauss-Seidel over-relaxation procedure. The results of the rigid-perfectly plastic analysis confirm the more limited results obtained by other investigators through a numerical solution of the Hill-Handelman stress-function equation. But, because of the better convergence properties of the Piechnik equation, the solution easily gives any point on the torque-moment interaction curve.

Equations, considering the effect of work-hardening, are developed for both the generalized J_2 deformation theory and the counterpart flow theory. With each theory, a stress-function and a warping-function formulation is given. This development, in all cases, leads to a system of two simultaneous partial differential equations. The first is the governing equation, corresponding to a compatibility equation with the stress function and to an equilibrium equation with the warping function, while the second equation represents the non-linear behavior of the constitutive relation.

In determining the discrete analogue for the flow-theory equations, a backward-difference quotient is applied to derivatives taken with respect to the time-like variable. This approach leads to a system of finite-difference equations, whose solution is comparable to the solutions of the discrete deformation-theory system of equations.

The numerical algorithms apply the Gauss-Seidel over-relaxation iteration to the discrete analogue of the governing equation in a manner analogous to the corresponding linear elasticity problem. Concurrently, the Newton-Raphson iteration is applied to the discrete representation of the constitutive relation. During a sweep through the cross-sectional mesh, these iterations are performed successively on each unknown discrete variable at all points. The sweeps are continued until the greatest change in any of the unknown discrete values of the governing equation due to the last iteration is less than a preassigned convergence parameter.

The results of work-hardening analysis lead to the following conclusions: (1) In both the deformation and flow-theory calculations, the stress-function equations and the warping-function equations give comparable results with approximately the same amount of computation. (2) The results for the deformation theory agree with those of flow theory when a constant ratio is maintained between the curvature and unit angle of twist variables. (3) The two work-hardening theories predict different results for a given deformation when this ratio is allowed to vary. (4) Because the backward-difference quotient was used with flow-theory formulation, the numerical solution of the flow-theory equation is of the same degree of numerical difficulty as that for the deformation-theory equations.

NUMERICAL ANALYSIS OF COMBINED BENDING AND TORSION OF A PRISMATIC BAR USING RIGID-PLASTIC AND WORK-HARDENING PLASTICITY THEORIES

By

Patrick M. Miller

A THESIS

Submitted to
Michigan State University
in partial fulfillment of the requirements
for the degree of

DOCTOR OF PHILOSOPHY

Department of Metallurgy, Mechanics and Materials Science

1966

ACKNOWLEDGMENTS

The author expresses his appreciation to Professor L. E. Malvern for help in formulation and solution of this problem, to Professors W. A. Bradley and C. S. Duris for suggestions which contributed to the solution, and to Professors G. E. Mase and T. Triffet for serving on the guidance committee.

TABLE OF CONTENTS

Page

ACKNOWLEDGMENTS. ii

LIST OF TABLES vi

LIST OF ILLUSTRATIONS. viii

LIST OF APPENDICES x

Chapter

I. INTRODUCTION 1

1.1 Review of Related Investigations. 1
1.2 Objectives and General Discussion of the Present Study 5

II. DERIVATION OF EQUATIONS. 10

2.1 General Principles of Mechanics 10
2.2 Rigid-Perfectly Plastic Material Governed by Hencky Deformation Theory . . 15
2.2.1 Warping-Function Formulation . . . 18
2.2.2 Stress-Function Formulation. . . . 20
2.3 Rigid-Perfectly Plastic Material Governed by Levy-Mises Theory 23
2.3.1 Warping-Rate Function Formulation. 25
2.3.2 Stress-Function Formulation. . . . 27
2.4 Work-Hardening Material Governed by a Generalized J_2 Deformation Law. 29
2.4.1 Warping-Function Formulation . . . 31
2.4.2 Stress-Function Formulation. . . . 33
2.5 Work-Hardening Material Governed by a Generalized J_2 Flow Law 34
2.5.1 Warping-Rate Function Formulation. 36
2.5.2 Stress-Function Formulation. . . . 37

III. NUMERICAL SOLUTIONS FOR A UNIT SQUARE CYLINDER 40

3.1 Symmetry Properties of the Solution . . . 40
3.2 Discretization and Finite-Difference Operators 41

CONTENTS (continued)

Chapter			Page
	3.3	Piechnik Equation for Rigid-Perfectly Plastic Material.	44
	3.4	Warping-Function Equations for Work-Hardening Generalized J_2 Deformation Theory.	49
	3.5	Stress-Function Equations for Work-Hardening Generalized J_2 Deformation Theory.	54
	3.6	Warping-Function Equations for Work-Hardening Generalized J_2 Flow Theory. . .	59
	3.7	Stress-Function Equations for Work-Hardening Generalized J_2 Flow Theory. . .	68
IV.	NUMERICAL SOLUTION FOR A CIRCULAR BAR OF UNIT RADIUS.		74
	4.1	Transformation of Equations to Polar Coordinates	74
	4.2	Polar-Coordinate Discretization and Finite-Difference Representation.	78
	4.3	Piechnik Equation for Rigid-Perfectly Plastic Material.	80
	4.4	Warping-Function Equation for Work-Hardening Generalized J_2 Deformation Theory.	84
V.	RESULTS AND DISCUSSION		88
	5.1	Effect of Mesh Refinement	88
	5.2	Effect of Over-Relaxation Factor and Choice of Convergence Parameter	90
	5.3	Results of the Piechnik Equation for Rigid-Perfectly Plastic Material.	94
	5.4	Generalized J_2 Deformation-Theory Solutions	98
		5.4.1 Warping-Function Solution for Unit Square Bar.	99
		5.4.2 Stress-Function Solution for Unit Square Bar.	100
		5.4.3 Warping-Function Solution for a Unit Circular Bar.	101
		5.4.4 Approximation of the Elastic-Plastic Boundary for an Elastic-Perfectly Plastic Material	101
		5.4.5 Comparisons of the Deformation-Theory Solutions	102

CONTENTS (continued)

Chapter			Page
	5.5	Generalized J_2 Flow-Theory Solutions. . .	107
		5.5.1 Warping-Function Solutions	107
		5.5.2 Stress-Function Solutions.	107
		5.5.3 Comparisons for Flow Theory. . . .	107
	5.6	Comparison Between Flow and Deformation Theory.	108
		5.6.1 Conditions Where the Theories Agree.	108
		5.6.2 Examples of Load Paths Where the Theories Do Not Agree.	115
	5.7	Conclusions	118
VI.	POSSIBLE EXTENSIONS OF THE RESEARCH.		121
	6.1	Related Mechanics Problems.	121
		6.1.1 More General Loading Conditions. .	121
		6.1.2 General Boundaries	122
		6.1.3 Other Theories	123
		6.1.4 Work-Hardening Equations Not Related to Combined Bending and Torsion.	125
		6.1.5 Experimental Verification.	126
	6.2	Mathematical Investigations	128
		6.2.1 Bound on the Theta Increment . . .	128
		6.2.2 Effect of Newton-Raphson Iteration.	129
		6.2.3 General Convergence.	129
APPENDICES			132
BIBLIOGRAPHY			201

LIST OF TABLES

Table		Page
1.	Effect of mesh refinement on normalized torque and moment	89
2.	Comparison between numerical and perturbation solutions for unit radial cross section	98
3.	Comparison between deformation-theory solution approximation to perfectly-plastic material and the Piechnik solution	106
4.	Comparison of torques and moments for different load paths	116
5.	Effect of grid dimension on Piechnik equation warping function and stresses for $\mu = 1/\sqrt{3}$	173
6.	Comparison between stresses computed from Piechnik equation and Hill-Handelman equation for $\mu = 1/\sqrt{3}$	175
7.	Normalized stress resultants for warping-function deformation-theory analysis of a square section	176
8.	Typical stress output for warping-function deformation-theory with n = 2, μ = 1.00, and Θ = 3.00	180
9.	Normalized stress resultants for stress-function deformation-theory analysis of a square section	181
10.	Typical stress output for stress-function deformation-theory with n = 2, μ = 1.00, and Θ = 3.00	183
11.	Normalized stress resultants for warping-function deformation-theory analysis of a circular section	184

TABLES (continued)

Table		Page
12.	Normalized stress resultants for warping-function flow-theory analysis of a square section	186
13.	Typical stress output for warping-function flow-theory with n = 2, μ = 1.00, and Θ = 3.00	190
14.	Normalized stress resultants for stress-function flow-theory analysis of a square section	191
15.	Typical stress output for stress-function flow-theory with n = 2, μ = 1.00, and Θ = 3.00	193

LIST OF ILLUSTRATIONS

Figure		Page
1.	Coordinate system	10
2.	Relation between unit normal vector and direction cosines	14
3.	Ramberg-Osgood stress-strain curves	29
4.	Coordinate system for unit square cross section	40
5.	Lattice spacings for square mesh.	41
6.	Arbitrary integration paths for a given deformation (κ, θ)	67
7.	Relationship between unit normal direction cosines and coordinate angle.	77
8.	Lattice spacings for polar-coordinate mesh. . .	79
9.	Effect of relaxation factor	91
10.	Normalized torque vs. bending moment interaction curve for a unit square bar.	95
11.	Comparison of the normalized torque vs. bending moment interaction curves for the square and circular bar.	97
12.	Approximation to elastic-plastic boundaries . .	103
13.	Normalized second invariant J_2 vs. y.	105
14.	Functions C_β vs. $\frac{G\theta}{k}$ showing non-radial stresses.	112
15.	Paths chosen for comparing the deformation and flow-theory calculations at the point (3.00,3.00)	116
16.	Estimation of new approximation by tangent. . .	138

ILLUSTRATIONS (continued)

Figure		Page
17.	Basic flow chart pattern for program WARPI. . .	140
18.	Basic flow chart pattern for program WARPO. . .	141
19.	Basic flow chart pattern for program STRO . . .	142
20.	Basic flow chart pattern for program WARPLV . .	143
21.	Basic flow chart pattern for program STPLDT . .	144
22.	Basic flow chart pattern for program POLARR . .	145
23.	Basic flow chart pattern for program POLARO . .	146
24.	Torque-moment vs. unit angle of twist for warping-function deformation-theory solutions of a square section	195
25.	Torque-moment vs. unit angle of twist for warping-function deformation-theory solutions of a circular section	199

LIST OF APPENDICES

Appendix		Page
I.	SOLUTION TO FINITE-DIFFERENCE EQUATIONS BY GAUSS-SEIDEL OVER-RELAXATION METHOD	132
II.	NEWTON-RAPHSON ITERATIVE METHOD FOR SOLVING A NON-LINEAR EQUATION	137
III.	BASIC FLOW CHART PATTERNS	139
IV.	FORTRAN PROGRAMS.	147
V.	TORQUE, MOMENT, AND STRESS OUTPUTS.	173
VI.	GRAPHICAL REPRESENTATION OF TORQUES AND MOMENTS	194

I. INTRODUCTION

In the elastic analysis of combined bending and torsion, the solutions may be determined separately for pure bending and pure torsion, and then superimposed to give the solution for the combined problem. In a plastic medium, this principle of superposition no longer applies, and the problem must be formulated so that these two phenomena and the interaction between them are considered simultaneously. This interaction gives rise to a system of non-linear equations. In general, closed form solutions are not available for these equations; however, the development of high speed digital computers permits the problem to be treated by approximate numerical methods.

1.1 Review of Related Investigations

The problem of combined bending and torsion of a rigid-perfectly plastic bar has been considered by several investigators. In 1944, Handelman [7], using a stress-function approach, formulated the governing differential equation, assuming a material obeying Levy-Mises flow theory. The work of Handelman was extended to a more general loading situation by Hill [11]. The stress-function equation, governing the combined bending and torsion of a prismatic bar, known as the Hill-Handelman

equation, is highly non-linear and, in addition, is singular along the cross-sectional neutral axis of bending.

Because of the non-linear nature of the equation, early efforts to establish the interaction curve between the applied moment and torque were confined to the application of energy methods. Hill and Siebel [13], in 1953, established energy techniques which permit the calculation of upper and lower bounds for the torque and moment interaction curve. Using these energy methods, Steele [30] determined the upper and lower bounds for a square cross section. The maximum deviation between these upper and lower bounds was found not to exceed 14 per cent. In addition, Steele used Southwell's relaxation method to determine two points on the interaction curve.

Employing an approach similar to that of Steele, Imegwu [15] obtained additional points on the interaction curve. It appears that the line singularity mentioned above gave the most difficulty in obtaining the numerical solutions to the Hill-Handelman equation.

In 1961, Piechnik [24] formulated the problem using the warping function, as opposed to the stress-function formulation of Hill and Handelman. Piechnik determined the interaction curve in the region where the bending may be treated as a perturbation of the problem of pure torsion. Later in 1961, Piechnik and Zyczkowski [25]

solved the problem where the torsion may be considered as a perturbation of the situation of pure bending. Using both the perturbation solutions and the conditions of isotropy, these authors fitted a smooth fourth order interaction curve whose constants were evaluated so that the location, slope, and curvature at both intercepts agree with the two perturbation solutions. This curve was found to lie almost exactly between the upper and lower bounds of Hill and Siebel.

Concurrently, other researchers were considering the problem of work-hardening from both the standpoints of a deformation theory and of a flow theory.[1] Ramberg and Osgood [27] had introduced an empirical three-parameter uniaxial stress-strain law including the effect of work-hardening. This law was extended by Nadai to what is called the generalized J_2 deformation theory. Prager [26] formulated a procedure giving the counterpart flow theory to a given deformation theory. Using Prager's method, a counterpart generalized J_2 flow theory has been developed by Prager and Laning [6].

Greenberg, Dorn, and Wetherell [6] applied both generalized J_2 deformation theory and the generalized J_2 flow theory to the problem of a unit square bar subjected

---

[1] Some authors designate the deformation and flow type theories as "total strain" and "incremental" theories, respectively.

to pure torsion. In the deformation theory, their governing equation is a non-linear second order partial differential equation. For flow theory, the governing equation is treated as a non-linear second order partial differential equation in the space variables at each level of the time-like variable. The finite difference approximations to these equations were solved by methods of numerical analysis.

The numerical solution of the deformation-theory governing equation tended to converge at a reasonable rate, but with the flow-theory equation, the rate was much slower; and, consequently, comparisons between the theories were made only for a very limited range of the Ramberg-Osgood parameters. In all of the cases compared, the two theories were found to agree, even though the stress paths were non-radial.

A point in the body is said to be subjected to a radial stress path if the stress components at that point maintain the same ratios during the loading, that is, if $\sigma_{ij} = C\sigma^{\circ}_{ij}$, where the σ°_{ij}'s are constants and C is a monotonically increasing parameter. For such a radial path, the flow-theory equations are integrable to those of the deformation theory [12], [8]. With non-radial stress paths the two theories are generally expected to give different results, but the torsion solution of the square bar seems to indicate that while the radial stress path is

a sufficient condition for agreement of the two theories, it may not be a necessary condition.

Based on Drucker's assumptions [3], Budiansky [1] proposed a criterion under which a deformation theory would be an "acceptable competitor" to its counterpart flow theory even under the conditions of a non-radial stress path. Thus, on the basis of the "physical soundness" of a plasticity theory, one might expect the deformation and flow theories to yield comparable results even though the stresses deviate from a radial path during the loading. However, it should be emphasized that this criterion deals only with the physical acceptability of the deformation theory and not with the question of integrability of the flow-theory equations to those of the deformation theory.

1.2 Objectives and General Discussion of the Present Study

The principal objectives achieved in this study are threefold: (1) to better establish the torque-moment interaction curve for the perfectly plastic material, (2) to provide a solution to the combined bending and torsion problem for both generalized J_2 deformation theory and generalized J_2 flow theory, and (3) to compare these solutions for different loadings.

In the establishment of the interaction curve for a rigid-perfectly plastic material, Piechnik's warping-

function equation is solved numerically for a wide range of combined bending and torsion. Solutions are obtained for prismatic bars having either a unit square or a unit radial cross section. Since the warping-function formulation avoids the singularity of the Hill-Handelman equation, the numerical solution appears to converge throughout the range of the load parameters. In Section 5.3, these interaction curves are given, and it is found that they agree with those points calculated by previous investigators.

The application of generalized J_2 deformation or flow theory implicitly assumes the entire bar to be plastic. Thus, upon initial loading, yielding takes place immediately, followed by isotropic work-hardening, so that the material properties are governed by an expanding yield surface in a stress-representation space. In this study no unloading is considered, i.e., the second invariant of stress always increases.

Since governing equations including work-hardening in the combined bending and torsion problem were not available for either deformation or flow theory, systems of equations were developed for each theory. The development of these governing equations departs somewhat from the standard approach since it was not possible to determine a single governing equation. Instead, in both instances, the governing equations are presented as a

system of implicit non-linear partial differential equations for the unknown functions. These equations are solved simultaneously by numerical methods.

In the usual processes of determining work-hardening solutions, the flow-theory solution to a problem is generally much more difficult to obtain than its counterpart deformation-theory solution. The application of the backward finite-difference representation with respect to the time-like variable in the flow-theory equations (Section 3.6) leads to a flow-theory system of equations in which the difficulty in getting the numerical solution through iteration is comparable to that for deformation theory. The significance of this result is further analyzed in Section 5.7.

This approach, in the case of flow theory, seems to offer a distinct advantage for numerical solution over the method which Greenberg, Dorn, and Wetherell [6] applied to the case of pure torsion. Thus, numerous comparisons between the two theories may be made without difficulty, including cases of combined bending and torsion not previously treated.

Numerical solutions for both the generalized J_2 deformation and flow theories are obtained for a prismatic bar of a unit square cross section. With each theory, the solutions are obtained for both a stress-function and a warping-function formulation. The stress-function and

warping-function formulations appear to be equally competitive, with neither offering any computational advantage, and their results were found to agree within the assumed numerical accuracy.

Differences appear between the flow and deformation-theory predictions for combined bending and torsion when the bending curvature κ and the torsional angle of twist per unit length θ do not maintain a constant ratio during the deformation. When $\frac{\kappa}{\theta}$ was constant throughout the loading, the numerical solutions for the two theories agreed. This agreement would seem to indicate that a radial straining in the $\kappa - \theta$ generalized-strain space may be a sufficient condition for integrability of the flow theory for combined bending and torsion. The results of Greenberg, Dorn, and Wetherell are a special case of this since for pure torsion $\frac{\kappa}{\theta} = 0$ throughout the loading. At the present time a proof has not been given that the condition of a constant ratio is in fact a sufficient condition for integrability, but the numerical solutions obtained for the square bar support this hypothesis.

A numerical solution for the generalized J_2 deformation theory was also developed for the circular bar, using polar coordinates. This solution is given only to illustrate the feasibility of the method in instances where the coordinates are chosen so as to correspond to the cross-sectional geometry.

The basic equations are developed in Chapter II. The rigid-perfectly plastic formulation essentially repeats the work of Piechnik [24]. This formulation is presented in order to acquaint the reader with the basic differences between the rigid-perfectly plastic equations and the work-hardening formulations. The numerical algorithms for the square bar and the circular bar are given in Chapters III and IV, respectively. Chapter V is devoted to the presentation of the results and general conclusions of the study. Chapter VI suggests possibilities for additional investigations.

II. DERIVATION OF EQUATIONS

2.1 General Principles of Mechanics

A long prismatic bar with a simply-connected cross section having at least one axis of symmetry is acted on by a combined bending moment and torque at each end (Figure 1).

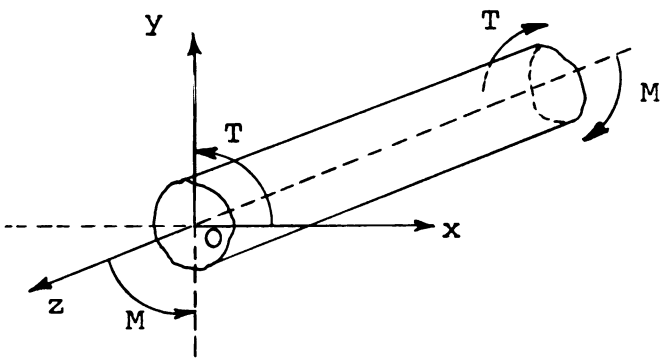

Figure 1. Coordinate system

The bending moment M acts in the yz-plane of symmetry about the Ox axis and the torque T acts in the xy-plane. The z-axis is parallel to the generators of the cylinder and is also the axis of twist.

The equilibrium equations for no body forces and the boundary conditions are

$$\frac{\partial \sigma_{xx}}{\partial x} + \frac{\partial \sigma_{xy}}{\partial y} + \frac{\partial \sigma_{xz}}{\partial z} = 0$$

$$\frac{\partial \sigma_{xy}}{\partial x} + \frac{\partial \sigma_{yy}}{\partial y} + \frac{\partial \sigma_{yz}}{\partial z} = 0$$

$$\frac{\partial \sigma_{xz}}{\partial x} + \frac{\partial \sigma_{yz}}{\partial y} + \frac{\partial \sigma_{zz}}{\partial z} = 0$$

$$P_{nx} = \ell \sigma_{xx} + m\sigma_{xy} + n\sigma_{xz} \qquad (2.1)$$

$$P_{ny} = \ell \sigma_{xy} + m\sigma_{yy} + n\sigma_{yz}$$

$$P_{nz} = \ell \sigma_{xz} + m\sigma_{yz} + n\sigma_{zz}$$

where (P_{nx}, P_{ny}, P_{nz}) are the traction vector components at a boundary point with outer unit normal $\hat{n}$.

The relationship between the displacements and the small strain components is

$$\varepsilon_{xx} = \frac{\partial u}{\partial x} \qquad \varepsilon_{xy} = \frac{1}{2}\left[\frac{\partial v}{\partial x} + \frac{\partial u}{\partial y}\right]$$

$$\varepsilon_{yy} = \frac{\partial v}{\partial y} \qquad \varepsilon_{yz} = \frac{1}{2}\left[\frac{\partial w}{\partial y} + \frac{\partial v}{\partial z}\right] \qquad (2.2)$$

$$\varepsilon_{zz} = \frac{\partial w}{\partial z} \qquad \varepsilon_{xz} = \frac{1}{2}\left[\frac{\partial w}{\partial x} + \frac{\partial u}{\partial z}\right].$$

The total displacement of the prismatic bar is assumed to be the sum of the displacement due to pure bending and that due to pure torsion. For an

incompressible bar, assuming bending parallel to the yz-plane, this sum is [12], for $\theta z \ll 1$,

$$u = -\frac{1}{2}\kappa xy - \theta yz$$

$$v = -\frac{1}{4}\kappa(2z^2 - x^2 + y^2) + \theta xz \qquad (2.3)$$

$$w = \kappa yz + f(x,y,\theta),$$

where κ is curvature, θ the angle of twist per unit length and $f(x,y,\theta)$ the warping function.

The terms $u' = -\theta yz$ and $v' = \theta xz$ represent a rigid rotation of the cross section around the z-axis through the angle θz, provided θz is small compared to one radian. Since finite rotations are considered, these displacement expressions are accurate only for small values of z. But the strain components derived from them are independent of z and are assumed to apply along the whole length of the bar.

The strain components for the prismatic bar are determined from Equations (2.2) and (2.3). Thus,

$$\varepsilon_{xx} = -\frac{1}{2}\kappa y \qquad \varepsilon_{xy} = 0$$

$$\varepsilon_{yy} = -\frac{1}{2}\kappa y \qquad \varepsilon_{yz} = \frac{1}{2}\left[\frac{\partial f}{\partial y} + \theta x\right] \qquad (2.4)$$

$$\varepsilon_{zz} = \kappa y \qquad \varepsilon_{xz} = \frac{1}{2}\left[\frac{\partial f}{\partial x} - \theta y\right].$$

This strain tensor satisfies the incompressibility assumption of the material since

$$3\varepsilon_m = \varepsilon_{xx} + \varepsilon_{yy} + \varepsilon_{zz} = -\frac{1}{2}\kappa y - \frac{1}{2}\kappa y + \kappa y = 0. \qquad (2.5)$$

Therefore, the strain tensor of (2.4) is also the strain deviator tensor.

The stresses σ_{xx}, σ_{yy}, and σ_{xy} are identically zero for the combined bending and torsion problem in elasticity. By analogy with the elastic problem, these stresses are assumed to be zero for the corresponding problem in plasticity [11]. In addition, the bar is taken to be of sufficient length so that the stresses are independent of z. As a result of these assumptions, the equilibrium equations and lateral boundary condition (2.1) reduce to

$$\frac{\partial \sigma_{xz}}{\partial x} + \frac{\partial \sigma_{yz}}{\partial y} = 0 \qquad \text{(a)}$$

$$P_{nz} = \ell \sigma_{xz} + m\sigma_{yz}. \qquad \text{(b)} \qquad (2.6)$$

The components of the unit normal vector $\hat{n}$ at any point on the lateral boundary are $\hat{n}$ (ℓ,m,0) and for the load vector they are $\vec{P}$ (0,0,0). Therefore, the boundary condition (2.6b) takes the form

$$\sigma_{xz}\ell + \sigma_{yz}m = 0. \qquad (2.7)$$

From Figure 2 it is observed that the components ℓ and m of the unit normal vector are given by [34]

$$\ell = \cos nx = \frac{dy}{ds}, \quad m = \cos ny = -\frac{dx}{ds}. \tag{2.8}$$

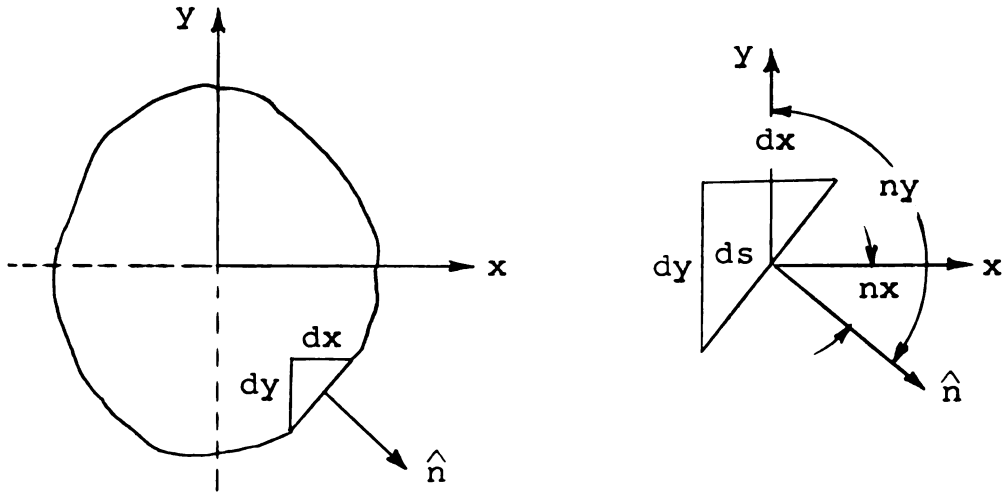

Figure 2. Relation between unit normal vector and direction cosines

Using Equations (2.8), Equation (2.7) is expressed

$$\sigma_{xz}dy - \sigma_{yz}dx = 0. \tag{2.9}$$

For the complete specification of a mechanics problem, the above equations must be supplemented by appropriate constitutive equations. These physical equations define the material relationship between stress and strain.

In the following sections the problem will be formulated for the constitutive relations of:

1. Rigid-perfectly plastic material governed by Hencky deformation theory.
2. Rigid-perfectly plastic material governed by Levy-Mises flow theory.
3. Work-hardening material governed by generalized J_2 deformation theory.
4. Work-hardening material governed by generalized J_2 flow theory.

Each theory will lead to a different formulation of the problem. In all cases the entire bar will be assumed to be plastic. Surfaces across which the interior normal component of stress is discontinuous are permitted, e.g., the neutral surface in pure bending.

The development of the rigid-perfectly plastic equations (Sections 2.2 and 2.3) essentially repeats the derivation given by Piechnik [24]. The work-hardening equations (Sections 2.4 and 2.5) represent a formulation which is original with this study.

2.2 Rigid-Perfectly Plastic Material Governed by Hencky Deformation Theory

For a rigid-perfectly plastic material obeying Hencky deformation theory the strain deviator tensor is proportional to the stress deviator tensor [9], [12]. Thus,

$$\varepsilon'_{ij} = \Phi\sigma'_{ij}, \tag{2.10}$$

where Φ is an unspecified proportionality function, ε'_{ij} the strain deviator tensor, and σ'_{ij} the stress deviator tensor. For this material, the function Φ is usually determined through the specification of a yield condition [12]. The Mises yield condition [19] is used in the following development, namely

$$(\sigma_{xx} - \sigma_{yy})^2 + (\sigma_{yy} - \sigma_{zz})^2 + (\sigma_{zz} - \sigma_{xx})^2$$

$$+ 6(\sigma_{xz}^2 + \sigma_{yz}^2 + \sigma_{xy}^2) = 6k^2, \qquad (2.11)$$

where k is the yield stress in pure torsion. According to the elastic analogy assumptions, $\sigma_{xx} = \sigma_{yy} = \sigma_{xy} = 0$, and this yield condition becomes

$$\sigma_{zz}^2 + 3\sigma_{xz}^2 + 3\sigma_{yz}^2 = 3k^2. \qquad (2.12)$$

From the assumption that $\sigma_{xx} = \sigma_{yy} = 0$ it follows that the deviatoric components of normal stress are $\sigma'_{xx} = \sigma'_{yy} = -\frac{1}{3}\sigma_{zz}$ and $\sigma'_{zz} = \frac{2}{3}\sigma_{zz}$. Hence, the following independent equations follow from the application of Equation (2.10) and the elastic analogy assumptions on the stress tensor:

$$\sigma_{zz} = \frac{3}{2\Phi} K y$$

$$\sigma_{yz} = \frac{1}{2\Phi}\left[\frac{\partial f}{\partial y} + \theta x\right] \qquad (2.13)$$

$$\sigma_{xz} = \frac{1}{2\Phi}\left[\frac{\partial f}{\partial x} - \theta y\right] .$$

The solution of the problem requires the determination of functions f and Φ such that the equilibrium equation (2.6a) and the yield condition (2.12) are satisfied identically throughout the cross section, and the boundary condition (2.9) is satisfied at each boundary point.

These functions may be determined by two different approaches [24], corresponding respectively to the warping-function approach or to the stress-function approach for the pure torsion problem.

The two approaches are summarized here, and the details carried out in the following sections.

(a) Warping-function method. The stress components (2.13) are substituted into the yield condition (2.12), giving Φ as a function of the warping-function f. The parameter Φ found in this manner is substituted along with Equation (2.13) into the equilibrium Equation (2.6a). These substitutions result in a single second-order partial differential equation for the unknown function f.

(b) Stress-function method. A stress-function ψ, defined by Equations (2.14), is introduced into the system as a new unknown:

$$\frac{\sigma_{xz}}{k} = \frac{\partial \psi}{\partial y}, \quad \frac{\sigma_{yz}}{k} = - \frac{\partial \psi}{\partial x}. \tag{2.14}$$

Stresses defined in this manner in terms of the function ψ satisfy the equilibrium Equation (2.6a) identically. The warping-function f is now eliminated from the shear strain Equations (2.4) to obtain the following compatibility equation for the shear strains:

$$\frac{\partial \varepsilon_{yz}}{\partial x} - \frac{\partial \varepsilon_{xz}}{\partial y} = \theta . \tag{2.15}$$

The stress components (2.13), represented in terms of ψ, are substituted into the yield condition (2.12), giving Φ as a function of ψ. Substitution of ψ along with these same stress component expressions into (2.15) produces a single second-order partial differential equation for the unknown function ψ.

2.2.1 Warping-Function Formulation

As a consequence of the stress-strain relations (2.13) the equilibrium Equation (2.6a) is

$$\frac{\partial}{\partial x}\left[\frac{1}{2\Phi}\left(\frac{\partial f}{\partial x} - \theta y\right)\right] + \frac{\partial}{\partial y}\left[\frac{1}{2\Phi}\left(\frac{\partial f}{\partial y} + \theta x\right)\right] = 0. \tag{2.16}$$

The yield condition (2.12) becomes

$$\frac{9}{4}\frac{\kappa^2}{\varphi^2}y^2 + \frac{3}{4\varphi^2}\left[\left(\frac{\partial f}{\partial x} - \theta y\right)^2 + \left(\frac{\partial f}{\partial y} + \theta x\right)^2\right] = 3k^2. \tag{2.17}$$

Equation (2.17) is solved for φ as a function of f. Thus,

$$\varphi = \frac{1}{2k}[3\kappa^2y^2 + f_x^2 - 2f_x\theta y + \theta^2y^2 + f_y^2 + 2f_y\theta x + \theta^2x^2]^{1/2}, \tag{2.18}$$

where the subscript represents differentiation with respect to that variable.

Equation (2.16), after multiplication by $2\varphi^2$ yields

$$\varphi(f_{xx} + f_{yy}) - \varphi_x(f_x - \theta y) - \varphi_y(f_y + \theta x) = 0. \tag{2.19}$$

Upon substitution for φ and its respective derivatives from (2.18), Equation (2.19) takes the following form:

$$3[\kappa^2y^2(f_{xx} + f_{yy}) - \kappa^2yf_y - \kappa^2\theta xy] + f_y^2f_{xx} + f_x^2f_{yy} + \theta^2y^2f_{yy} + 2\theta xf_yf_{xx} - 2\theta yf_xf_{yy} - 2f_xf_yf_{xy} + 2\theta yf_yf_{xy} - 2\theta xf_xf_{xy} + 2\theta^2xyf_{xy} + \theta^2x^2f_{xx} = 0. \tag{2.20}$$

Equation (2.20) was first developed by Piechnik [24] and is referred to as the Piechnik equation.

By introducing into (2.20) the dimensionless coordinates

$$x = a\xi, \quad y = a\eta \tag{2.21}$$

and the function

$$t = \frac{f}{a^2\theta} \tag{2.22}$$

and denoting

$$\mu = \frac{K}{\theta}, \tag{2.23}$$

the Piechnik equation is transformed to

$$3\mu^2\eta^2(t_{\xi\xi} + t_{\eta\eta}) + t_{\xi\xi}(t_\eta + \xi)^2 + t_{\eta\eta}(t_\xi - \eta)^2 - 2t_{\xi\eta}(t_\xi - \eta)(t_\eta + \xi) - 3\mu^2\eta t_\eta - 3\mu^2\xi\eta = 0. \tag{2.24}$$

Expressed in terms of the dimensionless coordinates ξ and η and the function t, the boundary condition (2.9) is

$$(t_\xi - \eta)d\eta - (t_\eta + \xi)d\xi = 0. \tag{2.25}$$

2.2.2 Stress-Function Formulation

As a result of the stress-strain relations (2.10) and the Equations (2.14) defining ψ, the shear strains become

$$\varepsilon_{xz} = k\varphi\frac{\partial\psi}{\partial y}, \quad \varepsilon_{yz} = -k\varphi\frac{\partial\psi}{\partial x}. \tag{2.26}$$

Substitution of these strains into the compatibility Equation (2.15) gives

$$\frac{\partial}{\partial x}\left(\varphi\frac{\partial\psi}{\partial x}\right) + \frac{\partial}{\partial y}\left(\varphi\frac{\partial\psi}{\partial y}\right) + \frac{\theta}{k} = 0. \tag{2.27}$$

From the yield condition (2.12), the normal stress σ_{zz} is, if ψ_x and ψ_y denote partial derivatives,

$$\sigma_{zz} = \pm\sqrt{3}\, k[1 - \psi_x^2 - \psi_y^2]^{1/2}, \tag{2.28}$$

where choice of sign corresponds to the sign of the coordinate y. Since symmetry conditions permit restricting an analysis to the region where y is positive, the positive sign will be taken for the following development. According to (2.13) the stress σ_{zz} is

$$\sigma_{zz} = \frac{3}{2\Phi}\kappa y. \tag{2.29}$$

Equating Equations (2.28) and (2.29) and solving for φ yields

$$\varphi = \frac{\sqrt{3}}{2k}\frac{\kappa y}{[1 - \psi_x^2 - \psi_y^2]^{1/2}}. \tag{2.30}$$

Substitution of Φ from (2.30) into Equation (2.27) produces the following partial differential equation for the unknown function ψ:

$$\frac{\partial}{\partial x}\left[\chi\frac{\partial\psi}{\partial x}\right] + \frac{\partial}{\partial y}\left[\chi\frac{\partial\psi}{\partial y}\right] + \frac{2}{\sqrt{3}}\frac{\theta}{\kappa} = 0, \tag{2.31}$$

where

$$\chi = \frac{y}{[1 - \psi_x^2 - \psi_y^2]^{1/2}}.$$

Through the use of energy principles, Equation (2.31) was first developed by Handelman [7] and later extended to more general loading situations by Hill [11]. This equation is referred to as the Hill-Handelman equation.

From Equations (2.9) and (2.14) the boundary condition on ψ for the Hill-Handelman equation is expressed as

$$d\psi = \frac{\partial\psi}{\partial y}dy + \frac{\partial\psi}{\partial x}dx = 0, \tag{2.32}$$

or

$$\psi = \text{constant} \tag{2.33}$$

on the boundary. However, since only derivatives of ψ are required, the constant is taken as zero, making the boundary condition

$$\psi = 0. \tag{2.34}$$

2.3 Rigid-Perfectly Plastic Material Governed by Levy-Mises Theory

For a material obeying Levy-Mises theory, the rate-of-deformation deviator tensor is proportional to the stress deviator tensor [12]. That is

$$\dot{\varepsilon}'_{ij} = \dot{\lambda}\,\sigma'_{ij} \tag{2.35}$$

where the dot represents differentiation with respect to an appropriate time-like variable and $\dot{\lambda}$ is an unspecified proportionality function.

The kinematical relation between the velocities and the rate of deformation tensor, which for small displacements may be identified with the time derivative of the strain tensor, is

$$\begin{aligned}
\dot{\varepsilon}_{xx} &= \frac{\partial \dot{u}}{\partial x} & \dot{\varepsilon}_{xy} &= \frac{1}{2}\left[\frac{\partial \dot{v}}{\partial x} + \frac{\partial \dot{u}}{\partial y}\right] \\
\dot{\varepsilon}_{yy} &= \frac{\partial \dot{v}}{\partial y} & \dot{\varepsilon}_{yz} &= \frac{1}{2}\left[\frac{\partial \dot{w}}{\partial y} + \frac{\partial \dot{v}}{\partial z}\right] \\
\dot{\varepsilon}_{zz} &= \frac{\partial \dot{w}}{\partial z} & \dot{\varepsilon}_{xz} &= \frac{1}{2}\left[\frac{\partial \dot{w}}{\partial x} + \frac{\partial \dot{u}}{\partial z}\right].
\end{aligned} \tag{2.36}$$

The velocities are determined by differentiating the displacement (2.3), with respect to time. For small-displacement theory, these velocities are (for small z)

$$\dot{u} = -\frac{1}{2}\dot{\kappa}xy - \dot{\theta}yz$$

$$\dot{v} = -\frac{1}{4}\dot{\kappa}(2z^2 - x^2 + y^2) + \dot{\theta}xy \qquad (2.37)$$

$$\dot{w} = \dot{\kappa}yz + F(x,y,\theta),$$

where $F(x,y,\theta)$ is the derivative of the warping function with respect to time. For small-displacement theory the coordinates may be considered as material coordinates giving the initial position of the particle.

The rate of deformation tensor is assumed to be independent of z and is determined from Equations (2.37) through the kinematical relations (2.36). Thus,

$$\dot{\varepsilon}_{xx} = -\frac{1}{2}\dot{\kappa}y \qquad \dot{\varepsilon}_{xy} = 0$$

$$\dot{\varepsilon}_{yy} = -\frac{1}{2}\dot{\kappa}y \qquad \dot{\varepsilon}_{yz} = \frac{1}{2}\left[\frac{\partial F}{\partial y} + \dot{\theta}x\right] \qquad (2.38)$$

$$\dot{\varepsilon}_{zz} = \dot{\kappa}y \qquad \dot{\varepsilon}_{xz} = \frac{1}{2}\left[\frac{\partial F}{\partial x} - \dot{\theta}y\right].$$

As a consequence of relation (2.35) the non-zero components of the stress tensor are

$$\sigma_{xx} = \frac{3}{2\dot{\lambda}}\dot{\kappa}y$$

$$\sigma_{yz} = \frac{1}{2\dot{\lambda}}\left[\frac{\partial F}{\partial y} + \dot{\theta}x\right] \qquad (2.39)$$

$$\sigma_{xz} = \frac{1}{2\dot{\lambda}}\left[\frac{\partial F}{\partial x} - \dot{\theta}y\right].$$

By a procedure analogous to Section 2.2, a warping-rate function equation and a stress-function equation are derived.

2.3.1 Warping-Rate Function Formulation

The stresses from (2.39) are substituted into the equilibrium Equation (2.6a). Differentiation and multiplication of this equation by $2\dot{\lambda}^2$ result in

$$\dot{\lambda}(F_{xx} + F_{yy}) - \dot{\lambda}_x(F_x - \dot{\theta}y) - \dot{\lambda}_y(F_y + \dot{\theta}x) = 0. \qquad (2.40)$$

The proportionality factor $\dot{\lambda}$ is obtained through substitution of (2.39) into the yield condition (2.12). After simplification, $\dot{\lambda}$ is expressed as

$$\dot{\lambda} = \frac{1}{2k}[3\dot{\kappa}^2y^2 + F_x^2 - 2F_x\dot{\theta}y + \dot{\theta}^2y^2 + F_y^2$$

$$+ 2F_y\dot{\theta}x + \dot{\theta}^2x^2]^{1/2}. \qquad (2.41)$$

The proportionality factor $\dot{\lambda}$ is eliminated from (2.40) through (2.41) to give

$$3\left[\dot{\kappa}^2 y^2 (F_{xx} + F_{yy}) - \dot{\kappa}^2 y F_y - \dot{\kappa}^2 \dot{\theta} xy\right] + F_y^2 F_{xx} + F_x^2 F_{yy}$$

$$+ \dot{\theta}^2 y^2 F_{yy} + 2\dot{\theta} x F_y F_{xx} - 2\dot{\theta} y F_x F_{yy} - 2F_x F_y F_{xy} + 2\dot{\theta} y F_y F_{xy}$$

$$- 2\dot{\theta} x F_x F_{xy} + 2\dot{\theta}^2 xy F_{xy} + \dot{\theta}^2 x^2 F_{xx} = 0. \qquad (2.42)$$

With the dimensionless coordinates ξ and η defined in (2.21) and with

$$\mu^* = \frac{\dot{\kappa}}{\dot{\theta}}, \qquad (2.43)$$

$$T = \frac{F}{a^2 \dot{\theta}} \qquad (2.44)$$

Equation (2.42) becomes

$$3\mu^{*2}\eta^2 (T_{\xi\xi} + T_{\eta\eta}) + T_{\xi\xi} (T_\eta + \xi)^2 + T_{\eta\eta} (T_\xi - \eta)^2$$

$$- 2T_{\xi\eta} (T_\xi - \eta)(T_\eta + \xi) - 3\mu^{*2}\eta T_\eta - 3\mu^{*2}\xi\eta = 0. \qquad (2.45)$$

In this notation the boundary condition (2.9) is expressed as

$$(T_\xi - \eta)d\eta - (T_\eta + \xi)d\xi = 0. \qquad (2.46)$$

If $\mu = \mu^*$, then Equations (2.45) and (2.24) are identical. This means $\frac{\kappa}{\theta} = \frac{\dot{\kappa}}{\dot{\theta}}$, or $\frac{\dot{\kappa}}{\kappa} = \frac{\dot{\theta}}{\theta}$, which implies $\ln \kappa = \ln \theta$ + constant, and consequently $\frac{\kappa}{\theta}$ = constant during the test. This type of loading is "proportional straining" in terms of the generalized variables κ and θ. Under the condition of proportional straining, there is no difference between the Hencky and Levy-Mises rigid-perfectly plastic interaction curves for combined bending and torsion. This was first noted by Piechnik [24].

2.3.2 Stress-Function Formulation

By eliminating the warping-rate function from the kinematical relations (2.38), the following compatibility relation is obtained:

$$\frac{\partial \dot{\varepsilon}_{yz}}{\partial x} - \frac{\partial \dot{\varepsilon}_{xz}}{\partial y} = \dot{\theta}. \qquad (2.47)$$

With use of the stress-strain relations (2.35), and Equation (2.14) defining ψ, this compatibility equation becomes

$$\frac{\partial}{\partial x}\left[\dot{\lambda}\frac{\partial \psi}{\partial x}\right] + \frac{\partial}{\partial y}\left[\dot{\lambda}\frac{\partial \psi}{\partial y}\right] + \frac{\dot{\theta}}{k} = 0. \qquad (2.48)$$

Paralleling the procedure used to determine Φ, the following relation for $\dot{\lambda}$ is derived from the yield condition:

$$\dot{\lambda} = \frac{\sqrt{3}}{2k} \frac{\dot{\kappa}\, y}{[1 - \psi_x^2 - \psi_y^2]^{1/2}}. \tag{2.49}$$

Substitution for $\dot{\lambda}$ from (2.49) produces (2.50), a single second-order partial differential equation for the unknown ψ:

$$\frac{\partial}{\partial x}\left[\chi \frac{\partial \psi}{\partial x}\right] + \frac{\partial}{\partial y}\left[\chi \frac{\partial \psi}{\partial y}\right] + \frac{2}{\sqrt{3}} \frac{\dot{\theta}}{\dot{\kappa}} = 0, \tag{2.50}$$

where

$$\chi = \frac{y}{[1 - \psi_x^2 - \psi_y^2]^{1/2}}.$$

The boundary condition for (2.50) is also

$$\psi = 0. \tag{2.51}$$

Again, if $\frac{\theta}{\kappa} = \frac{\dot{\theta}}{\dot{\kappa}}$, Equation (2.50) is identical to (2.31) and the two theories agree.

Equation (2.50) has been solved numerically by both Steele [30] and Imegwu [15] and [16]. In his second solution, Imegwu examines Hill's version of (2.50), which represents a more general loading condition than considered here.

2.4 Work-Hardening Material Governed by a Generalized J_2 Deformation Law

Ramberg and Osgood [27] introduced the following three-parameter stress-strain curves for uniaxial tension:

$$\varepsilon = \frac{1}{E}\left[1 + \left(\frac{\sigma}{\sqrt{3k}}\right)^{2n}\right]\sigma, \tag{2.52}$$

where ε is strain and σ stress. The law fits a variety of metals and includes work-hardening effects. These stress-strain curves for $n = 1$, $n = 9$, and $n \to \infty$ are shown in Figure 3. For $n \to \infty$ the curve approaches the elastic-perfectly plastic law.

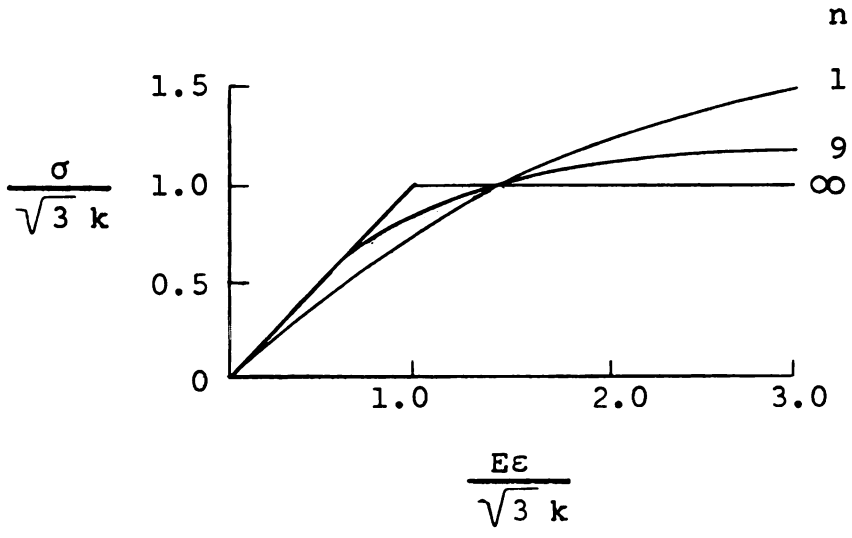

Figure 3. Ramberg-Osgood stress-strain curves

The uniaxial stress-strain law (2.52) has been extended by Nadai [6] to the following generalized

Ramberg-Osgood J_2 deformation theory:

$$2G\varepsilon'_{ij} = \left[1 + J_2^n\right]\sigma'_{ij}, \tag{2.53}$$

where J_2 is the normalized second invariant of deviatoric stress,

$$J_2 = \frac{1}{2k^2}\sigma'_{ij}\sigma'_{ij}. \tag{2.54}$$

The development is again analogous to Section 2.2. However, the yield condition is no longer required since the proportionality factor is now specified. Letting

$$\Phi = 1 + J_2^n, \tag{2.55}$$

Equation (2.53) becomes

$$2G\varepsilon'_{ij} = \Phi\sigma'_{ij}. \tag{2.56}$$

The kinematic equations (2.3) and (2.4) remain valid for the incompressible material. According to the stress-strain relation (2.56) and Equations (2.3) and (2.4), the normalized non-zero stresses are

$$\frac{\sigma_{zz}}{\sqrt{3}k} = \frac{\sqrt{3}}{\Phi}\Theta\mu y$$

$$\frac{\sigma_{yz}}{k} = \frac{\Theta}{\Phi}\left[\frac{\partial t}{\partial y} + x\right] \qquad (2.57)$$

$$\frac{\sigma_{xz}}{k} = \frac{\Theta}{\Phi}\left[\frac{\partial t}{\partial x} - y\right],$$

where

$$\Theta = \frac{G\theta}{k}, \quad \mu = \frac{\kappa}{\theta}$$

and

$$t = \frac{f}{\theta}.$$

2.4.1 Warping-Function Formulation

The shear stresses of (2.57) are introduced into the equilibrium Equation (2.6a) to obtain

$$\frac{\partial}{\partial x}\left[\frac{1}{\Phi}\left(\frac{\partial t}{\partial x} - y\right)\right] + \frac{\partial}{\partial y}\left[\frac{1}{\Phi}\left(\frac{\partial t}{\partial y} + x\right)\right] = 0. \qquad (2.58)$$

The normalized second invariant of stress J_2 is

$$J_2 = \left(\frac{\sigma_{zz}}{\sqrt{3}k}\right)^2 + \left(\frac{\sigma_{xz}}{k}\right)^2 + \left(\frac{\sigma_{yz}}{k}\right)^2. \qquad (2.59)$$

If the stresses from (2.57) are employed in (2.59), then

$$J_2 = \frac{\Theta^2}{\Phi^2}\left[3\mu^2 y^2 + (t_x - y)^2 + (t_y + x)^2\right]. \qquad (2.60)$$

Thus, Equation (2.55) becomes

$$\Phi = 1 + \frac{\Theta^{2n}}{\Phi^{2n}}\left[3\mu^2 y^2 + (t_x - y)^2 + (t_y + x)^2\right]^n. \qquad (2.61)$$

Differentiation and simplification of (2.58) lead to

$$\Phi(t_{xx} + t_{yy}) - \Phi_x(t_x - y) - \Phi_y(t_y + x) = 0, \qquad (2.62)$$

where Φ is obtained from the $(2n+1)^{th}$ degree polynomial representation of (2.61). Thus,

$$\Phi^{2n+1} - \Phi^{2n} - S^n = 0, \qquad (2.63)$$

where

$$S = \Theta^2\left[3\mu^2 y^2 + (t_x - y)^2 + (t_y + x)^2\right].$$

The boundary condition on the function t according to Equation (2.9) is

$$(t_x - y)dy - (t_y + x)dx = 0. \qquad (2.64)$$

Equations (2.62) and (2.63) are solved simultaneously for the unknown functions t and Φ.

2.4.2 Stress-Function Formulation

In view of the stress-strain relation (2.56) and Equations (2.14) defining the stress function, the shear strains are expressed as

$$\varepsilon_{xz} = \frac{k}{2G}\Phi\frac{\partial\psi}{\partial y}, \quad \varepsilon_{yz} = -\frac{k}{2G}\Phi\frac{\partial\psi}{\partial x}. \tag{2.65}$$

Since Equations (2.3) and (2.4) remain valid, the compatibility Equation (2.15) must be satisfied. Substituting from (2.65) into (2.15) yields

$$\frac{\partial}{\partial x}\left[\Phi\frac{\partial\psi}{\partial x}\right] + \frac{\partial}{\partial y}\left[\Phi\frac{\partial\psi}{\partial y}\right] + \frac{2G\theta}{k} = 0. \tag{2.66}$$

Equations (2.14), the first Equation (2.57), and Equation (2.59) then bring Equation (2.55) into the form

$$\Phi = 1 + \left[3\frac{\Theta^2}{\Phi^2}\mu^2 y^2 + \psi_x^2 + \psi_y^2\right]^n. \tag{2.67}$$

These equations can be brought into a form superficially similar to those for the warping-function formulation. Equation (2.66) takes the form

$$\Phi(\psi_{xx} + \psi_{yy}) + \Phi_x\psi_x + \Phi_y\psi_y + 2\Theta = 0. \tag{2.68}$$

Equation (2.67) is expressed as a $(2n+1)^{th}$ degree polynomial,

$$\Phi^{2n+1} - \Phi^{2n} - S^n = 0, \tag{2.69}$$

where

$$S = 3\Theta^2\mu^2 y^2 + \Phi^2(\psi_x^2 + \psi_y^2). \tag{2.70}$$

It should be noted that Equation (2.69) is not really of the same form as Equation (2.63), since S now contains the unknown Φ. But in the numerical algorithms both equations are treated in the same manner.

The boundary condition on the function ψ is $\psi = 0$ on the surface contour.

Equations (2.68) and (2.69) are solved simultaneously for the unknown functions ψ and Φ.

2.5 Work-Hardening Material Governed by a Generalized J_2 Flow Law

According to Prager-Laning type flow theory [6], [26], the generalized Ramberg-Osgood law takes the form,

$$2G\dot{\varepsilon}'_{ij} = \dot{\sigma}'_{ij} + \frac{2n+1}{2} J_2^{n-1} \dot{J}_2 \sigma'_{ij}, \tag{2.71}$$

where the dot represents differentiation with respect to an appropriate time-like variable. Since θ is assumed to increase monotonically with time, we may take θ as the time-like variable. In the following, the dot refers specifically to differentiation with respect to θ.

Letting

$$\dot{\lambda} = \frac{2n+1}{2} J_2^{n-1} \dot{J}_2, \tag{2.72}$$

permits (2.71) to be expressed as

$$2G\dot{\varepsilon}'_{ij} = \dot{\sigma}'_{ij} + \dot{\lambda}\sigma'_{ij}. \tag{2.73}$$

Differentiation of the displacement Equations (2.3), with respect to θ, yields the velocity components,

$$\begin{aligned}
\dot{u} &= -\frac{1}{2}\frac{dK}{d\theta} xy - yz \\
\dot{v} &= -\frac{1}{4}\frac{dK}{d\theta} (2z^2 - x^2 + y^2) + xy \\
\dot{w} &= \frac{dK}{d\theta} yz + \dot{f}(x,y,\theta).
\end{aligned} \tag{2.74}$$

From the kinematical relations (2.36), the corresponding strain rates are

$$\begin{aligned}
\dot{\varepsilon}_{xx} &= -\frac{1}{2}\dot{K}y \qquad & \dot{\varepsilon}_{xy} &= 0 \\
\dot{\varepsilon}_{yy} &= -\frac{1}{2}\dot{K}y \qquad & \dot{\varepsilon}_{yz} &= \frac{1}{2}\left[\frac{\partial F}{\partial y} + x\right] \\
\dot{\varepsilon}_{zz} &= \dot{K}y \qquad & \dot{\varepsilon}_{xz} &= \frac{1}{2}\left[\frac{\partial F}{\partial x} - y\right]
\end{aligned} \tag{2.75}$$

where $\dot{K} = \frac{dK}{d\theta}$ and F is the derivative of the warping function with respect to θ.

2.5.1 Warping-Rate Function Formulation

Equations (2.73) and (2.75) are combined to obtain the following non-zero stress relations:

$$\dot{\sigma}_{zz} + \dot{\lambda}\sigma_{zz} = 3G\dot{\kappa}y$$

$$\dot{\sigma}_{yz} + \dot{\lambda}\sigma_{yz} = G(F_y + x) \qquad (2.76)$$

$$\dot{\sigma}_{xz} + \dot{\lambda}\sigma_{xz} = G(F_x - y).$$

The shear stresses must satisfy the equilibrium equation

$$\frac{\partial \sigma_{xz}}{\partial x} + \frac{\partial \sigma_{yz}}{\partial y} = 0, \qquad (2.77)$$

and, on the contour surface, the boundary condition,

$$\sigma_{xz}dy - \sigma_{yz}dx = 0. \qquad (2.78)$$

In order to determine an equation representing (2.77) in terms of the warping-rate function F, the first order differential equations (2.76) would have to be solved explicitly for the stresses as functions of the strain rates.

Since Equations (2.76) represent a coupled set of non-linear equations, they will not be solved explicitly. Rather, in Chapter III, by means of a backwards difference

scheme for θ, a discrete system of equations will be developed. This system, in the discrete sense, will be shown to satisfy Equations (2.76) and (2.77).

2.5.2 Stress-Function Formulation

By virtue of the constitutive relation (2.73) and (2.14) defining ψ, the shear strain rates are

$$\dot{\varepsilon}_{xy} = \frac{k}{2G}\left(\dot{\psi}_y + \dot{\lambda}\psi_y\right)$$
$$\dot{\varepsilon}_{yz} = \frac{-k}{2G}\left(\dot{\psi}_x + \dot{\lambda}\psi_x\right). \tag{2.79}$$

Eliminating the warping-rate function from the shear strain rate expressions in (2.75) produces the following compatibility equation:

$$\frac{\partial \dot{\varepsilon}_{yz}}{\partial x} - \frac{\partial \dot{\varepsilon}_{xz}}{\partial y} = 1. \tag{2.80}$$

After substitution of the shear strain rates from (2.79) and further simplification, the compatibility equation (2.80) becomes

$$\dot{\psi}_{xx} + \dot{\psi}_{yy} + \dot{\lambda}(\psi_{xx} + \psi_{yy}) + \dot{\lambda}_x \psi_x + \dot{\lambda}_y \psi_y + \frac{2G}{k} = 0, \tag{2.81}$$

where, according to (2.72),

$$\dot{\lambda} = \frac{2n+1}{2} J_2^{n-1} \dot{J}_2.$$

From (2.59), the normalized second invariant J_2 is

$$J_2 = \left(\frac{\sigma_{zz}}{\sqrt{3}k}\right)^2 + \left(\frac{\sigma_{xz}}{k}\right)^2 + \left(\frac{\sigma_{yz}}{k}\right)^2 \qquad (2.82)$$

or

$$J_2 = \left(\frac{\sigma_{zz}}{\sqrt{3}k}\right)^2 + \psi_y^2 + \psi_x^2. \qquad (2.83)$$

In order to determine a system of equations comparable to the deformation-theory stress-function Equations (2.68) and (2.69), J_2 must be expressed explicitly as a function of $\dot{\kappa}y$, ψ_x, and ψ_y. In Chapter III, this will be accomplished, in the discrete sense, through the use of a backward difference in the θ variable.

The governing deformation-theory equations for both the warping function and the stress function are represented as a system of two equations in terms of two unknown functions. This formulation for a combined bending and torsion of a Nadai work-hardening material is believed to be new. For a numerical analysis approach, it will be shown in Chapter III that this formulation leads to a reasonable computational algorithm.

The equations for the flow-theory formulation cannot be expressed as two explicit continuous equations in a form analogous to those of the deformation theory. But, through the use of a backward difference in θ, it

will be shown that both the warping-function and the stress-function formulations may be represented, at each discrete level of θ, as a system analogous to that of the deformation theory. In addition, the computational algorithm for these equations will be shown to be almost equivalent to the deformation-theory algorithm.

It is generally believed that a flow-theory formulation leads to a much more difficult problem than its counterpart deformation-theory formulation [2], [6], [18]. The results of the present formulation indicate that both theories, in the case of combined bending and torsion, lead to problems in which the solutions are obtained through comparable numerical computations.

III. NUMERICAL SOLUTIONS FOR A UNIT SQUARE CYLINDER

3.1 Symmetry Properties of the Solution

The unit square cross section is geometrically symmetric with respect to both the x and y axes (Figure 4).

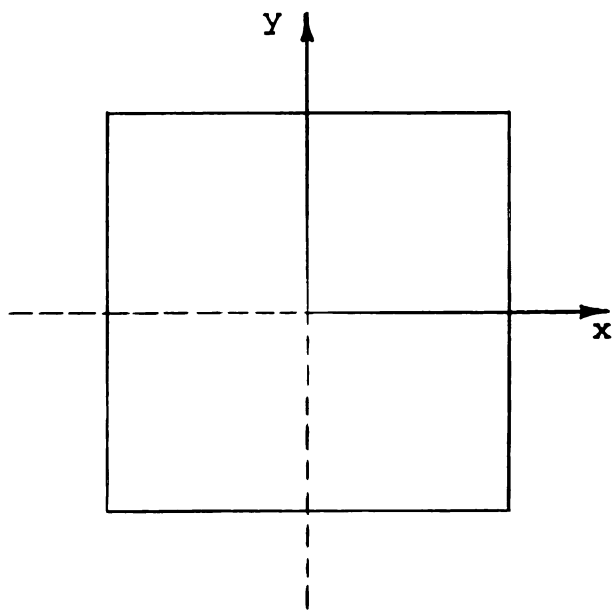

Figure 4. Coordinate system for unit square cross section

Since the bending moment acts about the x-axis, the normal stresses are symmetrical with respect to the y-axis. Because the material is isotropic, the normal stresses are anti-symmetric with respect to the x-axis. Moreover, only the square of the normal stress enters into the calculation of the stress function and warping function, since the

normal stress is considered only in the second invariant of deviatoric stress J_2. This implies that the normal stresses produce only symmetric effects on the governing equations. Hence, the solutions to the differential equations have the same symmetry properties as in the case of pure torsion.

When a square bar is subjected to pure torsion, the stress function is symmetrical with respect to the x and y axes, and the warping function is anti-symmetric with respect to these axes [34].

3.2 Discretization and Finite Difference Operators

A square mesh of equally spaced horizontal and vertical lines is superimposed on the positive quadrant of the cross section (Figure 5).

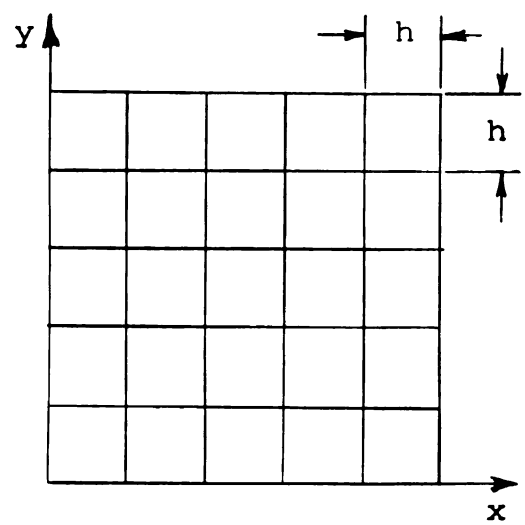

Figure 5. Lattice spacings for square mesh

The intersections of these lines are called mesh points or nodal points. The values of x and y at the nodal points are given by

$$\begin{aligned} x &= (i-1)h \qquad 1 \leq i \leq N \\ y &= (j-1)h \qquad 1 \leq j \leq N \end{aligned} \tag{3.1}$$

where i and j are integers, h the lattice spacing, and N the number of nodal points in either the x or y direction. A function g(x,y) defined at the point (x,y) has the discrete analogue g(i,j) defined at the point (i,j).

For the cross section, continuous physical parameters are replaced by discrete functions defined only at the mesh points. Discretization of the problem is accomplished through replacing the governing differential equation by its discrete analogue. Thus, the problem is reduced to that of solving a system of algebraic equations for the values of the discrete function.

The spatial derivatives are represented by the following finite-difference operators:

a) first derivatives at an interior point,

$$\begin{aligned} g_x &= [g(i+1,j) - g(i-1,j)]/2h \\ g_y &= [g(i,j+1) - g(i,j-1)]/2h, \end{aligned} \tag{3.2}$$

b) second derivatives at an interior point,

$$g_{xx} = [g(i+1,j) - 2g(i,j) + g(i-1,j)]/h^2$$

$$g_{yy} = [g(i,j+1) - 2g(i,j) + g(i,j-1)]/h^2, \tag{3.3}$$

c) mixed second derivative at an interior point,

$$g_{xy} = [g(i+1,j+1) - g(i-1,j+1) + g(i-1,j-1)$$

$$- g(i+1,j-1)]/4h^2, \tag{3.4}$$

d) first derivatives at a boundary point,

$$g_x = [3g(N,j) - 4g(N-1,j) + g(N-2,j)]/2h$$

$$g_y = [3g(i,N) - 4g(i,N-1) + g(i,N-2)]/2h. \tag{3.5}$$

The error for each of the above spatial derivative operators is of order h^2 [29].

In the flow-theory considerations, a function $g(x,y,\theta)$ is defined at the point (x,y,θ) and has the discrete analogue $g(i,j,\ell)$ defined at the point (i,j,ℓ). The derivative with respect to θ, at the point (i,j,ℓ), is represented by a backward difference quotient. Thus,

$$g_\theta = [g(i,j,\ell) - g(i,j,\ell-1)]/\Delta\theta, \tag{3.6}$$

and this approximation has an error of order $\Delta\theta$ [29].

Quadrature is performed by the repeated use of the two-dimensional form of Simpson's $\frac{1}{3}$ quadrature formula. The integral of the function over the area bounded by $(i-1)h \leq x \leq (i+1)h$ and $(j-1)h \leq y \leq (j+1)h$ is approximated by

$$\iint_A g(x,y)dxdy = \frac{h^2}{9}\Big[g(i+1,j+1) + g(i-1,j+1) + g(i-1,j-1) + g(i+1,j-1) + 4[g(i+1,j) + g(i,j+1) + g(i-1,j) + g(i,j-1)] + 16g(i,j)\Big] . \qquad (3.7)$$

The error of this quadrature formula is of order h^4 [6].

3.3 Piechnik Equation for Rigid-Perfectly Plastic Material

As was observed in Section 2.3.1, the warping-function equations for flow and deformation theory of rigid-perfectly plastic material are identical. Consequently, a solution is provided only for the case of deformation theory.

The Piechnik Equation (2.24) is quasi-linear in the unknown function $t(x,y)$ and may be expressed as

$$At_{xx} + 2Bt_{xy} + Ct_{yy} + Dt_y + E = 0 \qquad (3.8)$$

where the non-linear terms are contained in the coefficients

$$A = 3\mu^2 y^2 + (t_y + x)^2$$

$$B = -(t_x - y)(t_x - y)^2$$

$$C = 3\mu^2 y^2 + (t_x - y)^2$$

$$D = -3\mu^2 y$$

$$E = -3\mu^2 xy$$

In view of the boundary conditions (2.9) and the anti-symmetry property of the warping function, t must satisfy the additional constraints,

$$\begin{aligned} t_x &= y \quad \text{if} \quad x = 0.5 \\ t_y &= -x \quad \text{if} \quad y = 0.5 \\ t &= 0 \quad \text{if} \quad x = 0 \quad \text{or} \quad y = 0, \end{aligned} \tag{3.9}$$

on the first quadrant of the unit cross section.

Following the Gauss-Seidel over-relaxation procedure outlined in Appendix I, the values of $t_{m+1}(i,j)$ for the $(m+1)^{th}$ sweep through the mesh are calculated by

$$t_{m+1}(i,j) = t_m(i,j) + \omega[\bar{t}_{m+1}(i,j) - t_m(i,j)] \tag{3.10}$$

where ω is the over-relaxation factor and the $\bar{t}_{m+1}(i,j)$

values are furnished by

$$\bar{t}_{m+1}(i,j) = \frac{1}{2(\bar{A}+\bar{C})}\Big\{\bar{A}[t_m(i+1,j) + t_{m+1}(i-1,j)]$$

$$+ (\bar{C}+\bar{D})t_m(i,j+1) + (\bar{C}-\bar{D})t_{m+1}(i,j-1) + \bar{B}[t_m(i+1,j+1)$$

$$- t_{m+1}(i-1,j+1) - t_m(i+1,j-1) + t_{m+1}(i-1,j-1)] + \bar{E}\Big\} \qquad (3.11)$$

where

$$t_x = [t_m(i+1,j) - t_{m+1}(i-1,j)]/2h$$

$$t_y = [t_m(i,j+1) - t_{m+1}(i,j-1)]/2h$$

$$\bar{A} = 3\mu^2y^2 + (t_y + x)^2$$

$$\bar{B} = -[(t_x - y)(t_y + x)]/2$$

$$\bar{C} = 3\mu^2y^2 + (t_x - y)^2$$

$$\bar{D} = -1.5\mu^2yh$$

$$\bar{E} = 3\mu^2xyh^2,$$

and the discrete values of x and y are determined by Equations (3.1). At the boundaries, x = 0.5 or y = 0.5, the respective derivatives are known from (3.9) and these are incorporated into the above equations. For points on

the center lines, $x = 0$ or $y = 0$, the values of $t(i,j)$ are known.

For each sweep through the mesh, the cyclic order is prescribed so that the rows of the unknown matrix $t(i,j)$ are successively displaced. Thus, for each i, the index j runs through the range $1 \leq j \leq N$, before i is increased through its range $1 \leq i \leq N$.

The iterations are continued until

$$\text{Max} \left| t_{m+1}(i,j) - t_m(i,j) \right| < \varepsilon, \qquad (3.12)$$

for a preassigned convergence parameter ε, where the maximum is taken over all mesh points. More specific information on the choice of the over-relaxation factor and the convergence parameter ε for all algorithms is provided in Chapter V, Section 5.2.

The stresses are calculated by the finite-difference analogue of the stress-strain relations (2.13). The parameter φ is obtained through the analogue of (2.18). The difference representations of these quantities are

$$\varphi_k(i,j) = k\varphi(i,j) = \theta \left(\frac{9}{4}\mu^2 y^2 + \frac{3}{4}[(t_x - y)^2 + (t_y + x)^2] \right)^{1/2}$$

$$\frac{\sigma_{zz}(i,j)}{\sqrt{3}\,k} = \frac{\sqrt{3}\mu\theta y}{2\Phi_k(i,j)}$$

$$\frac{\sigma_{xy}(i,j)}{k} = \frac{\theta\left[\frac{t(i+1,j) - t(i-1,j)}{2h} - y\right]}{2\Phi_k(i,j)} \qquad (3.13)$$

$$\frac{\sigma_{yz}(i,j)}{k} = \frac{\theta\left[\frac{t(i,j+1) - t(i,j-1)}{2h} + x\right]}{2\Phi_k(i,j)},$$

where x and y are determined by (3.1). The values computed according to (3.13) are normalized stresses.

The normalized stress resultants, bending moment m_n, and torque t_n, are determined by the following integrals:

$$m_n = \frac{1}{M_o}\int_A y\sigma_{zz}\,dA$$

$$t_n = \frac{1}{T_o}\int_A (x\sigma_{yz} - y\sigma_{xz})\,dA \qquad (3.14)$$

where M_o is the moment for pure bending and T_o is the torque for pure torsion. The integrals of Equations (3.14) are approximated by repeated use of Simpson's $\frac{1}{3}$ quadrature formula, Equation (3.7).

The numerical calculations for the solution to the Piechnik equation are performed by a FORTRAN program, WARPI. A flow chart showing the sequence of operations

for program WARPI is provided in Appendix III, Figure 17. The listing of FORTRAN statements is given in Appendix IV.

3.4 Warping-Function Equations for Work-Hardening Generalized J_2 Deformation Theory

Equation (2.62) may be expressed as a non-linear Poisson equation,

$$t_{xx} + t_{yy} - E(t_x, t_y, x, y) = 0, \tag{3.15}$$

where

$$E = \frac{\Phi_x(t_x - y) + \Phi_y(t_y + x)}{\Phi}$$

and Φ is obtained from the polynomial,

$$\Phi^{2n+1} - \Phi^{2n} - S^n = 0, \tag{3.16}$$

where

$$S = \Theta^2[3\mu^2 y^2 + (t_x - y)^2 + (t_y + x)^2].$$

Equations (3.15) and (3.16) are treated as two simultaneous equations for the unknown functions $t(x,y)$ and $\Phi(x,y)$. Equation (3.15) is a second-order partial differential equation and the Equation (3.16) is a $(2n+1)^{th}$ degree polynomial in Φ.

The solution t(x,y) to the system must satisfy the conditions of anti-symmetry and the boundary condition (2.9). Thus, the constraints,

$$t_x = y \quad \text{if} \quad x = 0.5$$

$$t_y = -x \quad \text{if} \quad y = 0.5 \tag{3.17}$$

$$t = 0 \quad \text{if} \quad x = 0 \quad \text{or} \quad y = 0,$$

must be satisfied.

Each equation is represented by its corresponding finite-difference analogue. Using the Gauss-Seidel over-relaxation procedure (Appendix I), Equation (3.15) is solved as a Poisson equation.

Since this technique assumes values of the unknown function t(i,j) at each grid point, the difference estimate of E(i,j) is made at each point using the current estimates of t(i,j). Thus, in the approximate discrete sense, E is considered as a function of the spatial variables. This means, that to some degree, the convergence of the system to the solution t(x,y) depends on the manner in which E(i,j) converges to the function $E(t_x,t_y,x,y)$.

At each point, after the new estimate for the function t(i,j) has been determined, a new estimate to $\Phi(i,j)$ is made by means of the Newton-Raphson method

(Appendix II) applied to Equation (3.16). Thus, the two iteration processes are performed during the same sweep through the mesh. It appears that the calculation of these corrected values for the two functions in this successive manner tends to accelerate the convergence of the system.

To begin the iteration, initial solutions for $t(i,j)$ and $\Phi(i,j)$ are assumed. These values are corrected by succeeding sweeps through the net. According to the Gauss-Seidel procedure, the values of $t_{m+1}(i,j)$ for the $(m+1)^{th}$ sweep are calculated by

$$t_{m+1}(i,j) = t_m(i,j) + \omega[\bar{t}_{m+1}(i,j) - t_m(i,j)] \qquad (3.18)$$

where

$$\bar{t}_{m+1}(i,j) = \left[t_m(i+1,j) + t_m(i,j+1) + t_{m+1}(i-1,j) + t_{m+1}(i,j-1) - E_{m+1}\right]/4, \qquad (3.19)$$

and

$$E_{m+1} = [\Phi_m(i+1,j) - \Phi_{m+1}(i-1,j)][t_m(i+1,j) - t_{m+1}(i-1,j) - 2hy] + [\Phi_m(i,j+1) - \Phi_{m+1}(i,j-1)][t_m(i,j+1) - t_{m+1}(i,j-1) + 2hx] \; /4\Phi_m(i,j). \qquad (3.20)$$

The discrete values of x and y are obtained from (3.1). Modifications in Equations (3.18) through (3.20) are made at the boundaries, x = 0.5 and y = 0.5, so that the constraints of (3.17) are satisfied. Furthermore, on the center-lines, x = 0 and y = 0, the values of t(i,j) are known.

During the same sweep, the values of $\Phi_{m+1}(i,j)$ are calculated by the Newton-Raphson iteration for a $(2n+1)^{th}$ degree polynomial

$$\Phi_{m+1}(i,j) = \Phi_m(i,j) - \frac{\Phi_m^{2n}(i,j)[\Phi_m(i,j) - 1] - S_{m+1}^n}{\Phi_m^{2n-1}(i,j)[(2n+1)\Phi_m(i,j) - 2n]}, \tag{3.21}$$

where S_{m+1} is the difference representation of

$$S = \Theta^2 \left[3\mu^2 y^2 + (t_x - y)^2 + (t_y + x)^2 \right].$$

The iterations are continued until

$$\text{Max} \left| t_{m+1}(i,j) - t_m(i,j) \right| < \varepsilon, \tag{3.22}$$

with a preassigned convergence parameter ε, where the maximum is taken over all mesh points.

In general, if the necessary and sufficient conditions stated in Appendix I are satisfied, then the Gauss-Seidel method will converge for an arbitrary initial solution $t_o(i,j)$. However, as shown in Appendix II, the

Newton-Raphson method requires an initial estimate of $\Phi_o(i,j)$ near the exact solution. Therefore, to ensure convergence, the process is initiated near Θ equal zero. At this starting point, with Θ equal to zero, the exact values for $t(i,j)$ and $\Phi(i,j)$ are known. Consequently, if Θ is increased by a small amount $\Delta\Theta$, and this known solution for $\Theta = 0$ is used as an initial estimate, the process may converge. In fact, if $\Delta\Theta$ is small enough, one would expect the Newton-Raphson technique to converge rapidly.

Thus, the mathematical algorithm assumes the solution to be known at $\Theta = \ell\,\Delta\Theta$. This solution is used as the initial estimate for the solution at $\Theta = (\ell+1)\Delta\Theta$. Iteration is continued until the convergence criterion (3.22) is satisfied, giving the solution at $(\ell+1)\Delta\Theta$. Experience indicates that if $\Delta\Theta$ is kept small enough, this procedure will provide convergence throughout the desired range of Θ.

After a solution is obtained for a given Θ, the normalized stresses are calculated by the following relations:

$$\frac{\sigma_{zz}(i,j)}{\sqrt{3}k} = \frac{\sqrt{3}\Theta_{\mu y}}{\Phi(i,j)}$$

$$\frac{\sigma_{xz}(i,j)}{k} = \frac{\Theta\left[\frac{t(i+1,j) - t(i-1,j)}{2h} - y\right]}{\Phi(i,j)} \qquad (3.23)$$

$$\frac{\sigma_{yz}(i,j)}{k} = \frac{\Theta\left[\frac{t(i,j+1) - t(i,j-1)}{2h} + x\right]}{\Phi(i,j)}.$$

The normalized bending moment and torque for this Θ are calculated according to Equation (3.14) using the two-dimensional Simpson's $\frac{1}{3}$ rule.

The calculations for this system of equations are performed by a FORTRAN program, WARPO. A flow chart depicting the sequence of operations is shown in Appendix III, Figure 18. The FORTRAN listing of this program is provided in Appendix IV.

3.5 Stress-Function Equations for Work-Hardening Generalized J_2 Deformation Theory

The solution to the stress-function equation for deformation theory parallels the solution presented in Section 3.4 for the warping-function equation. Equation (2.68) is expressed as the non-linear Poisson equation,

$$\psi_{xx} + \psi_{yy} + E(\psi_x, \psi_y, x, y) = 0, \qquad (3.24)$$

where

$$E = \frac{\Phi_x \psi_x + \Phi_y \psi_y + 2\Theta}{\Phi},$$

and Φ is obtained from the $(2n+1)^{th}$ degree polynomial,

$$\Phi^{2n+1} - \Phi^{2n} - S^n = 0 \qquad (3.25)$$

where

$$S = 3\Theta^2\mu^2y^2 + \Phi^2(\psi_x^2 + \psi_y^2).$$

By virtue of Equation (2.34) and the symmetry properties of ψ, indicated in Section 3.1, the following conditions must be satisfied:

$$\begin{aligned} \psi &= 0 \quad \text{if} \quad x = 0.5 \quad \text{or } y = 0.5 \\ \psi_x &= 0 \quad \text{if} \quad x = 0 \\ \psi_y &= 0 \quad \text{if} \quad y = 0. \end{aligned} \qquad (3.26)$$

As in Section 3.4, Equations (3.24) and (3.25) are treated as two simultaneous equations for the unknown functions $\psi(x,y)$ and $\Phi(x,y)$. Equation (3.24) is a second-order partial differential equation and (3.25) is a $(2n+1)^{th}$ degree polynomial in Φ. Each equation is represented by its finite-difference analogue. Consequently, the Gauss-Seidel method (Appendix I) is employed on the analogue of (3.24) and the Newton-Raphson technique (Appendix II) is

used on (3.25). This algorithm is completely analogous to that applied in Section 3.4 to the warping-function equations.

The iteration begins with assumed initial solutions for $\psi(i,j)$ and $\Phi(i,j)$. These are subsequently corrected by successive sweeps through the mesh. The values of $\psi_{m+1}(i,j)$ for the $(m+1)^{th}$ sweep are given by

$$\psi_{m+1}(i,j) = \psi_m(i,j) + \omega[\bar{\psi}_{m+1}(i,j) - \psi_m(i,j)], \quad (3.27)$$

where

$$\bar{\psi}_{m+1}(i,j) = [\psi_m(i+1,j) + \psi_m(i,j+1) + \psi_{m+1}(i-1,j) + \psi_{m+1}(i,j-1) + E_{m+1}]/4, \quad (3.28)$$

and

$$E_{m+1} = \Big\{[\Phi_m(i+1,j) - \Phi_{m+1}(i-1,j)][\psi_m(i+1,j) - \psi_{m+1}(i-1,j)] + [\Phi_m(i,j+1) - \Phi_{m+1}(i,j-1)][\psi_m(i,j+1) - \psi_{m+1}(i,j-1)] + 8\Theta h^2\Big\}/4\Phi_m(i,j). \quad (3.29)$$

During the same sweep, the values of $\Phi_{m+1}(i,j)$ are calculated according to the Newton-Raphson iteration,

$$\Phi_{m+1}(i,j) = \Phi_m(i,j) - \frac{\Phi_m^{2n}(i,j)[\Phi_m(i,j) - 1] - S_{m+1}^n}{\Phi_m^{2n-1}(i,j)[(2n+1)\Phi_m(i,j) - 2n]}, \quad (3.30)$$

where S_{m+1} is the difference representation of

$$S = 3\Theta^2\mu^2 y^2 + \Phi^2[\psi_x^2 + \psi_y^2] \quad .$$

The iterations are continued until

$$\text{Max} \left| \psi_{m+1}(i,j) - \psi_m(i,j) \right| < \varepsilon, \tag{3.31}$$

with a preassigned convergence parameter ε, where the maximum is taken over all mesh points.

The algorithm for the deformation-theory stress-function formulation proceeds in a manner identical to that for the warping function in Section 3.4. Thus, the computations are initiated at Θ equal to $\Delta\Theta$ and Θ is incremented until the desired stresses and stress resultants are obtained for a given range of Θ.

The normalized stresses are calculated by the difference analogues of the first equation of (2.57) and Equations (2.14). These difference representations are, respectively,

$$\begin{aligned}
\frac{\sigma_{zz}(i,j)}{\sqrt{3}k} &= \frac{\sqrt{3}\Theta\mu y}{\Phi(i,j)} \\
\frac{\sigma_{xz}(i,j)}{k} &= \frac{\psi(i,j+1) - \psi(i,j-1)}{2h} \\
\frac{\sigma_{yz}(i,j)}{k} &= -\frac{\psi(i+1,j) - \psi(i-1,j)}{2h}.
\end{aligned} \tag{3.32}$$

For the stress-function formulation, the torque is calculated directly from the stress-function $\psi(x,y)$. From the last equation of (3.14), the normalized torque is

$$t_n = \frac{1}{T_o} \iint (x\sigma_{yz} - y\sigma_{xz})dxdy. \tag{3.33}$$

Introducing ψ_x and ψ_y from (2.14) yields

$$t_n = \frac{1}{T_o} \left[- \iint y\psi_y dxdy - \iint x\psi_x dxdy \right]. \tag{3.34}$$

The integrals of (3.34) are integrated by parts, and since $\psi = 0$ on the boundary, the expression for t_n becomes

$$t_n = \frac{2}{T_o} \iint \psi dxdy. \tag{3.35}$$

The normalized bending moment is calculated by

$$m_n = \frac{1}{M_o} \iint y\sigma_{zz} dxdy. \tag{3.36}$$

Numerical integration of (3.35) and (3.36) is performed through Simpson's $\frac{1}{3}$ rule according to (3.7).

The computations for the stress-function system of equations are furnished by the FORTRAN program STRO. The sequential flow chart for the program is given in Appendix III, Figure 19, and the FORTRAN listing in Appendix IV.

3.6 Warping-Function Equations for Work-Hardening Generalized J_2 Flow Theory

The warping-rate function $F(x,y,\theta)$ depends not only on the spatial coordinates, x and y, but also on the time-like variable θ. Thus, the difference analogue of the function must be described by three integers i, j, ℓ, where

$$x = (i-1)h$$

$$y = (j-1)h \tag{3.37}$$

$$\theta = \ell \Delta\theta .$$

Using the backward difference quotient (3.6) for $\dot{\sigma}_{zz}$, $\dot{\sigma}_{xz}$, $\dot{\sigma}_{yz}$, but not for $\dot{\lambda}$, and denoting

$$\sigma'_{zz} = \frac{\sigma_{zz}}{\sqrt{3}k}, \quad \sigma'_{xz} = \frac{\sigma_{xz}}{k}, \quad \sigma'_{yz} = \frac{\sigma_{yz}}{k}$$

and $\Theta = \frac{G}{k}\theta$, the stresses at the level $\Theta = \ell \Delta\Theta$, according to (2.76), are

$$\sigma'_{zz}(\ell) = \frac{\sqrt{3}\Delta\Theta \dot{\kappa} y + \sigma'_{zz}(\ell-1)}{\Lambda(\ell)}$$

$$\sigma'_{xz}(\ell) = \frac{\Delta\Theta(F_x - y) + \sigma'_{xz}(\ell-1)}{\Lambda(\ell)} \tag{3.38}$$

$$\sigma'_{yz}(\ell) = \frac{\Delta\Theta(F_y + x) + \sigma'_{yz}(\ell-1)}{\Lambda(\ell)},$$

where

$$\Lambda(\ell) = 1 + \Delta \dot{\lambda}(\ell).$$

The quantity $\dot{\lambda}(\ell)$ is obtained from the backwards difference representation of (2.72). Hence,

$$\Lambda(\ell) = 1 + \frac{2n+1}{2} J_2^{n-1}(\ell)[J_2(\ell) - J_2(\ell-1)], \tag{3.39}$$

where $J_2(\ell)$ is the normalized second invariant of stress at the $\ell\Delta\Theta$ level.

For convenience, the notation,

$$T = \Delta\Theta F, \tag{3.40}$$

is introduced. The shear stresses of (3.38) are substituted into the equilibrium Equation (2.77) to give

$$\frac{\partial}{\partial x}\left[\frac{\frac{\partial T}{\partial x} - \Delta\Theta y + \sigma'_{xz}(\ell-1)}{\Lambda(\ell)}\right] + \frac{\partial}{\partial y}\left[\frac{\frac{\partial T}{\partial y} + \Delta\Theta x + \sigma'_{yz}(\ell-1)}{\Lambda(\ell)}\right] = 0, \tag{3.41}$$

which after differentiation and simplification becomes

$$\Lambda(\ell)\left[\frac{\partial^2 T}{\partial x^2} + \frac{\partial^2 T}{\partial y^2}\right] - \Lambda_x(\ell)\left[\frac{\partial T}{\partial x} - \Delta\Theta y + \sigma'_{xz}(\ell-1)\right] - \Lambda_y(\ell)\left[\frac{\partial T}{\partial y} + \Delta\Theta x + \sigma'_{yz}(\ell-1)\right] + \Lambda(\ell)\left[\frac{\partial \sigma'_{xz}(\ell-1)}{\partial x} + \frac{\partial \sigma'_{yz}(\ell-1)}{\partial y}\right] = 0. \tag{3.42}$$

The unknown function $\Lambda(\ell)$ is obtained from Equation (3.39).

The boundary condition (2.9) takes the form

$$\left[\frac{\partial T}{\partial x} - \Delta\Theta y + \sigma'_{xz}(\ell - 1)\right] dy$$

$$+ \left[\frac{\partial T}{\partial y} + \Delta\Theta x + \sigma'_{yz}(\ell - 1)\right] dx = 0. \qquad (3.43)$$

For a unit square cross section, Equation (3.43) and the anti-symmetry properties of Section 3.1 imply

$$T_x = \Delta\Theta y \quad \text{if} \quad x = 0.5$$

$$T_y = -\Delta\Theta x \quad \text{if} \quad y = 0.5 \qquad (3.44)$$

$$T = 0 \quad \text{if} \quad x = 0 \quad \text{or} \quad y = 0.$$

In Equation (3.44), the conditions

$$\sigma'_{xz}(\ell - 1) = 0 \quad \text{if} \quad x = 0.5$$

and

$$\sigma'_{yz}(\ell - 1) = 0 \quad \text{if} \quad y = 0.5$$

have been used.

The three equations, (3.42), (3.39), and (3.43), represent a discrete system in terms of the Θ variable and a continuous system in terms of the spatial variables

x and y. In addition, the entire system represents an initial value problem, requiring the additional condition that the solution is known for Θ equal zero.

These equations now represent a system which is discrete in the time-like variable Θ and continuous in the spatial variables x and y. At each discrete level of Θ, the system may be considered as a continuous system very similar to the continuous system given for the deformation theory (Section 3.4). The solution to this system at a given Θ level will be somewhat equivalent to the solution of the deformation system. Since, in general, the solution is required for a range of Θ, the two systems may be solved by similar algorithms, which will depend on incrementing $\Delta\Theta$. This formulation, through the backwards difference on the Θ variable, yields a system of flow-theory equations which are essentially like the counterpart deformation-theory equations, and are solvable through numerical calculations of comparable difficulty.

The technique for solving this system of equations is very similar to that used in the case of deformation theory. However, now not only the iteration but also the solution to the system at the $\ell\Delta\Theta$ level depends on the solution at the previous level.

If the solution is known at the previous level, then the continuous equations at the present level take

the form,

$$T_{xx} + T_{yy} + E(T_x, T_y, x, y) = 0, \tag{3.45}$$

where

$$E = -\frac{\Lambda_x(\ell)}{\Lambda(\ell)}\left[\frac{\partial T}{\partial x} - \Delta\Theta y + \sigma'_{xz}(\ell-1)\right] - \frac{\Lambda_y(\ell)}{\Lambda(\ell)}\left[\frac{\partial T}{\partial y} + \Delta\Theta x + \sigma'_{yz}(\ell-1)\right] + \frac{\partial\sigma'_{xz}(\ell-1)}{\partial x} + \frac{\partial\sigma'_{yz}(\ell-1)}{\partial y}.$$

The variable $\Lambda(\ell)$ is obtained from the $(2n+1)^{th}$ degree polynomial

$$\Lambda^{2n+1}(\ell) - \Lambda^{2n}(\ell) - K(\ell) = 0, \tag{3.46}$$

where

$$K(\ell) = \frac{2n+1}{2} S^{n-1}(\ell)[S(\ell) - \Lambda^2(\ell)J_2(\ell-1)], \tag{3.47}$$

and the parameter $S(\ell)$ is given by

$$S(\ell) = \left[\sqrt{3}\,\Delta\Theta\dot{\kappa}\,y + \sigma'_{zz}(\ell-1)\right]^2 + \left[\frac{\partial T}{\partial x} - \Delta\Theta y + \sigma'_{xz}(\ell-1)\right]^2 + \left[\frac{\partial T}{\partial y} + \Delta\Theta x + \sigma'_{yz}(\ell-1)\right]^2.$$

At a given Θ level, Equations (3.45) and (3.46) are treated as two simultaneous equations in the unknown functions $T(x,y,\ell)$ and $\Lambda(x,y,\ell)$. Each is represented

by its corresponding difference analogue, and simultaneously (3.45) is solved as a non-linear Poisson equation (Appendix I) and (3.46) as a $(2n+1)^{th}$ degree polynomial (Appendix II).

To begin the iteration, initial solutions for $T(i,j,\ell)$ and $\Lambda(i,j,\ell)$ are assumed to be the final solutions at the previous level. These values are corrected by successive sweeps through the mesh. The values $T_{m+1}(i,j,\ell)$ for the $(m+1)^{th}$ sweep are furnished by

$$T_{m+1}(i,j,\ell) = T_m(i,j,\ell) + \omega[\bar{T}_{m+1}(i,j,\ell) - T_m(i,j,\ell)], \tag{3.48}$$

where

$$\bar{T}_{m+1}(i,j,\ell) = [T_m(i+1,j,\ell) + T_m(i,j+1,\ell)$$

$$+ T_{m+1}(i-1,j,\ell) + T_{m+1}(i,j-1,\ell) - E_{m+1}]/4, \tag{3.49}$$

and

$$E_{m+1} = \left[\left\{[\Lambda_m(i+1,j,\ell) - \Lambda_{m+1}(i-1,j,\ell)][T_m(i+1,j,\ell) - T_{m+1}(i-1,j,\ell) - 2h\Delta\Theta y + 2h\sigma'_{xz}(\ell-1)] + [\Lambda_m(i,j+1,\ell) - \Lambda_{m+1}(i,j-1,\ell)][T_m(i,j+1,\ell) - T_{m+1}(i,j-1,\ell) + 2h\Delta\Theta x + 2h\sigma'_{yz}(\ell-1)]\right\}/4\Lambda_m(i,j,\ell)\right] - 2h[\sigma'_{xz}(i+1,j,\ell-1) - \sigma'_{xz}(i-1,j,\ell-1) + \sigma'_{yz}(i,j+1,\ell-1) - \sigma'_{yz}(i,j-1,\ell-1)].$$

At the boundaries, the constraints of Equations (3.44) are incorporated into the above equations.

During the same sweep, the values $\Lambda_{m+1}(i,j,\ell)$ are calculated by the Newton-Raphson iteration. Thus,

$$\Lambda_{m+1}(i,j,\ell) = \Lambda_m(i,j,\ell) - \frac{\Lambda_m^{2n}(i,j,\ell)[\Lambda_m(i,j,\ell) - 1] - K_{m+1}}{\Lambda_m^{2n-1}(i,j,\ell)[(2n+1)\Lambda_m(i,j,\ell) - 2n]} \quad (3.50)$$

where K_{m+1} is the difference analogue of (3.47).

Experience indicates that a one-to-one correspondence between the number of iterations for the Gauss-Seidel and Newton-Raphson methods is not sufficient to give general convergence. Thus, at each point an additional convergence requirement is placed on the Newton-Raphson iteration of $\Lambda_{m+1}(i,j,\ell)$.

Temporarily, the notation $\Lambda_{m+1,n}(i,j,\ell)$ is introduced. At each point in the mesh the Newton-Raphson iteration is continued on $\Lambda_{m+1,n}(i,j,\ell)$ until

$$\left|\Lambda_{m+1,n}(i,j,\ell) - \Lambda_{m+1,n-1}(i,j,\ell)\right| < \varepsilon_1, \quad (3.51)$$

for a preassigned convergence parameter ε_1, at that particular point.

It is worth noting that the primary difference between the flow-theory calculation and deformation-theory

calculation (Section 3.4) is this additional iteration. From a computer standpoint, these additional calculations represented a very small difference in the two solutions for the combined bending and torsion problem.

After inequality (3.51) is satisfied, the $(m+1)^{th}$ sweep is continued. The number of sweeps are continued until

$$\text{Max} \left| T_{m+1}(i,j,\ell) - T_m(i,j,\ell) \right| < \varepsilon, \qquad (3.52)$$

for a preassigned convergence parameter ε, where the maximum is taken over all mesh points.

As in the deformation-theory solution, the computations are begun for the undeformed bar. However, in flow theory a particular path for the forward integration is prescribed. The iteration at any level takes the previous solution as an initial estimate and iterations are continued until condition (3.52) is satisfied.

To better illustrate the method of solution, the curvature K and unit angle of twist θ space is considered (Figure 6).

Any point (K, θ) in this space may be reached by any number of paths p_1, p_2, p_3, etc. The only restriction is that θ be a monotonically increasing function. Specification of $dK/d\theta$ as a function of θ, with the initial condition, $K = 0$ when $\theta = 0$, defines the load path.

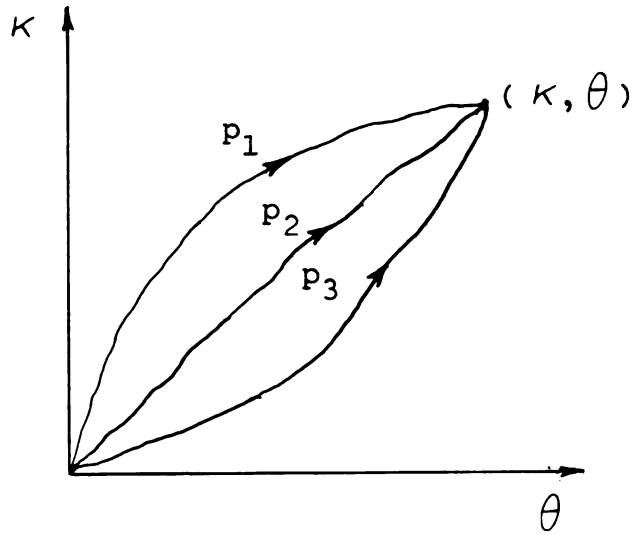

Figure 6. Arbitrary integration paths for a given deformation (κ, θ)

Experience indicates that if $\Delta\Theta$ is kept small enough the method will converge at each level of Θ, in a manner analogous to that of deformation theory. However, in flow theory an additional reason for keeping $\Delta\Theta$ small is that according to the difference representation, the error in the forward integration is of order $\Delta\Theta$.

At each level, the normalized stresses are calculated by

$$\sigma'_{zz}(i,j,\ell) = \frac{\sqrt{3}\Delta\Theta\dot{\kappa}y + \sigma'_{zz}(i,j,\ell-1)}{\Lambda(i,j,\ell)} \tag{3.53}$$

$$\sigma'_{xz}(i,j,\ell) = \frac{\frac{T(i+1,j,\ell)-T(i-1,j,\ell)}{2h} - \Delta\Theta y + \sigma'_{xz}(i,j,\ell-1)}{\Lambda(i,j,\ell)}$$

$$\sigma'_{yz}(i,j,\ell) = \frac{\frac{T(i,j+1,\ell)-T(i,j-1,\ell)}{2h} + \Delta\Theta x + \sigma'_{yz}(i,j,\ell-1)}{\Lambda(i,j,\ell)}.$$

The normalized bending moments and torque are determined by substitution of (3.53) into (3.14) and carrying out the integration by Simpson's $\frac{1}{3}$ rule.

The computations for this system of equations are furnished by a FORTRAN program WARPLV. The flow chart and FORTRAN listing of WARPLV are shown in Appendix III, Figure 20, and Appendix IV, respectively.

3.7 Stress-Function Equations for Work-Hardening Generalized J_2 Flow Theory

In flow theory, the stress-function $\psi(x,y,\theta)$ is a function of the three variables x, y, and θ. The difference analogue is represented by the integers i, j, and ℓ as defined by (3.37).

Through application of the backwards difference on θ, in the same manner as in Section 3.6, Equation (2.81) becomes

$$\Lambda(\ell)[\psi_{xx}(\ell) + \psi_{yy}(\ell)] + \Lambda_x(\ell)\psi_x(\ell) + \Lambda_y(\ell)\psi_y(\ell)$$

$$+ 2\Delta\Theta - \psi_{xx}(\ell-1) - \psi_{yy}(\ell-1) = 0, \qquad (3.54)$$

where $\Lambda(\ell)$ is again defined by (3.39). But the normalized second stress invariant $J_2(\ell)$ is now given by

$$J_2(\ell) = \left[\frac{\sqrt{3}\Delta\Theta\dot{\kappa}y + \sigma'_{zz}(\ell-1)}{\Lambda(\ell)}\right]^2 + \psi_x^2(\ell) + \psi_y^2(\ell). \qquad (3.55)$$

Equation (3.54) is expressed as the non-linear Poisson equation,

$$\psi_{xx}(\ell) + \psi_{yy}(\ell) + E(\psi_x, \psi_y, x, y) = 0, \qquad (3.56)$$

where

$$E = [\Lambda_x(\ell)\psi_x(\ell) + \Lambda_y(\ell)\psi_y(\ell) + 2\Delta\Theta - \psi_{xx}(\ell-1)$$

$$- \psi_{yy}(\ell-1)]/\Lambda(\ell).$$

The function $\Lambda(\ell)$ is obtained from the $(2n+1)^{th}$ degree polynomial,

$$\Lambda^{2n+1}(\ell) - \Lambda^{2n}(\ell) - K(\ell) = 0, \qquad (3.57)$$

where

$$K(\ell) = \frac{2n+1}{2} S^{n-1}(\ell)[S(\ell) - \Lambda^2(\ell)J_2(\ell-1)], \qquad (3.58)$$

and the parameter $S(\ell)$ is provided by

$$S(\ell) = [\sqrt{3}\Delta\Theta\dot{\kappa}y + \sigma'_{zz}(\ell-1)]^2$$

$$+ \Lambda^2(\ell)[\psi_x^2(\ell) + \psi_y^2(\ell)]. \qquad (3.59)$$

Since the stress function ψ is still defined by (2.14), the boundary conditions on ψ given by (3.26) are valid for any level of Θ. The condition of the unstressed bar, ψ identically zero throughout the cross section, is assumed as the initial condition at Θ equal zero.

Equations (3.56) and (3.57) are represented by their discrete analogues and solved simultaneously by an algorithm identical to that employed in Section 3.6.

At a given level $\ell\Delta\Theta$, the values $\psi_{m+1}(i,j,\ell)$ for the $(m+1)^{th}$ sweep are furnished by the Gauss-Seidel over-relaxation (Appendix I),

$$\psi_{m+1}(i,j,\ell) = \psi_m(i,j,\ell) + \omega[\bar{\psi}_{m+1}(i,j,\ell) - \psi_m(i,j,\ell)], \qquad (3.60)$$

where

$$\bar{\psi}_{m+1}(i,j,\ell) = [\psi_m(i+1,j,\ell) + \psi_m(i,j+1,\ell)$$

$$+ \psi_{m+1}(i-1,j,\ell) + \psi_{m+1}(i,j-1,\ell) + E_{m+1}]/4, \qquad (3.61)$$

and

$$E_{m+1} = \Big| [\Lambda_m(i+1,j,\ell) - \Lambda_{m+1}(i-1,j,\ell)][\psi_m(i+1,j,\ell) - \psi_{m+1}(i-1,j,\ell)] + [\Lambda_m(i,j+1,\ell) - \Lambda_{m+1}(i,j-1,\ell)] [\psi_m(i,j+1,\ell) - \psi_{m+1}(i,j-1,\ell)] + 8\Delta\Theta h^2 + 4[\psi(i+1,j,\ell-1) + \psi(i,j+1,\ell-1) + \psi(i-1,j,\ell-1) + \psi(i,j-1,\ell-1) - 4\psi(i,j,\ell-1)\Big| / 4\Lambda_m(i,j,\ell).$$

At the boundaries, the constraints of Equations (3.26) are incorporated into the above equations.

During the same sweep, the values $\Lambda_{m+1}(i,j,\ell)$ are calculated by the Newton-Raphson iteration (Appendix II),

$$\Lambda_{m+1}(i,j,\ell) = \Lambda_m(i,j,\ell) - \frac{\Lambda_m^{2n}(i,j,\ell)[\Lambda_m(i,j,\ell) - 1] - K_{m+1}}{\Lambda_m^{2n-1}(i,j,\ell)[(2n+1)\Lambda_m(i,j,\ell) - 2n]}, \quad (3.62)$$

where K_{m+1} is the difference analogue of (3.58).

Again, an inner iteration is performed on $\Lambda_{m+1}(i,j,\ell)$ at each spatial point, until condition (3.51) is satisfied. The $(m+1)^{th}$ sweep is then continued. The sweeps are continued until

$$\text{Max} \left| \psi_{m+1}(i,j,\ell) - \psi_m(i,j,\ell) \right| < \varepsilon, \quad (3.63)$$

for a preassigned convergence parameter ε, where the maximum is taken over all mesh points.

As in Section 3.6, a load path is specified in the curvature-twist space. This specification indicates the dependency of the stresses and stress resultants on the load history.

At each level, the normalized stresses are determined

$$\sigma'_{zz}(i,j,\ell) = \frac{\sqrt{3}\Delta\Theta\,\dot{\kappa}\,y + \sigma'_{zz}(i,j,\ell-1)}{\Lambda(i,j,\ell)}$$

$$\sigma'_{xz}(i,j,\ell) = \frac{\Psi(i,j+1,\ell) - \Psi(i,j-1,\ell)}{2h} \qquad (3.64)$$

$$\sigma'_{yz}(i,j,\ell) = -\frac{\Psi(i+1,j,\ell) - \Psi(i-1,j,\ell)}{2h}.$$

The normalized torque and bending moment are obtained by substitution of the above results into Equations (3.35) and (3.36). These integrals are evaluated by Simpson's $\frac{1}{3}$ rule, (3.7).

The computations for this system of equations are performed by a FORTRAN program STPLDT. The flow chart and FORTRAN listing of STPLDT are presented in Appendix III, Figure 21, and Appendix IV, respectively.

The numerical results for the unit square bar calculations are given in Chapter V. In order to demonstrate the feasibility of applying this technique to other

coordinate systems, a circular bar of unit radius is considered in Chapter IV, using polar coordinates.

IV. NUMERICAL SOLUTION FOR A CIRCULAR BAR OF UNIT RADIUS

4.1 Transformation of Equations to Polar Coordinates

A point P, defined by the polar-coordinates (r,α), may be transformed into rectangular coordinate (x,y) through equations

$$x = r \cos \alpha \quad \text{and} \quad y = r \sin \alpha. \tag{4.1}$$

The inverse form of relations (4.1) is

$$r = (x^2 + y^2)^{1/2} \quad \text{and} \quad \alpha = \arctan \frac{y}{x}. \tag{4.2}$$

If u is a function of r and α, then according to the chain rule and the inverse relations (4.2), the rectangular coordinate derivatives are determined by the following formulas:

$$\begin{aligned} \frac{\partial u}{\partial x} &= \cos \alpha \frac{\partial u}{\partial r} - \frac{\sin \alpha}{r} \frac{\partial u}{\partial \alpha} \\ \frac{\partial u}{\partial y} &= \sin \alpha \frac{\partial u}{\partial r} + \frac{\cos \alpha}{r} \frac{\partial u}{\partial \alpha}. \end{aligned} \tag{4.3}$$

Similar expressions may be developed for the second derivatives $\partial^2 u / \partial x^2$, $\partial^2 u / \partial y^2$, and $\partial^2 u / \partial x \, \partial y$.

Substituting relations (4.3) into the Piechnik Equation (2.24) yields

$$3\mu^2 r^3 \sin^2\alpha(r^2 t_{rr} + r t_r + t_{\alpha\alpha}) + r t_{rr}(t_\alpha + r^2)^2$$

$$- 2t_r(r t_{r\alpha} - t_\alpha)(r^2 + t_\alpha) + r t_r^2(r t_r + t_{\alpha\alpha})$$

$$- 3\mu^2 r^3 \sin\alpha(r t_r \sin\alpha + t_\alpha \cos\alpha) - 3\mu^2 r^5 \sin\alpha\cos\alpha = 0. \tag{4.4}$$

From equation (2.18), the parameter φ given in terms of r and α is

$$\varphi_k = k\varphi = \frac{\theta}{2}\left[3\mu^2 r^2 \sin^2\alpha + t_r^2 + \left(\frac{t_\alpha}{r}\right)^2 + r^2 + 2t_\alpha\right]^{1/2}. \tag{4.5}$$

The non-zero stresses (2.13) are transformed to

$$\frac{\sigma_{zz}}{\sqrt{3k}} = \frac{\sqrt{3}\theta}{2\varphi_k}\mu r \sin\alpha$$

$$\frac{\sigma_{yz}}{k} = \frac{\theta}{2\varphi_k}\left(t_r \sin\alpha + t_\alpha \frac{\cos\alpha}{r} + r\cos\alpha\right) \tag{4.6}$$

$$\frac{\sigma_{xz}}{k} = \frac{\theta}{2\varphi_k}\left(t_r \cos\alpha - t_\alpha \frac{\sin\alpha}{r} - r\sin\alpha\right).$$

Equations (4.3) permit the deformation-theory Equations (2.62) and (2.63) to be transformed to their respective polar-coordinate representations. These equations become

$$\Phi\left(t_{rr} + \frac{1}{r}\,t_r + \frac{1}{r^2}\,t_{\alpha\alpha}\right) - \Phi_r t_r - \frac{\Phi_\alpha t_\alpha}{r^2} - \Phi_\alpha = 0, \tag{4.7}$$

and

$$\Phi^{2n+1} - \Phi^{2n} - S^n = 0, \tag{4.8}$$

where

$$S = \Theta^2\left[3\mu^2 r^2 \sin^2\alpha + t_r^2 + \left(\frac{t_\alpha}{r}\right)^2 + r^2 + 2t_\alpha\right]^2. \tag{4.9}$$

Equations (4.7) and (4.8) may be treated as two simultaneous equations for the unknown functions $t(r,\alpha)$ and $\Phi(r,\alpha)$.

The stresses are determined by the polar representation of Equations (2.57). These normalized stresses become

$$\frac{\sigma_{zz}}{\sqrt{3}k} = \frac{\sqrt{3}}{\Phi}\,\Theta\mu r \sin\alpha$$

$$\frac{\sigma_{yz}}{k} = \frac{\Theta}{\Phi}\left(t_r \sin\alpha + t_\alpha \frac{\cos\alpha}{r} + r\cos\alpha\right) \tag{4.10}$$

$$\frac{\sigma_{xz}}{k} = \frac{\Theta}{\Phi}\left(t_r \cos\alpha - t_\alpha \frac{\sin\alpha}{r} - r\sin\alpha\right).$$

The normalized bending moment and torque relations of (3.14) are transformed into their polar-coordinate

representation. That is,

$$m_n = \frac{1}{M_o} \int_A r \sin \alpha \, \sigma_{zz} dA$$

$$t_n = \frac{-1}{T_o} \int_A (r \sin \alpha \, \sigma_{xz} - r \cos \alpha \, \sigma_{yz}) dA \tag{4.11}$$

where dA is now given by $rd\alpha dr$.

The boundary conditions for both the Piechnik Equation (4.4) and the work-hardening deformation Equation (4.7) are given by the transformation of the general boundary condition (2.64). This equation may be expressed

$$(t_x - y) \frac{dy}{dS} - (t_y + x) \frac{dx}{dS} = 0. \tag{4.12}$$

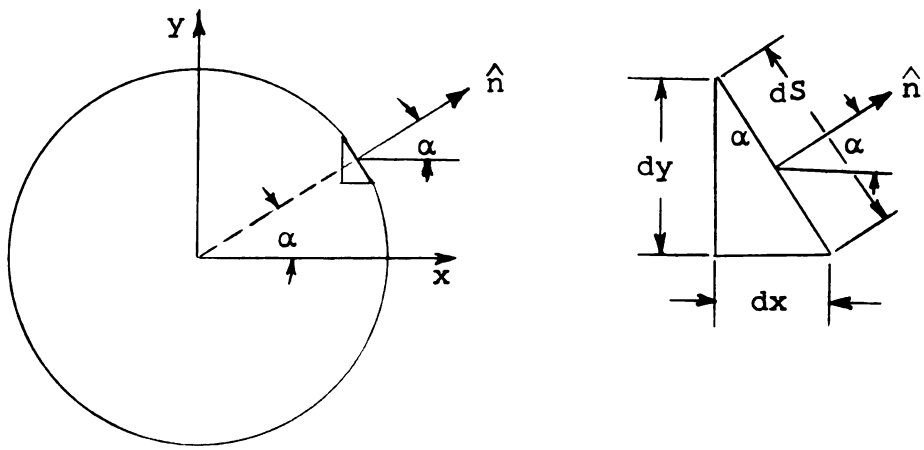

Figure 7. Relationship between unit normal direction cosines and coordinate angle

From Figure 7 the direction cosines are given by

$$\frac{dy}{ds} = \cos \alpha \qquad \text{and} \qquad \frac{dx}{ds} = -\sin \alpha,$$

and when x and y are on the surface of the unit circular cross section,

$$x = \cos \alpha \qquad \text{and} \qquad y = \sin \alpha.$$

Thus, (4.12) becomes

$$t_x \cos \alpha + t_y \sin \alpha = 0. \tag{4.13}$$

However, Equation (4.13) is recognized as the partial derivative of t with respect to r. Consequently, the general boundary condition (2.64) reduces to the following condition for the case of a unit circular cross section:

$$\frac{\partial t}{\partial r} = 0 \qquad \text{if} \qquad r = 1. \tag{4.14}$$

This boundary condition (4.14) is appropriate for both the rigid-perfectly plastic and the deformation-theory work-hardening formulations.

4.2 Polar-Coordinate Discretization and Finite-Difference Representation

A mesh of equally spaced concentric circles and radial lines is superimposed on the circular cross section (Figure 8). Again the symmetry arguments of Section 3.1 apply to the solution. Thus, in determining the solution,

only one-quarter of the cross section needs to be considered.

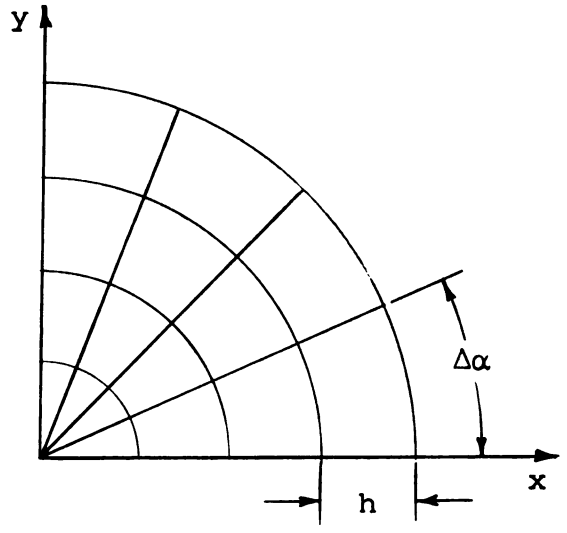

Figure 8. Lattice spacing for polar-coordinate mesh

Since the spacing between concentric circles is h and the angle between radial lines is $\Delta\alpha$, the values of r and α at each nodal point are given by

$$r = (i-1)h \qquad 1 \leq i \leq N$$
$$\alpha = (j-1)\Delta\alpha \qquad 1 \leq j \leq N. \tag{4.15}$$

The spatial derivatives of a function $g(r,\alpha)$ are represented by the following finite-difference operators:

a) first derivatives,

$$g_r = \frac{g(i+1,j) - g(i-1,j)}{2h}$$

$$g_\alpha = \frac{g(i,j+1) - g(i,j-1)}{2(\Delta\alpha)}, \tag{4.16}$$

b) second derivatives,

$$g_{rr} = \frac{g(i+1,j) - 2g(i,j) + g(i-1,j)}{h^2}$$

$$g_{\alpha\alpha} = \frac{g(i,j+1) - 2g(i,j) + g(i,j-1)}{(\Delta\alpha)^2}, \tag{4.17}$$

c) second mixed derivative,

$$g_{r\alpha} = \frac{g(i+1,j+1) - g(i-1,j+1) + g(i-1,j-1) - g(i+1,j-1)}{4h(\Delta\alpha)}. \tag{4.18}$$

The integral of the function $g(r,\alpha)$ over the region $(i-1)h \leq r \leq (i+1)h$ and $(j-1)r\Delta\alpha \leq r\alpha \leq (j+1)r\Delta\alpha$ is approximated by Simpson's $\frac{1}{3}$ rule for polar coordinates,

$$\iint g(r,\alpha)\,r\,d\alpha\,dr = \frac{(\Delta\alpha)hr(i)}{9}\Big[g(i+1,j+1) + g(i-1,j+1) + g(i+1,j-1) + g(i-1,j-1) + 4[g(i+1,j) + g(i,j+1) + g(i-1,j) + g(i,j-1)] + 16g(i,j)\Big]. \tag{4.19}$$

4.3 Piechnik Equation for Rigid-Perfectly Plastic Material

The polar-coordinate representation of the Piechnik Equation (4.4) is expressed as

$$At_{rr} + Bt_{r\alpha} + Ct_{\alpha\alpha} + Dt_r + Et_\alpha + F = 0, \quad (4.20)$$

where the coefficients are given by

$$A = 3\mu^2 r^5 \sin^2\alpha + r(t_\alpha + r^2)^2$$

$$B = -2rt_r(r^2 + t_\alpha)$$

$$C = 3\mu^2 r^3 \sin^2\alpha + rt_r^2$$

$$D = r^2 t_r^2$$

$$E = 2\,t_r(r^2 + t_\alpha) - 3\mu^2 r^3 \sin\alpha \cos\alpha$$

$$F = -3\mu^2 r^5 \sin\alpha \cos\alpha.$$

By virtue of the anti-symmetry property of $t(r,\alpha)$ and the boundary condition (4.14), the following conditions must be satisfied on the first quadrant of the unit circle:

$$\begin{aligned} &t = 0 \quad \text{if} \quad \alpha = 0 \quad \text{or} \quad \alpha = \frac{\pi}{2} \\ &t_r = 0 \quad \text{if} \quad r = 1. \end{aligned} \quad (4.21)$$

Equation (4.20) may be replaced by its respective finite-difference analogue. The Gauss-Seidel over-

relaxation procedure, outlined in Appendix I, applied to this system of algebraic equations, gives the numerical solution. Thus, the $t_{m+1}(i,j)$ for the $(m+1)^{th}$ sweep is given by

$$t_{m+1}(i,j) = t_m(i,j) + \omega[\bar{t}_{m+1}(i,j) - t_m(i,j)], \qquad (4.22)$$

where

$$\bar{t}_{m+1}(i,j) = \Big[(\bar{A}+\bar{D})t_m(i+1,j) + (\bar{A}-\bar{D})t_{m+1}(i-1,j)$$

$$+ (\bar{C}+\bar{E})t_m(i,j+1) + (\bar{C}-\bar{E})t_{m+1}(i,j-1) + \bar{B}[t_m(i+1,j+1)$$

$$-t_m(i+1,j-1) + t_{m+1}(i-1,j-1) - t_{m+1}(i-1,j+1)]$$

$$+ \bar{F}\Big] /[2(\bar{A}+\bar{C})], \qquad (4.23)$$

with the coefficients having been previously calculated according to

$$\bar{A} = (\Delta\alpha)^2 \left[3\mu^2 r^5 \sin^2\alpha + r\left(\frac{t_m(i+1,j) - t_{m+1}(i-1,j)}{2h} + r^2\right)^2\right],$$

$$\bar{B} = \frac{h(\Delta\alpha)r}{2}\left[\left(\frac{t_m(i+1,j) - t_{m+1}(i-1,j)}{2h}\right)\right.$$

$$\left.\left(r^2 + \frac{t_m(i,j+1) - t_{m+1}(i,j-1)}{2(\Delta\alpha)}\right)\right],$$

$$\bar{C} = h^2 \left[3\mu^2 r^3 \sin^2\alpha + r \left(\frac{t_m(i+1,j) - t_{m+1}(i-1,j)}{2h} \right)^2 \right],$$

$$\bar{D} = \frac{h(\Delta\alpha)^2 r^2}{2} \left(\frac{t_m(i+1,j) - t_{m+1}(i-1,j)}{2h} \right)^2,$$

$$\bar{E} = \frac{h^2(\Delta\alpha)}{2} \left[2 \left(\frac{t_m(i+1,j) - t_{m+1}(i-1,j)}{2h} \right) \right.$$

$$\left. \left(r^2 + \frac{t_m(i,j+1) - t_{m+1}(i,j-1)}{2(\Delta\alpha)} \right) + 3\mu^2 r^3 \sin\alpha \cos\alpha \right],$$

$$\bar{F} = -h^2(\Delta\alpha)^2(3\mu^2 r^5 \sin\alpha \cos\alpha).$$

The iterations are continued until the condition,

$$\text{Max} \left| t_{m+1}(i,j) - t_m(i,j) \right| < \varepsilon, \qquad (4.24)$$

is satisfied for a preassigned ε, where the maximum is taken over all nodal points.

The normalized stresses are calculated from the discrete analogues of (4.6). The normalized bending moment may then be obtained by successively applying Simpson's $\frac{1}{3}$ rule (4.18) to Equations (4.11). The computations for this system of equations are performed by the FORTRAN program POLARR. The flow chart and FORTRAN listing for POLARR are shown in Appendix III, Figure 22, and Appendix IV, respectively.

4.4 Warping-Function Equation for Work-Hardening Generalized J_2 Deformation Theory

Equation (4.7) is treated as a non-linear Poisson equation expressed in polar coordinates. That is,

$$t_{rr} + \frac{1}{r} t_r + \frac{1}{r^2} t_{\alpha\alpha} + E(t_r, t_\alpha, r, \alpha) = 0, \tag{4.25}$$

where

$$E = \frac{-\Phi_r t_r - \frac{\Phi_\alpha t_\alpha}{r^2} - \Phi_\alpha}{\Phi},$$

and Φ is obtained from the $(2n+1)^{th}$ degree polynomial,

$$\Phi^{2n+1} - \Phi^{2n} - \left[\Theta^2 \left(3\mu^2 r^2 \sin^2\alpha + t_r^2 \right. \right.$$

$$\left. \left. + \left(\frac{t_\alpha}{r} \right)^2 + r^2 + 2t_\alpha \right)^2 \right]^n = 0. \tag{4.26}$$

Equations (4.25) and (4.26) may be considered as two simultaneous equations for the unknown functions $t(r,\alpha)$ and $\Phi(r,\alpha)$. In addition, the function $t(r,\alpha)$ must satisfy the boundary conditions,

$$\begin{aligned} t &= 0 \quad \text{if} \quad \alpha = 0 \quad \text{or} \quad \alpha = \frac{\pi}{2} \\ t_r &= 0 \quad \text{if} \quad r = 1. \end{aligned} \tag{4.27}$$

Each of the simultaneous equations may be represented by its respective finite-difference analogue. Applying the Gauss-Seidel and the Newton-Raphson methods to these difference analogues yields the following sequence for correcting the initially assumed values for $t(i,j)$ and $\Phi(i,j)$. During the $(m+1)^{th}$ sweep, the values $t_{m+1}(i,j)$ are calculated by

$$t_{m+1}(i,j) = t_m(i,j) + \omega[\bar{t}_{m+1}(i,j) - t_m(i,j)], \tag{4.28}$$

where $\bar{t}_{m+1}(i,j)$ is given by

$$\bar{t}_{m+1}(i,j) = \Big[(\bar{A}+\bar{D})t_m(i+1,j) + (\bar{A}-\bar{D})t_{m+1}(i-1,j) + \bar{C}[t_m(i,j+1) + t_{m+1}(i,j-1)] - E_{m+1}\Big]/[2(\bar{A}+\bar{C})]. \tag{4.29}$$

The coefficients are determined according to

$$\begin{aligned}
\bar{A} &= (\Delta\alpha)^2 r^2 \\
\bar{C} &= h^2 \\
\bar{D} &= \frac{h(\Delta\alpha)^2 r}{2} \\
E_{m+1} &= \frac{h^2(\Delta\alpha)^2 r^2}{\Phi_m(i,j)}\left[\left(\frac{\Phi_m(i+1,j) - \Phi_{m+1}(i-1,j)}{2h}\right)\right. \\
&\left.\left(\frac{t_m(i+1,j) - t_{m+1}(i-1,j)}{2h}\right) + \left(\frac{\Phi_m(i,j+1) - \Phi_{m+1}(i,j-1)}{2(\Delta\alpha)}\right)\right. \\
&\left.\left(\frac{t_m(i,j+1) - t_{m+1}(i,j-1)}{2(\Delta\alpha)r^2} - 1\right)\right].
\end{aligned} \tag{4.30}$$

Furthermore, the corrected values of $\Phi_{m+1}(i,j)$ are calculated during this sweep according to

$$\Phi_{m+1}(i,j) = \Phi_m(i,j) - \frac{\Phi_m^{2n}(i,j)[\Phi_m(i,j) - 1] - S_{m+1}^n}{\Phi_m^{2n-1}(i,j)[(2n+1)\Phi_m(i,j) - 2n]}, \tag{4.31}$$

where the parameter S_{m+1} is given by the $(m+1)^{th}$ discrete representation of S in Equation (4.9).

The sweeps continue until

$$\text{Max} \left| t_{m+1}(i,j) - t_m(i,j) \right| < \varepsilon, \tag{4.32}$$

for a preassigned convergence parameter ε, where the maximum is taken over all nodal points.

The normalized stresses may now be obtained from the difference analogues of (4.10). As a result of Equations (4.11), these stresses determine the normalized stress resultants.

The calculations for this system of equations are performed by the FORTRAN program POLARO. The flow chart and FORTRAN listing in POLARO are shown in Appendix III, Figure 23, and Appendix IV, respectively.

The polar-coordinate solution was developed only for these two cases. However, due to the similarity between the algorithms for the deformation and flow theories in the case of a square bar, it is believed that a similar polar-coordinate algorithm could be developed

for flow theory. The purpose here is to demonstrate the feasibility of the technique applied to circular geometry rather than to compare the two theories.

V. RESULTS AND DISCUSSION

5.1 Effect of Mesh Refinement

Steele [30] observed, in his numerical solution of the Hill-Handelman equation, that a 9 x 9 mesh on the entire unit square cross section provides torque and moment values which vary by less than 0.5 per cent from those for a 13 x 13 mesh. Thus, assuming the finite-difference solution converges to the continuous solution as the lattice spacing approaches zero, the normalized torque and moment provided by the 9 x 9 mesh appear to be valid to at least two decimal places.

The present investigation utilizes a 12 x 12 cross-sectional mesh. As a consequence of the symmetry properties, the solution must be obtained for only a 7 x 7 set of lattice points or 49 discrete points. In order to estimate the effect of grid size, the number of grid spacings was doubled. This latter system, a 24 x 24 mesh, requires the determination of the solution for a 13 x 13 set of lattice points or 169 discrete points. Two solutions were obtained for the Piechnik rigid-perfectly plastic equation with N = 13. A comparison between the normalized torques and bending moments for the two mesh sizes is shown in Table 1.

Table 1. Effect of mesh refinement on normalized torque and moment (calculations at N x N points)

N	μ^2	t_n	m_n	Per cent difference Δt_n	Per cent difference Δm_n
7	0.333	0.8294	0.6388		
13	0.333	0.8350	0.6370	+0.67	-0.28
7	1.333	0.6417	0.8230		
13	1.333	0.6452	0.8188	+0.54	-0.51

The results of Table 1 indicate that the actual error in the torque and moment would tend to cause disagreement in the third decimal place. Thus, with the 49 discrete point solution, at least two place accuracy is assumed in the normalized torques and bending moments.

The variations in stresses for the above calculation on the Piechnik equation are presented in Table 5 of Appendix V. The stress results tend to show a difference in the second decimal place.

Greenberg, Dorn, and Wetherell [6], in their numerical solution to the plastic torsion problem, used an 8 x 8 mesh on one quadrant of the cross section. With this mesh size, a solution is required for 81 discrete points, and accuracy of the calculated torques was assumed to be valid to three decimal places.

Using N = 13, μ = 1.00, and n = 12, computer runs were performed for both the deformation-theory and the flow-theory warping-function equations. With each run,

the difference between the normalized torques and bending moments for N = 13 and those for N = 7 was of the same order as that shown for the Piechnik equation in Table 1.

In view of the large number of calculations required for the combined bending and torsion problem, and since the major emphasis of this study is confined to the torque and moment relationships, the remaining calculations use a discrete system of 49 points on the first quadrant of the cross section. The comparisons between calculated stresses and stress resultants according to different theories assume the numerical accuracy of the order presented in the above discussion.

5.2 Effect of Over-Relaxation Factor and Choice of Convergence Parameter

In the case of linear second-order equations, formulas are available for selecting an optimum relaxation factor [32]. Generally, these formulas are dependent on the mesh size h and the geometric shape of the cross section. Apparently, formulas of this nature are not available for the non-linear cases.

Since most of the computer runs were for a system of 49 discrete points, various relaxation factors were considered in an experimental analysis. Data, showing the effect of the over-relaxation factor ω, was determined for the Piechnik equation, the warping-function equation, and the warping-rate function equation. This information is presented in Figures 9a, 9b, and 9c.

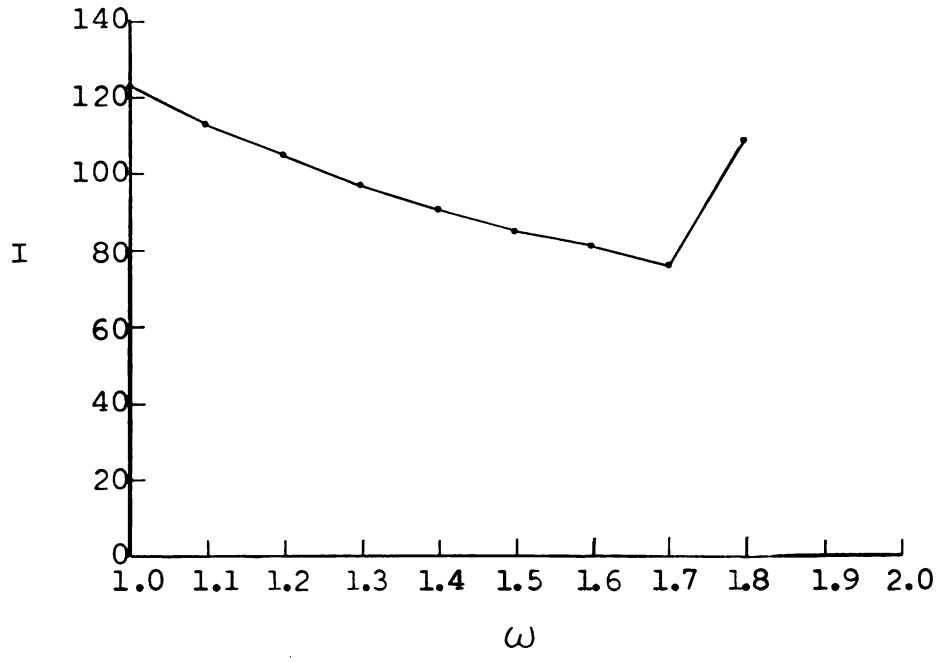

Figure 9a. Effect of relaxation factor ω on the number of iterations I for the Piechnik equation with N = 7 and μ = 1.00

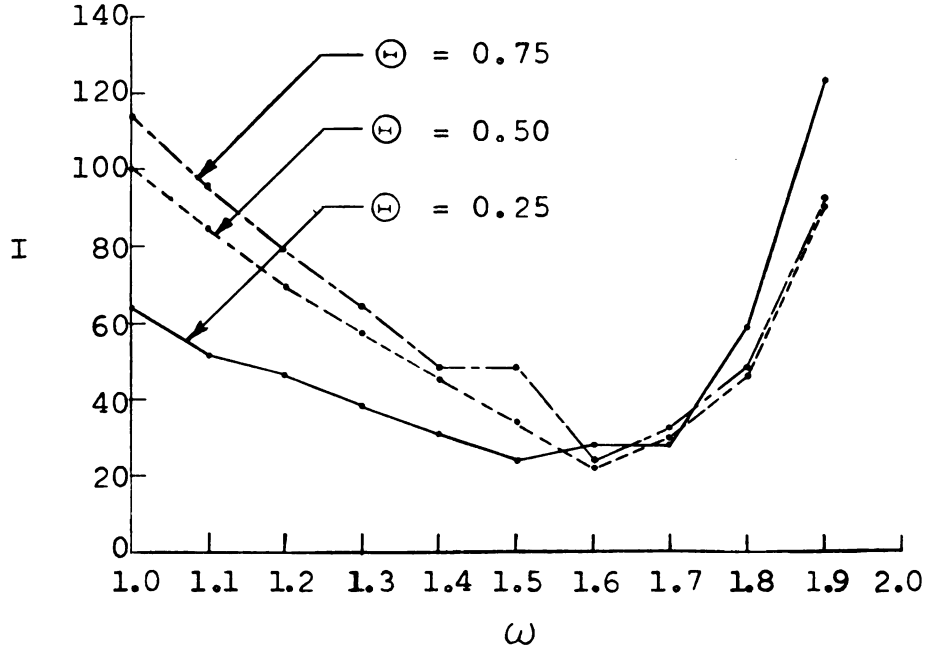

Figure 9b. Effect of relaxation factor ω on the number of iterations I for the warping-function deformation-theory equations with N = 7, μ = 1.00, and n = 2

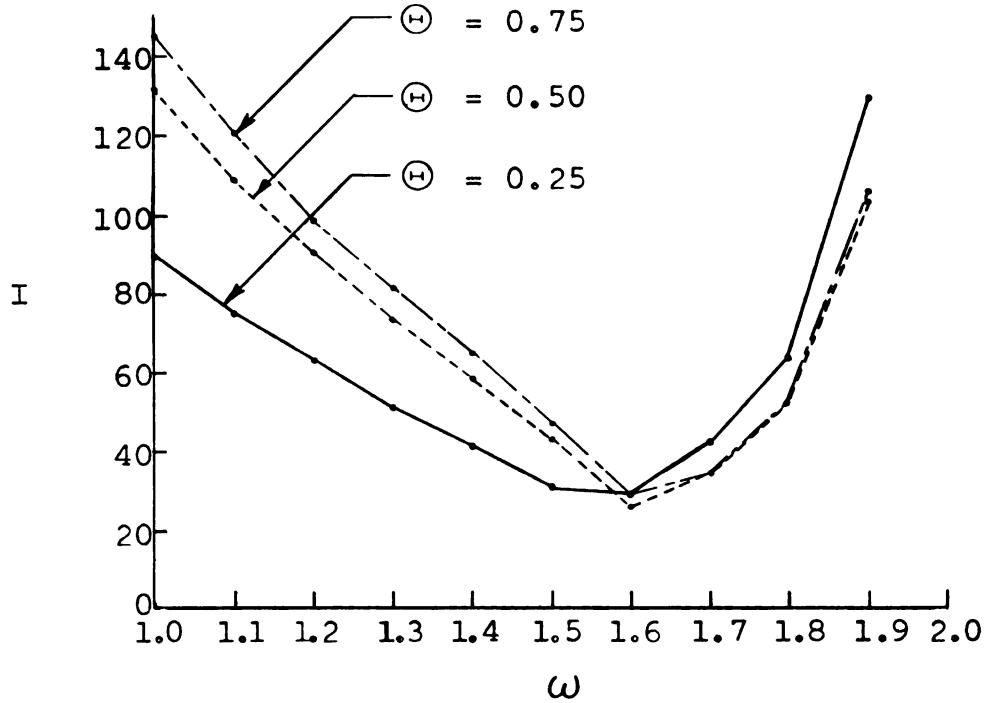

Figure 9c. Effect of relaxation factor ω on the number of iterations I for the warping-function flow-theory equations with N = 7, μ = 1.00, and n = 2

In the case of the Piechnik equation, Figure 9a, the system failed to converge after 250 iterations, for ω = 1.9. With the other two equations, the system converged for the entire range of ω. In all cases, the results indicate that the rate of convergence is quite dependent on the values of the relaxation factor. Values of ω from 1.5 to 1.6 appear to give reasonable convergence rates for the values of μ, n, and Θ tested.

The value of 1.55 for ω was used in all calculations except for the experimentation just described. This

implicitly assumes that the optimum over-relaxation factor is independent of μ, n, and Θ. As Figures 9b and 9c indicate, this probably is not exactly the case, since the optimum ω changes when n and μ are held constant and Θ is allowed to vary. However, a run for n = six and μ = zero for the case of deformation theory gave the optimum ω as approximately 1.45. In addition, with the optimum over-relaxation factor, these deformation and flow equations tend to converge faster than the Piechnik equation.

For the case where N = 13, the number of discrete points is 169, and the optimum over-relaxation factor is 1.80. Using the optimum over-relaxation factors, 1.55 for N = 7 and 1.80 for N = 13, the following comparisons were observed with the warping-function deformation-theory equations for μ = 1.00 and n = 12 with $0 \leq \Theta \leq 4.00$:

1) With the increase in grid lines, the average number of iterations increased from 23 to 38.
2) The execution time increased from 0.82 minutes to 4.27 minutes for the respectives runs.

Because of the large number of computer runs, it was felt that the most effective use of the computer time would be realized if the convergence parameter required the computed variable to have only four significant non-zero digits after the decimal place. Since only first derivatives of this function are needed, the accuracy

should be sufficient to allow the making of reasonable comparisons. The convergence parameter is given in each program listing (Appendix IV), under the variable name El. In each program El is set equal to the desired constant.

5.3 Results of the Piechnik Equation for Rigid-Perfectly Plastic Material

The Piechnik equation was solved numerically for the unit square and unit circular cross sections. The most important aspect of each solution is the interaction curve between the normalized torque and bending moment.

The interaction curve for the unit square cross section is shown in Figure 10. These results are compared with those obtained by Steele [30] and Imegwu [15] through a numerical solution of the Hill-Handelman equation. The numerical results are essentially equal, but in the present study the Piechnik equation has been solved throughout a greater range of μ. This is possible since the Piechnik equation does not have the line singularity present in the Hill-Handelman equation. In addition, Figure 10 contains the upper and lower bounds for a unit square section, obtained by Steele [30] by means of energy principles developed by Hill and Siebel [13].

Because of the line singularity in the Hill-Handelman equation, nodal points cannot be placed on the x-axis. Steele [30] and Imegwu [15], [16] begin the grid lines at a distance of $\frac{h}{2}$ from both the x and y axes. If

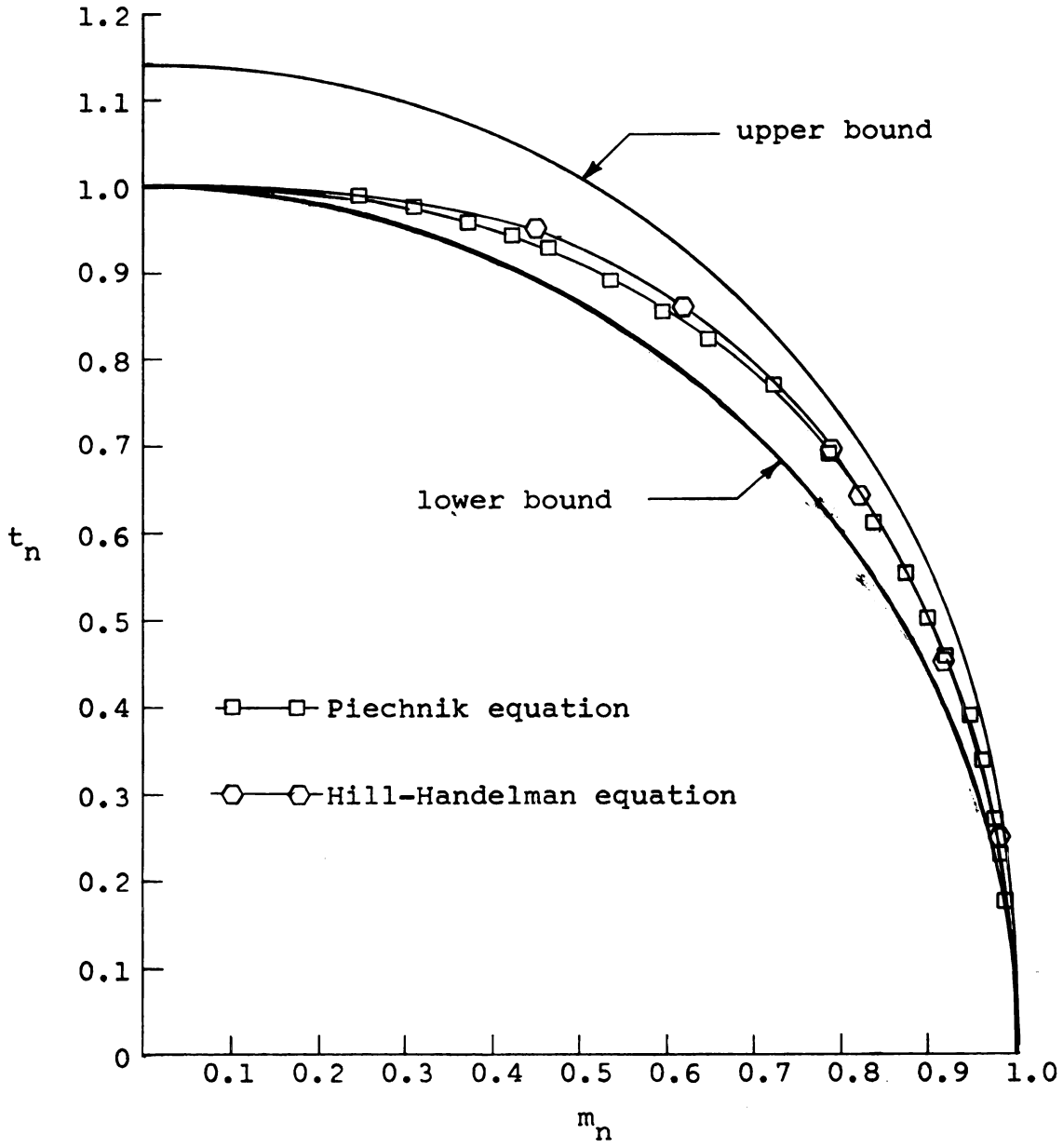

Figure 10. Normalized torque vs. bending moment interaction curve for a unit square bar

the Piechnik equation is solved with N = 10, then the stresses at selected spatial points may be compared with those obtained by Steele at these points. Steele computed the stresses for $\mu = \frac{1}{\sqrt{3}}$ and $\mu = \frac{2}{\sqrt{3}}$. The Piechnik equation was solved with N = 10 for these same values of μ. A comparison between the stresses given by Steele and those of the Piechnik solution for $\mu = \frac{1}{\sqrt{3}}$ are given in Table 6 of Appendix V. Because of the finer grid, the results of the Piechnik equation should be more accurate. However, general agreement between the stresses for the two solutions is observed.

A comparison between the interaction curve for the unit circular bar and unit square bar is illustrated in Figure 11. These results seem to indicate that the interaction curve is somewhat insensitive to the geometric cross section. Prager and Onat [20] obtained a similar result for the case of combined plastic bending and an axial load. In his more limited analysis, Imegwu [15] came to the conclusion that such an insensitivity appears to exist also for the case of combined bending and torsion.

Piechnik [24] solved his equation by assuming the bending to act as a perturbation on the pure plastic torsion. Due to mathematical difficulties, this solution was confined to a unit circular cross section. A comparison between the numerical and perturbation solutions is presented in Table 2. Piechnik states that his results

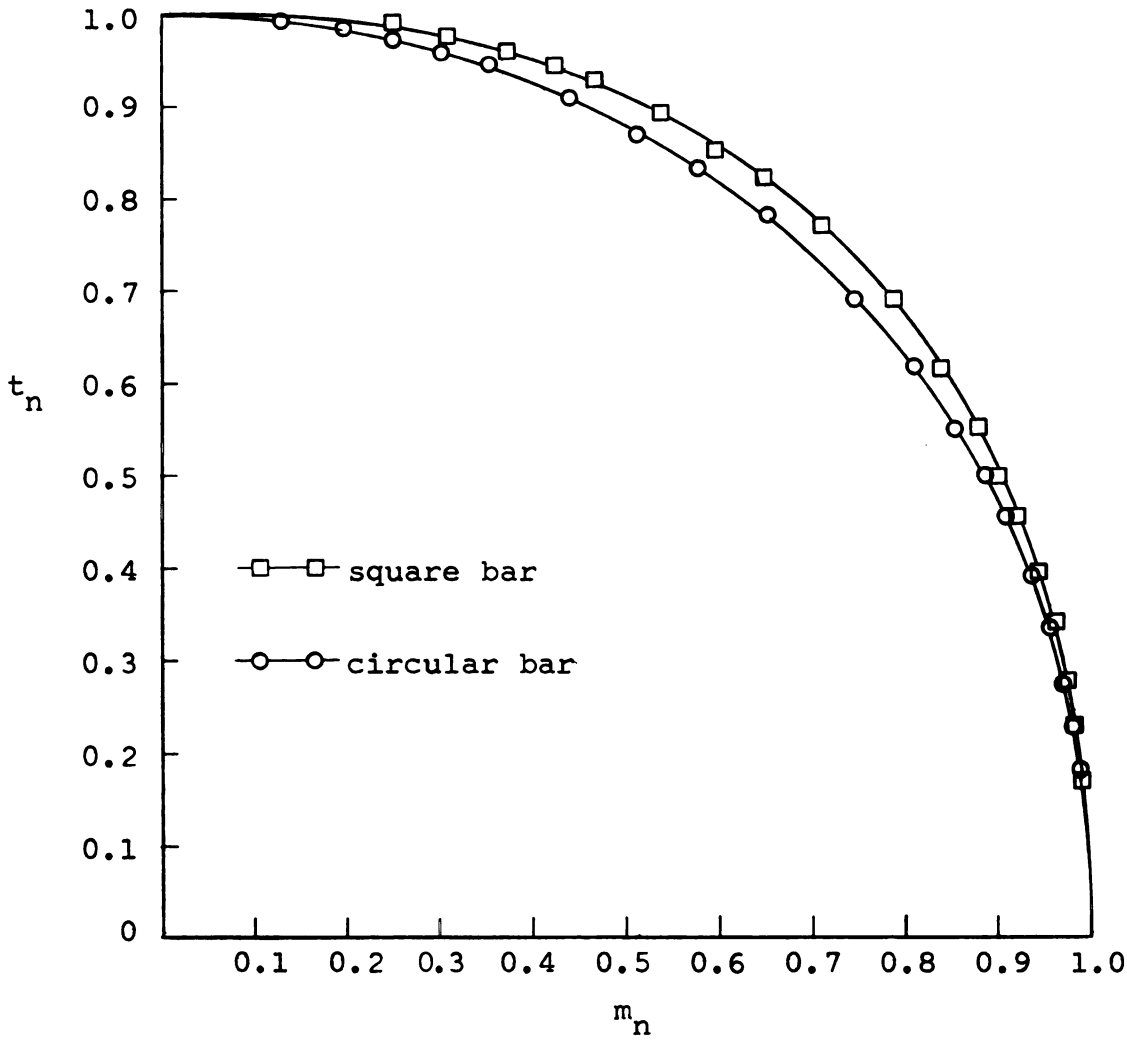

Figure 11. Comparison of the normalized torque vs. bending moment interaction curves for the square and circular bar

should be reasonably accurate for μ less than 0.25. The values shown in Table 2 indicate a favorable comparison within this range of μ.

Table 2. Comparison between numerical and perturbation solutions for unit radial cross section

	Numerical		Perturbation	
μ	t_n	m_n	t_n	m_n
0.10	0.9929	0.1329	0.9927	0.1328
0.15	0.9845	0.1945	0.9846	0.1951
0.20	0.9735	0.2518	0.9747	0.2529
0.25	0.9603	0.3050	0.9647	0.3240
0.30	0.9454	0.3542	0.9562	0.4107

The results for both of these numerical solutions of the Piechnik equation agree with those determined through energy, perturbation, and numerical methods, by other researchers. Thus, even though no mathematical justification is available to ensure convergence of the system to the correct result, the above comparisons strongly suggest the method indeed converges to a satisfactory solution.

5.4 Generalized J_2 Deformation-Theory Solutions

The combined bending and torsion problem for the generalized J_2 deformation theory was solved numerically by both a warping-function and a stress-function approach. For the case of the unit square bar, the two formulations provide essentially the same result.

This generalized J_2 deformation law was also used in the solution of the unit circular bar in polar coordinates. The polar-coordinate solution shows that the mathematical algorithm appears to be a tractable means to solve the problem when the coordinate system corresponds to the cross-sectional geometry.

5.4.1 Warping-Function Solution for Unit Square Bar

The warping-function deformation-theory equations were solved for the values of μ and n as shown in Tables 7 of Appendix V. The resulting normalized torques and bending moments are also given in these tables. For each particular combination of μ and n a given range for Θ is specified. The range of Θ and the given $\Delta\Theta$ may be obtained from inspection of the data in each table.

To illustrate the general effect of the work-hardening on the torques and moments, the normalized torques and bending moments vs. the unit angle of twist, for selected values of the Ramberg-Osgood exponent n, are shown in Figures 24 of Appendix VI.

Due to the large number of calculations, it is not convenient to present the entire stress output. However, Table 8 of Appendix V shows the typical stress output obtained by the warping-function formulation for some values of μ, n, and Θ .

5.4.2 Stress-Function Solution for Unit Square Bar

The solution to the stress-function equations serves as a check on the warping-function solution and was developed so that a comparison could be made with the above results. The equations were solved for the combinations of μ and n as presented in Tables 9 of Appendix V, and the normalized stress resultants obtained are also given in these tables.

Calculations of the stresses corresponding to the same values of μ, n, and Θ as given in Table 8 (warping-function results of Section 5.4.1) are presented in Table 10 of Appendix V. A comparison between the two stress calculations may be obtained by examining these two stress tables.

Since the results are only assumed to be accurate to two decimal places, the stress resultants for the warping and stress-function formulation are essentially equal. The computational algorithms are also essentially the same. Thus, it appears neither method offers an advantage, although, from the standpoint of error, the stress-function formulation would be expected to be better, since the values of the unknown function are prescribed on the boundary, while in the case of the warping function, the normal derivatives are prescribed at the boundary.

The warping-function approach has the advantage of giving directly the axial displacements, which might be of physical interest. For this reason, and because it represents a more novel approach in plasticity, the major effort in this study was made with the warping-function approach.

5.4.3 Warping-Function Solution for a Unit Circular Bar

The polar-coordinate deformation-theory warping-function equations for the circular bar were solved for the values of μ and n as shown in Tables 11 of Appendix V. The normalized stress resultants are presented graphically in Figures 25 of Appendix VI.

5.4.4 Approximation of the Elastic-Plastic Boundary for an Elastic-Perfectly Plastic Material

The generalized J_2 work-hardening deformation-theory approach provides a method of approximating the elastic-plastic boundary for an elastic-perfectly plastic material. As was pointed out in Section 2.4, as $n \rightarrow \infty$ the uniaxial Ramberg-Osgood stress-strain curve approaches the elastic-perfectly plastic curve represented by the curve consisting of two straight segments in Figure 3. When the tensor version, Equation (2.53), of the Ramberg-Osgood law is assumed to apply over the whole cross section in a deformation-theory analysis with no unloading,

it is reasonable to expect that the solution for n large will approximate the elastic-perfectly plastic solution. The region where J_2 approaches the constant unity approximates the perfectly-plastic region, and the boundary of this region is taken as the approximation to the elastic-plastic boundary.

On the basis of letting n become large, the elastic-plastic boundary was approximated for the square section for $\mu = 0$ and for $\mu = 1$, and for the circular section with $\mu = 1$. These boundaries for various values of Θ are shown in Figures 12.

By the sand hill-soap film analogy, the boundary is known for the case of pure torsion. Figure 12a has the appearance of the elastic-plastic boundary predicted by this familiar analogy. The boundary for the combined bending and torsion problem is not known. However, an indication that the solution is approximating a perfectly-plastic material is given since the second stress deviator invariant, J_2, approaches unity. Since J_2 approaches its greatest values along the y-axis, J_2 is plotted as a function of distance along the y-axis in Figures 13.

5.4.5. Comparisons of the Deformation-Theory Solutions

A general comparison between the stresses and stress resultants calculated by the warping function (Tables 7 and 8) and by the stress function (Tables 9

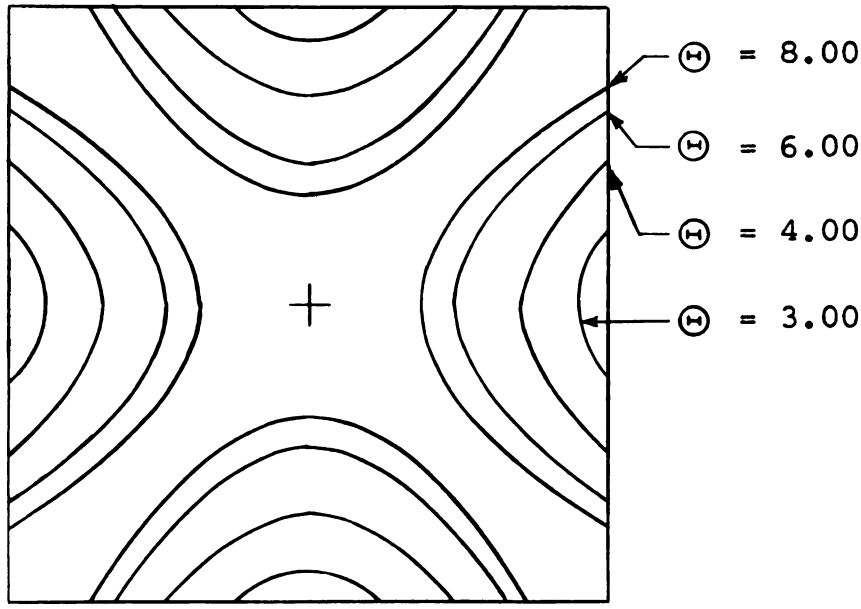

Figure 12a. Approximation to elastic-plastic boundary with $\mu = 0.00$ and $n = 12$

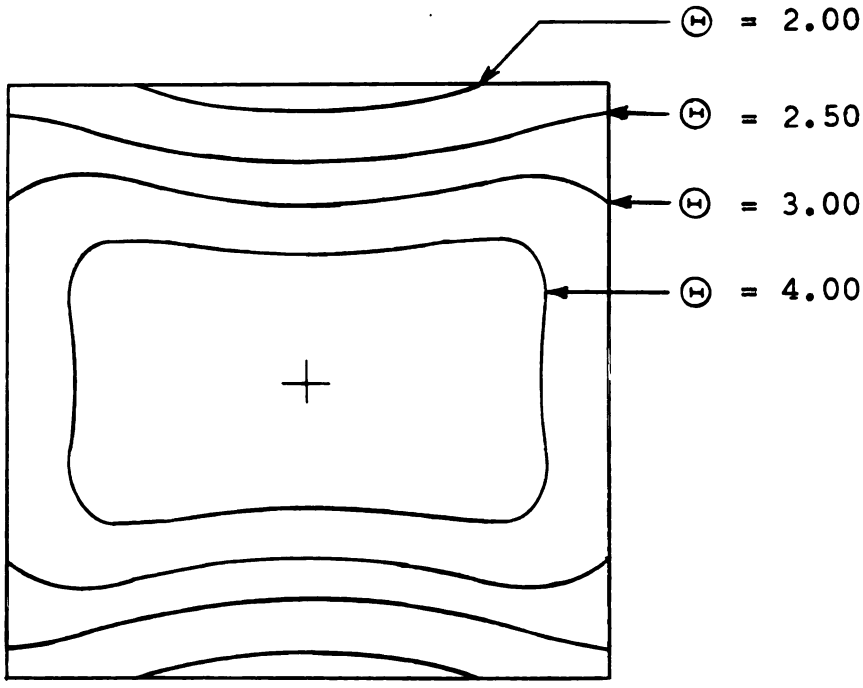

Figure 12b. Approximation to elastic-plastic boundary with $\mu = 1.00$ and $n = 12$

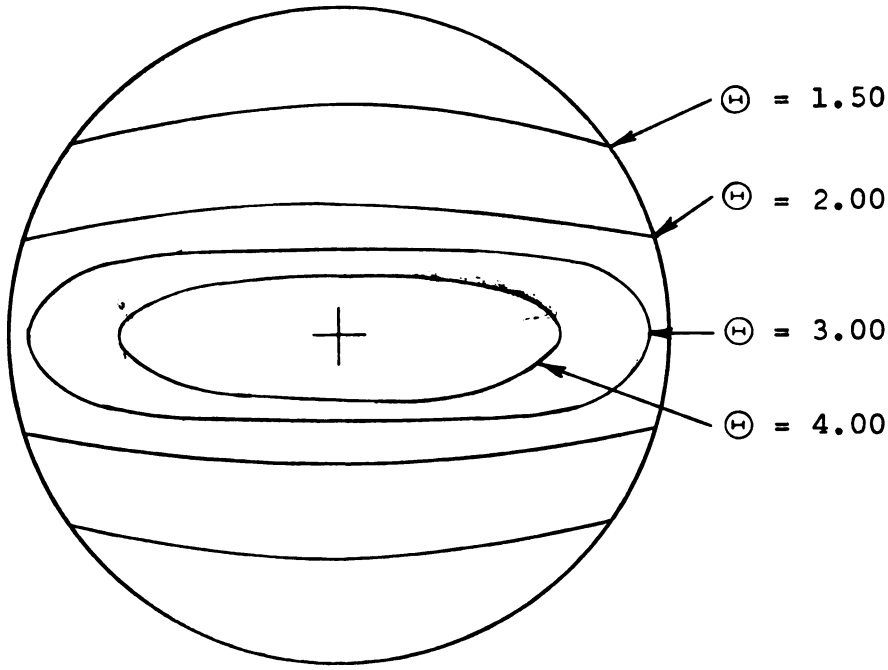

Figure 12c. Approximation to elastic-plastic boundary for circular section with $\mu = 1.00$ and $n = 15$

and 10) indicate that they agree within the limits of the assumed numerical accuracy. In addition, for the case of pure torsion, each method confirms the results presented by Greenberg, Dorn, and Wetherell [6]. As a final check, if n becomes large, then the moments and torques approach those given by the solution to the Piechnik equation. Typical comparisons for both the unit square and circular bars are shown in Table 3. These arguments offer physical assurance that the results are indeed converging to reasonable values.

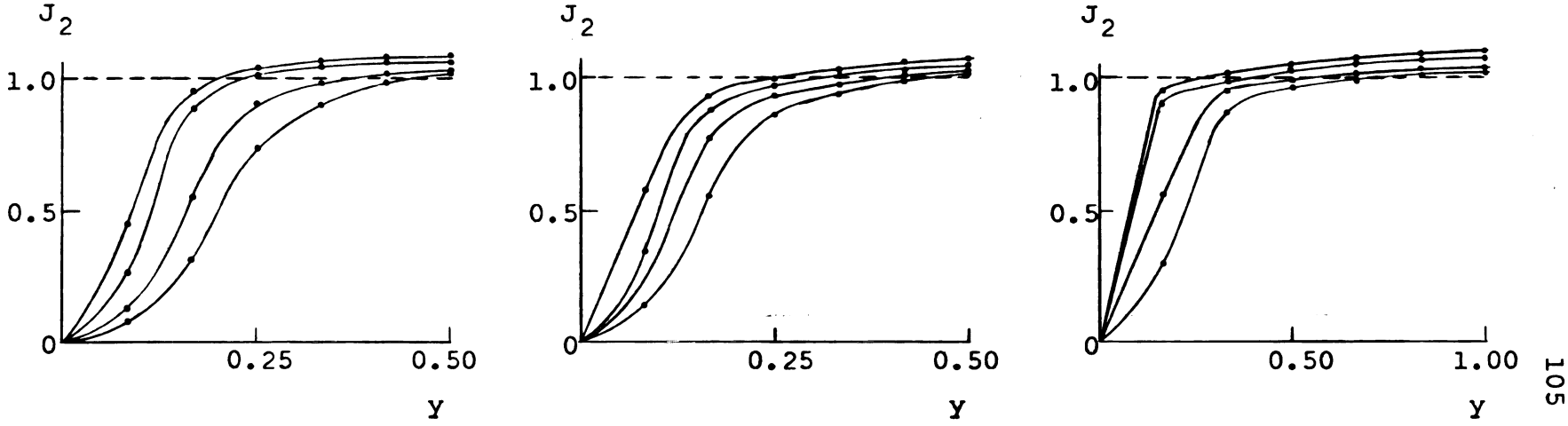

(a) Square section
μ = 0.00, n = 12
Ⓗ = 3.0, 4.0, 6.0, 8.0

(b) Square section
μ = 1.00, n = 12
Ⓗ = 2.0, 2.5, 3.0, 4.0

(c) Circular section
μ = 1.00, n = 15
Ⓗ = 1.5, 2.0, 3.0, 4.0

Figure 13. Normalized second invariant J_2 vs. y on y-axis

Table 3. Comparison between deformation-theory solution approximation to perfectly-plastic material and the Piechnik solution

Deformation theory		Piechnik equation	
Square Bar			
$n = 12$, $\mu = 1.00$, $\Theta = 4.00$		$\mu = 1.00$	
t_n	m_n	t_n	m_n
0.6834	0.8093	0.6874	0.7885
Circular Bar			
$n = 15$, $\mu = 1.00$, $\Theta = 4.00$		$\mu = 1.00$	
t_n	m_n	t_n	m_n
0.7119	0.7855	0.6936	0.7488

In the case of the unit circular bar, expressed in polar coordinates, the warping function offers an advantage over the stress-function formulation. That is, the governing equations in both cases are singular at the origin. However, with the warping function, the singularity is removable since the warping is known to be zero at the origin. Thus, the warping-function approach provides a numerically tractable way to approach the problem through the use of polar coordinates.

The flow-theory equations are solved in Section 5.5 for the same parameters as the deformation-theory equations. As will be shown, the two theories appear to give the same results under the condition of proportional straining in terms of the generalized variables κ and θ.

5.5 Generalized J_2 Flow-Theory Solutions

The generalized J_2 flow-theory analysis was also formulated for both the warping and stress functions. Both methods give essentially the same results for the stresses and the normalized torques and bending moments.

5.5.1 Warping-Function Solutions

The warping-function system of equations was solved for various values of n and μ; the resulting normalized stress resultants are given in Tables 12 of Appendix V. Typical values for calculated stresses are presented in Table 13 of Appendix V.

5.5.2 Stress-Function Solutions

The stress-function system of equations was solved for the various values of μ and n; the resulting normalized torques and bending moments are given in Tables 14 of Appendix V. Table 15 of Appendix V gives calculated values for the stresses which compare with those for the warping-rate function calculations given in Table 13.

5.5.3 Comparisons for Flow Theory

A comparison between the torques and moments for the warping function (Tables 12) and the stress function (Tables 14) shows that the two formulations provide results which agree within the assumed numerical accuracy.

An examination of Tables 13 and 15 shows a similar agreement between the stresses. Thus, both methods provide essentially the same results.

From a computational point of view, neither method offers an advantage, since the mathematical algorithms are practically equivalent.

5.6 Comparison Between Flow and Deformation Theory

5.6.1 Conditions Where the Theories Agree

Piechnik [24] showed that for a rigid-perfectly plastic material, the condition $\frac{\kappa}{\theta} = \frac{\dot{\kappa}}{\dot{\theta}}$ produces the same governing equation for flow theory as for deformation theory. The solution to the Piechnik equation is given by the interaction curve between torque and moment. In the case of deformation theory, this curve results from $0 \leq \frac{\kappa}{\theta} \leq \infty$. Similarly, in the case of flow theory, it results from $0 \leq \frac{\dot{\kappa}}{\dot{\theta}} \leq \infty$. Thus, the interaction curves for both theories are identical.

In the work-hardening materials, the solution to the system of equations is no longer an interaction curve but rather the relationships of the moments and torques to the deformation parameters κ and θ. These relationships depend on the Ramberg-Osgood constant n. A comparison between the results presented for deformation theory (Section 5.4) and flow theory (Section 5.5) indicates that

the two theories appear to agree under the condition $\frac{K}{\theta} = \frac{\dot{K}}{\dot{\theta}}$.

It should be noted that the solutions to the flow theory represent a forward integration in the Θ variable. This is accomplished through a backwards difference quotient in $\Delta\Theta$. The error in the system is of order $\Delta\Theta$ and it may tend to accumulate with increasing Θ. Thus, the two theories would not be expected to agree as well for Θ large as for Θ small.

In all cases tested, with N = 7, the calculations for deformation theory and for flow theory agree to two decimal places when Θ is small. As Θ assumes its maximum value in the specified range, there is a little less agreement. This difference is believed to be due to an accumulation in the error of the backwards difference quotient.

To investigate these numerical differences, computer runs were made with N = 13, μ = 1.00, and n = 12 for both the deformation and the flow-theory warping-function equations. In addition, with the flow theory the increment in Θ was $\Delta\Theta$ = 0.0625. The results of these calculations with the two theories agree to three places initially and gradually decrease to two places as Θ takes on its maximum value. This indicates the theories produce the same results if $\frac{K}{\theta}$ = constant and that any difference in results can be attributed to numerical error rather

than to actual differences in the predictions of the theories.

It is generally believed that the solutions for a deformation theory and its counterpart flow theory will agree only under the conditions of radial loading in the stress space. Greenberg, Dorn, and Wetherell [6] showed the two theories provided the same numerical result for pure torsion even though the stresses were non-radial. The present study shows that under the loading condition $\frac{\kappa}{\theta}$ = constant, where κ and θ are generalized strain parameters, the deformation and flow theories provide essentially the same numerical results. In this more general situation, the loading is such that the stresses follow a non-radial load path.

As was remarked in Section 1.1, a radial stress load path means $\sigma_{ij} = C\sigma^{\circ}_{ij}$ where σ°_{ij} are constants and C is a function which increases monotonically with the time-like variable. Thus, for the combined bending and torsion, a radial stress load path implies

$$\frac{\sigma_{zz}}{\sigma^{\circ}_{zz}} = \frac{\sigma_{xz}}{\sigma^{\circ}_{xz}} = \frac{\sigma_{yz}}{\sigma^{\circ}_{yz}} = C(\theta), \qquad (5.1)$$

where σ°_{zz}, σ°_{xz}, σ°_{yz} may be taken as the respective stresses when Θ equal $\Delta\Theta$.[2]

---

[2]This choice of the value of Θ at which the stresses σ°_{ij} are taken is arbitrary.

To better illustrate the non-radial nature of the combined bending and torsion problem, consider

$$\frac{\sigma_{zz}}{\sigma^{*}_{zz}} = C_1$$

$$\frac{\sigma_{xz}}{\sigma^{*}_{xz}} = C_2 \qquad (5.2)$$

$$\frac{\sigma_{yz}}{\sigma^{*}_{yz}} = C_3$$

where the C_β are functions of θ. A radial loading is indicated if $C_1 = C_2 = C_3$. If C_1, C_2, and C_3 are plotted as functions of the time-like variable θ, then the difference between the curves will tend to indicate the degree of non-radial stress loading.

Figures 14 show the functions C_β plotted as functions of θ for $\mu = 0$ and for $\mu = 1$ and for two choices of the Ramberg-Osgood exponent, $n = 2$ and $n = 12$. The stresses are taken at the spatial point where $i = 4$ and $j = 5$. The results for $\mu = 0$ confirm the results reported by Greenberg, Dorn, and Wetherell.

An analysis of these graphs shows that the stress paths tend to be more non-radial when μ is smaller and n larger. However, in the torque, moment, and stress results, it was found that the two theories agree under the condition $\frac{K}{\theta}$ = constant, and there appears to be no

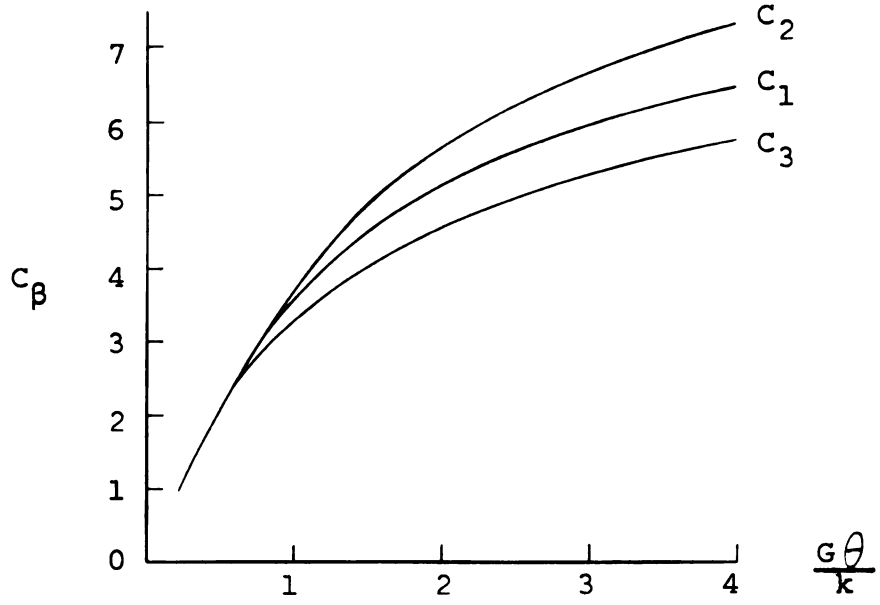

Figure 14a. Functions C_β vs. $\frac{G\theta}{k}$ showing non-radial stresses for $\mu = 1.00$ and $n = 2$ at the discrete point $i = 4$, $j = 5$

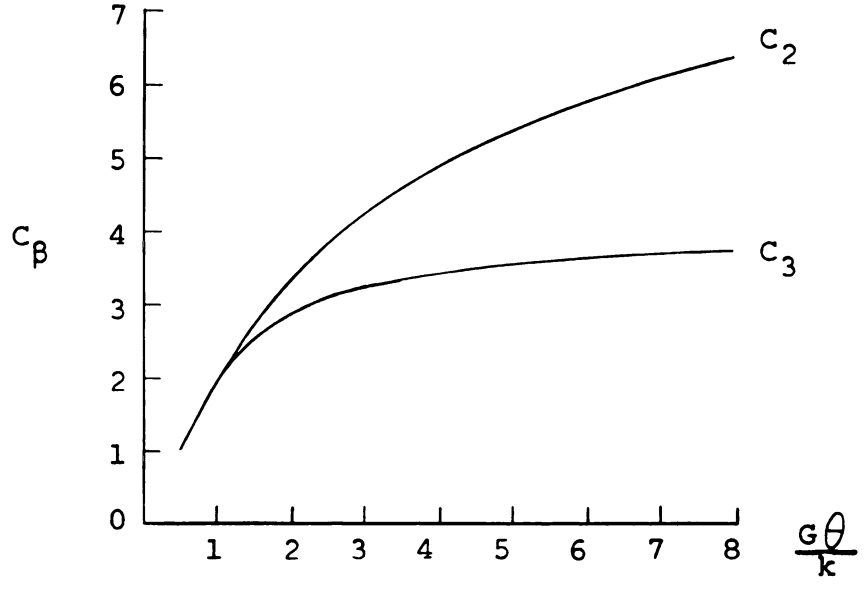

Figure 14b. Functions C_β vs. $\frac{G\theta}{k}$ showing non-radial stresses for $\mu = 0.00$ and $n = 2$ at the discrete point $i = 4$, $j = 5$

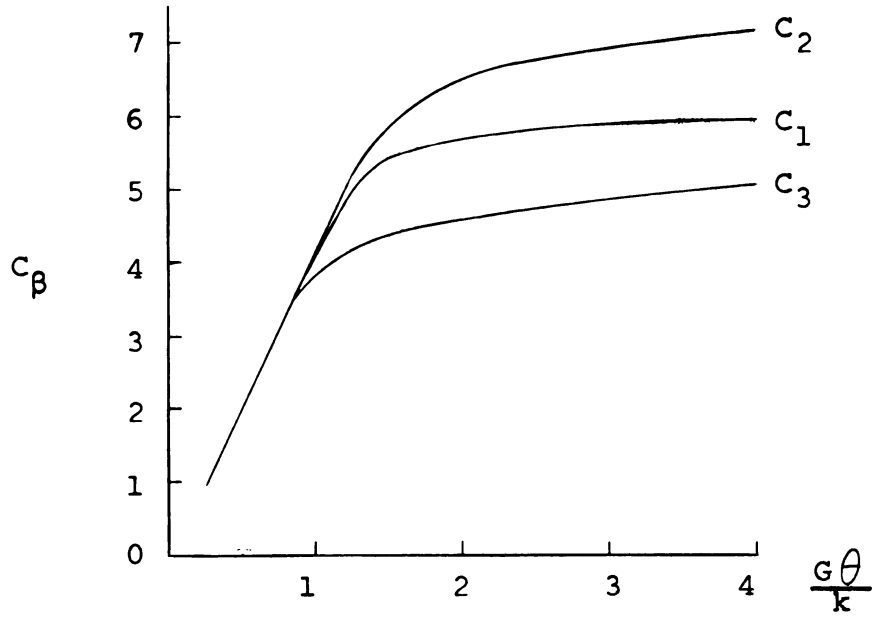

Figure 14c. Functions C_β vs. $\frac{G\theta}{k}$ showing non-radial stresses for $\mu = 1.00$ and $n = 12$ at the discrete point $i = 4$, $j = 5$

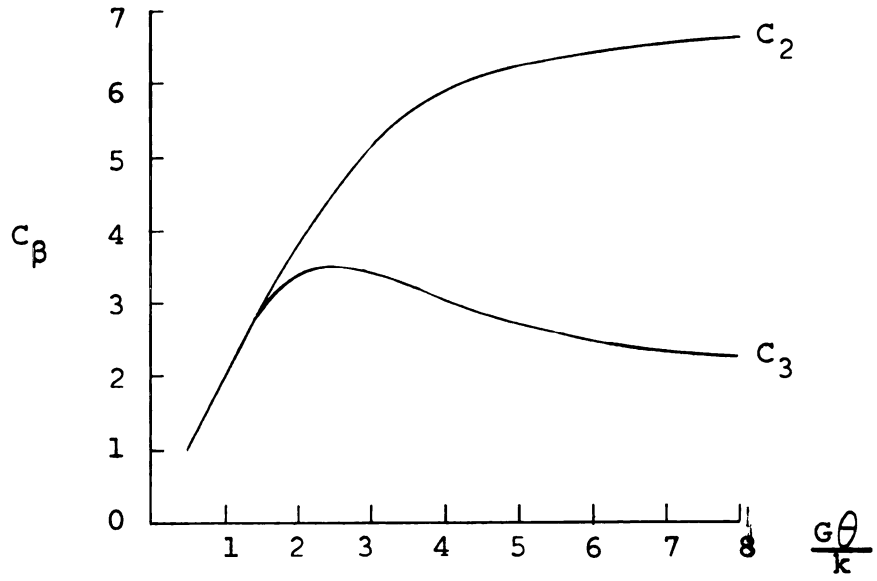

Figure 14d. Functions C_β vs. $\frac{G\theta}{k}$ showing non-radial stresses for $\mu = 0.00$ and $n = 12$ at the discrete point $i = 4$, $j = 5$

dependence on the values of n and μ, insofar as agreement between the two theories is concerned. The agreement between the numerical results from the two theories seems to suggest that, although the condition of a radial stress path is a sufficient condition for integrability of the flow-theory equations to those of deformation theory, it may not be a necessary condition. Otherwise, with non-radial stress paths, one would expect more disagreement between the two theories than that observed with this study.

Budiansky [1] has proposed a condition under which the deformation theory is an "acceptable competitor" to the flow theory even under the condition of non-radial stress paths. For the generalized J_2 deformation theory, this condition is [6]

$$\alpha < \tan^{-1}\sqrt{2n-1} \tag{5.3}$$

where

$$\alpha = \cos^{-1} \frac{\sigma'_{ij}\dot{\sigma}'_{ij}}{[\sigma'_{kl}\sigma'_{kl}]^{1/2}[\dot{\sigma}'_{pq}\dot{\sigma}'_{pq}]^{1/2}}. \tag{5.4}$$

Budiansky and Mangasarian [2], [18], for the case of an infinite plate with a circular hole, showed that generalized J_2 deformation theory and generalized J_2 flow theory give comparable results even if the stress paths are non-radial. However, in all cases the Budiansky criterion was satisfied.

Calculations with the combined bending and torsion problem indicate that under the condition $\frac{K}{\theta}$ = constant, the Budiansky criterion is satisfied. Thus, on the basis of Budiansky's physical arguments, perhaps one could expect the results of the two theories to be comparable. Nevertheless, this condition does not answer the question of integrability posed earlier in this section.

In Section 5.6.2 examples will be given where the theories do not agree. This disagreement between the theories will be shown to depend on how much the load variable $\frac{dK}{d\theta}$ is allowed to vary during the loading.

5.6.2 Examples of Load Paths Where the Theories Do Not Agree

To further compare the results of the deformation-theory and the flow-theory calculations, the parameter $\frac{dK}{d\theta}$ was allowed to vary during the loading. As was shown in Chapter III, Section 3.6, a point in the generalized $K-\theta$ space may be reached by any number of paths. For the paths A, B, C, and D shown in Figure 15, the values calculated at the point (3.00,3.00) for the normalized torque and moment are shown in Table 4. These calculations were made with n = 2 and with n = 12. This table shows the per cent difference between the normalized torques and moments and those for load path C. In this case, path C represents the loading where $\frac{K}{\theta}$ is constant. The values for the deformation-theory calculations are also included in

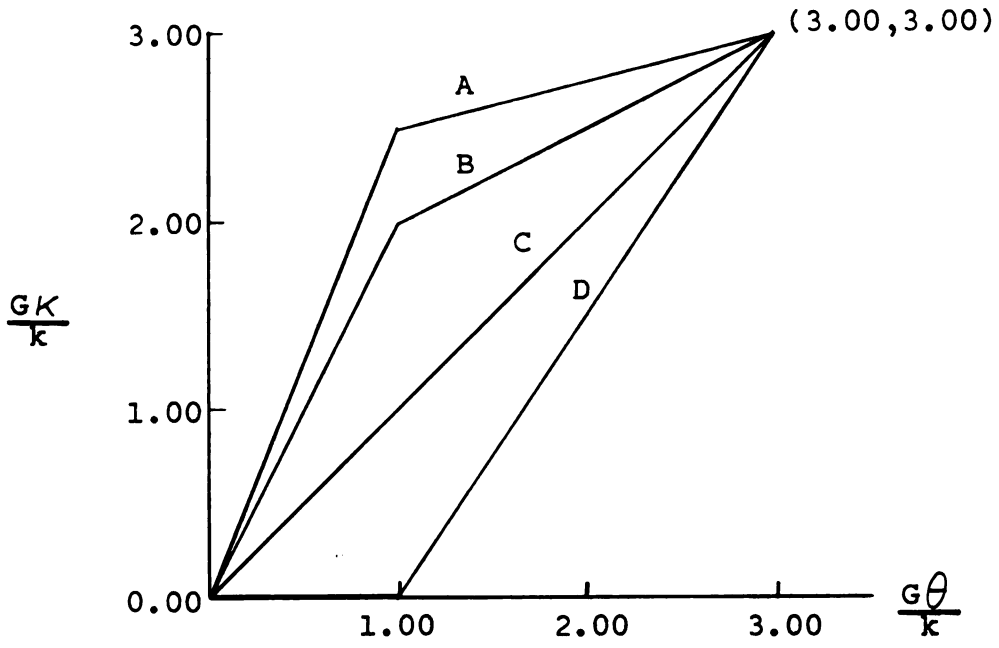

Figure 15. Paths chosen for comparing the deformation and flow-theory calculations at the point (3.00,3.00)

Table 4. Comparison of torques and moments for different load paths (see Figure 15)

Path	t_n	m_n	Per Cent Difference from C: torque	moment
Ramberg-Osgood exponent n = 2				
A	0.753	0.705	+17.65	-11.54
B	0.711	0.743	+11.09	- 6.77
C	0.640	0.797		
C (deformation)	0.642	0.807	+ 0.31	+ 1.38
D	0.593	0.836	- 7.34	+ 4.52
Ramberg-Osgood exponent n = 12				
B	0.719	0.733	+ 9.10	- 6.14
C	0.659	0.781		
C (deformation)	0.656	0.789	- 0.45	+ 1.11
D	0.625	0.807	- 5.16	+ 3.33

this table; deformation theory predicts the same results for all paths.

For the paths tested, the differences are not extremely large; however, they are of such magnitude that they cannot be attributed to numerical error. Thus, under the condition of non-radial loading in terms of the generalized strain parameters κ and θ, a difference in the predictions of the flow and deformation theories is observed. This difference becomes greater as the path in the $\kappa - \theta$ space becomes more non-radial.

The Budiansky criterion, Equations (5.3), was checked with deformation-theory calculations for paths A and B with the Ramberg-Osgood exponent n = 2. For n = 2, the maximum permissible value for the angle α is 65.9°. With path A the maximum calculated α was 76.2° while with path B the maximum calculated α was 63.9°. Thus path A violates the Budiansky criterion while path B does not violate this condition. These deformation-theory calculations deviated by as much as 14.8 per cent of the flow-theory values with path A while the maximum deviation was about 10.0 per cent of the flow-theory values with path B.[3] Although no definite conclusion may be drawn from this particular analysis, it would seem that if the Budiansky

---

[3]When calculated as a percentage of the deformation-theory values, the percentages for paths A and B were as high as 17.7 per cent and 11.1 per cent, respectively.

criterion is violated with a deformation theory then the results certainly should be questioned.

The development of the Budiansky criterion is predicated on the assumption that one wishes to set a limit on when the deformation theory may be considered as an "acceptable competitor" to a counterpart flow theory [1]. This implicitly assumes that one would prefer the flow-theory solution, but that generally it is easier to obtain the deformation-theory solution [2], [18]. The results of the present study indicate that the flow-theory analysis is comparable to the numerical calculations required for the deformation theory. If the flow theory is the preferable theory, then it may be more reasonable to proceed with a flow-theory analysis.

5.7 Conclusions

The following general conclusions relating to the combined bending and torsion problem are made as a result of this investigation:

1) The numerical solution of the Piechnik equation confirms the results of other investigators. But, from a computational point of view, the Piechnik equation has better convergence properties, and, consequently, all points on the interaction curve may now be calculated.
2) In both the flow-theory and the deformation-theory generalized J_2 work-hardening material calculations,

the stress-function equations and the warping-function equations give comparable results with approximately the same amount of numerical computation. Thus, neither method appears to offer any computational advantage. However, with more complicated geometric boundaries, the stress-function approach would be preferable.

3) The two work-hardening theories, deformation and flow, appear to agree under loading conditions where a constant ratio is maintained between the generalized strain parameters K and θ even though the stress load path is non-radial. This strongly suggests that a radial stress load path may be only a sufficient condition for integrating the flow-theory equations to those of deformation theory, but not a necessary one.

4) As the strain path is made non-radial in terms of the generalized variables K and θ, differences are observed in the results of the two theories. It is customarily believed that the flow theory should be the preferable theory [12], [17]. Thus, for this type of non-radial straining, the flow-theory results should be preferred to those of the deformation theory.

5) The numerical analysis calculations for the flow-theory solution are comparable to those for the

deformation theory. In all solutions, both flow and deformation, the times required for convergence at any given Θ level are comparable. The flow-theory calculations take slightly longer due to the additional iteration mentioned in Section 3.6, but this iteration is not significant in terms of the total time. The more important consideration between the theories is the size of the increment $\Delta\Theta$. In flow-theory computations, this must be kept small because of the error, and, consequently, more calculations are required for a given range of Θ.

It is generally believed that even with numerical analysis the flow-theory solutions are much more difficult to obtain than the deformation-theory solutions. With the iteration procedures of the present study, this was not the case for combined bending and torsion, and it is possible that similar procedures could be used in other problems to make flow-theory competitive with deformation theory from the standpoint of computational difficulty.

VI. POSSIBLE EXTENSIONS OF THE RESEARCH

It may be possible to extend the research along two primary avenues: (1) to apply the technique to other related problems in mechanics, and (2) to establish a mathematical criterion which would ensure the convergence of the iterative schemes.

6.1 Related Mechanics Problems

6.1.1 More General Loading Conditions

The equations should be extended to a more general loading situation. Hill [11], [12] extended Handelman's work [7] to the general case of combined torsion, bending about two orthogonal axes of symmetry and uniaxial extension. In a similar manner, the work-hardening formulations could be generalized to include these loadings.

In this generalization, the displacement Equations (2.3) would be replaced by the following displacements:

$$u = -\frac{1}{2}\kappa_1 xy + \frac{1}{4}\kappa_2(y^2 - x^2 - 2z^2) - \frac{1}{2}\delta x - \theta yz$$

$$v = \frac{1}{4}\kappa_1(x^2 - y^2 - 2z^2) - \frac{1}{2}\kappa_2 xy - \frac{1}{2}\delta y + \theta xz \qquad (6.1)$$

$$w = \kappa_1 yz + \kappa_2 xz + \delta z + f(x,y,\theta),$$

where κ_1 and κ_2 are curvatures, θ unit angle of twist and δ unit extension. These more general displacements represent the sum of the displacements for each loading considered separately.

Again, the elastic analogy assumption on the stresses would be made and an incompressible material assumed. The development should parallel that of Chapter II, but, in the solution, the manner in which the curvatures and the extension depend on the unit angle of twist would have to be specified. Numerical solutions could be obtained with algorithms similar to those used in this study. Since under the more general loading the effect of the unit angle of twist on the normal stress is greater, extreme care should be maintained in incrementing the unit angle of twist variable.

6.1.2 General Boundaries

From a more practical viewpoint, it may be reasonable to consider other geometric cross sections. The present analysis treated only the square and the circular bars. In each of these cases, the algorithms exhibit reasonable convergence rates. For these examples, the normal derivatives on the boundary are parallel to the grid lines, and neither the warping function nor the stress function offer a computational advantage. In the case of an irregular boundary, however, the stress-

function approach might give an advantage, since the value of the stress function is prescribed on the boundary while the normal derivative is prescribed for the warping function.

In the extension to a more general boundary, the major problem would be computer programming. The program must consider the different possibilities at each boundary point. In addition, an irregular geometric cross section may tend to cause some difficulty in the convergence of the algorithms. The convergence properties of the Gauss-Seidel method applied to the linear Poisson equation are known to depend on the boundary geometry [32].

6.1.3 Other Theories

A number of attempts have been made to determine mathematical stress-strain relations. Many of these are summarized by Osgood [21]. Some of these theories may be preferable to the ones used in this study. Since the present formulation considers the constitutive relation as a separate equation, the algorithm could be adapted to these other theories, and the results of different theories could be compared.

Perhaps one of the more interesting theories would be one due to Prager [12], assuming the tensile stress-strain curve as

$$\sigma = Y \tanh\left(\frac{E\varepsilon}{Y}\right) . \qquad (6.2)$$

Prager [26] and Hill [12] give the counterpart generalized flow theory for this stress-strain curve. From a physical standpoint, one of the objections to this relation is the difficulty in defining the parameters [21]. However, in the case where the material has a well-defined yield point and the actual stress-strain curve approaches the elastic-perfectly plastic situation, this formulation provides a good fit to the uniaxial physical data [12]. Thus, using Prager's relation for the whole body provides a numerical method of determining displacements when the material behavior approaches that of an ideal elastic-perfectly plastic medium.

Hill [12] gives an equation for determining the warping in the case of pure torsion of a prismatic bar with an elastic-perfectly plastic material. Hodge [14] has applied this equation to some special cross sections. In Hodge's formulation, the deformations must be such that the elastic strains may be neglected. This restriction would not be necessary in the numerical calculations with a smooth stress-strain curve such as Prager's hyperbolic tangent law.

The Ramberg-Osgood curve also approaches the elastic-perfectly plastic case when n approaches infinity. But, in the plastic region, the perfectly-plastic stress is approached from above, whereas with Prager's method it is approached from below. Consequently, in this special

case, it would seem that Prager's relation offers some advantage over that of Ramberg and Osgood for approximating an elastic-perfectly plastic curve by a smooth curve.

6.1.4 Work-Hardening Equations Not Related to Combined Bending and Torsion

The iteration procedure developed in this study permits the material non-linearity to be confined to a single equation. This non-linearity, resulting from the constitutive relation, is treated by the Newton-Raphson iterative procedure. The governing equation, i.e., the equilibrium equation with the warping function or the compatibility equation with the stress function, is still treated numerically in a manner analogous to the corresponding linear elasticity problem.

It may be possible to develop iterative procedures similar to those used in this study for other work-hardening problems not related to combined bending and torsion. For example, the governing work-hardening equations for an Airy's stress function in plane stress or plane strain problems may be developed. This development would assume the entire body to be governed by work-hardening plasticity equations so that no undetermined elastic-plastic boundary is involved. The governing equation would be a fourth-order partial differential equation which would be treated in a manner similar to the linear

biharmonic equation. The non-linear material properties would be contained in an equation similar to the polynomial equation considered in this study. The computational algorithm should somewhat parallel that employed with the stress-function approach of this investigation.

As in elasticity, the Airy stress-function approach would be suitable only for problems with traction boundary conditions. For displacement boundary conditions or mixed problems, it might be possible to develop a similar procedure for equations analogous to the Navier equations of elasticity. Another possible class of problems are those of axial symmetry including, but not limited to, torsion of bars of non-uniform cross section. Also, no consideration has yet been given to combined torsion and flexure with transverse loads, introducing dependence on the z-coordinate.

6.1.5 Experimental Verification

The validity of any engineering analysis must be measured by the degree to which it actually predicts the behavior of physical phenomena. To determine if this method produces reasonable results, one would have to compare these analytical results to experimental measurements. Since the deformation and flow theories produce different results under certain loading conditions, there is some question as to the physical validity of the methods. It

should be possible to develop experiments which would provide greater insight into the application of the theories.

It would be quite difficult to subject a prismatic bar simultaneously to arbitrary pure bending and torsion where the rates of curvature and rates of twist could be independently controlled. Hill and Siebel [13] have reported on an experiment with a steel circular bar where the ratio of moment to torque was held constant.

The problem of combined torsion and tension should exhibit similar differences between the theories. It should be feasible to design an experiment where the rate of extension and rate of twist are independently controlled to determine the relationship between tension and torsion. This type of experiment may be a possible way of checking the physical validity of the numerical procedures.

Ramberg and Osgood [21] suggest that their formulation will provide a reasonable fit to a variety of materials. For the uniaxial stress conditions, the three parameters are easily obtained [21].

In order to obtain a valid mathematical stress-strain relation for a given material, it may be necessary to consider other theories such as those suggested in 6.2.3. If a reasonable fit to a given material is made, then the above experiment should provide additional information concerning the range of application for both the deformation and the flow theories.

6.2 Mathematical Investigations

6.2.1 Bound on the Theta Increment

Experience indicates that the algebraic system for both the flow and deformation theories converges at reasonable rates if the increment in the angle Θ is small. Thus, at any given level of Θ, the convergence is possible only if the initial solution is near the actual solution. It appears that the governing factor on the "nearness" of the initial solution is the Newton-Raphson iteration on the $(2n+1)^{th}$ degree polynomial. That is, if the initially estimated roots provide a good approximation, then the system tends to converge.

The object of an additional investigation might be to determine a bound on the increment $\Delta\Theta$. Previous results show that this bound depends on the Ramberg-Osgood exponent n and on the curvature-twist (or curvature rate-twist rate) ratio μ.

By experimenting with different increments, a bound depending on n and μ could be established experimentally. Mathematically, the term S_{m+1} (for example, see Equation 3.21) must be bounded for a given increment. With this bound, a limit may be established on the degree of change in the root $\Phi(i,j)$ at an arbitrary point (i,j).

6.2.2 Effect of Newton-Raphson Iteration

The effect of the Newton-Raphson iteration should be further studied. It appears that an equation of the type,

$$A(u)u_{xx} + B(u)u_{xy} + C(u)u_{yy} + D(u)u_x + E(u)u_y + F(u) = 0, \tag{6.3}$$

solved by iteration will tend to converge if the estimates of the non-linear coefficients $A(u_m)$, $B(u_m)$, $C(u_m)$, $D(u_m)$, $E(u_m)$, and $F(u_m)$ approach their respective limits at a faster rate than u_m approaches u. This seems to indicate that, if values of u_m approximate u in a relatively coarse manner, some technique must be utilized by which the coefficients are predicted quite accurately. If such techniques can be developed, it seems reasonable to expect the system to converge.

In a certain sense, the Newton-Raphson iteration takes rather poor values of $t_m(i,j)$ and predicts quite accurate values for $E_m(i,j)$. Thus, this iteration scheme acts as a predictor in determining more accurate estimates. It may be possible that other predicting techniques may provide better convergence rates.

6.2.3 General Convergence

The question of general convergence must be considered from two standpoints: (1) will the discrete

system converge to the continuous system as the lattice parameter approaches zero, and (2) will the iterative method for the algebraic system converge. In non-linear problems, very little theory is available in regard to either of these two problems.

Recently, Parter and Greenspan [22], [23] considered these convergence problems with a mildly non-linear second-order partial differential equation. They considered the Dirichlet problem, on the union of R and S, with

$$\begin{aligned} \nabla^2 u &= f(u) \quad \text{on} \quad R \\ u &= g(x,y) \quad \text{on} \quad S, \end{aligned} \tag{6.4}$$

where R is the interior of the closed path S. In addition, the function f(u) must be such that both its first and second derivatives exist and are always greater than or equal to zero.

Parter [22] considered the convergence of the discrete system to the continuous system. Both authors [23] treat the convergence of a number of different algorithms for the solution of the discrete system. In each analysis, the most important restriction appears to be the bounds on the function f(u) and its first and second derivatives.

It may be that the equation considered in this study,

$$\nabla^2 t + E(t_x, t_y) = 0, \qquad (6.5)$$

also possesses similar non-linear properties. The problem is to establish certain bounds on the function $E(t_x, t_y)$. If this is accomplished, then perhaps a procedure analogous to that of Parter and Greenspan could aid in the establishment of a general convergence requirement of the system. In addition, with the warping-function formulations, the analysis requires the consideration of the Neumann boundary conditions.

APPENDIX I

SOLUTION TO FINITE-DIFFERENCE EQUATIONS BY THE GAUSS-SEIDEL OVER-RELAXATION METHOD

This method, also known as Liebmann's method or the method of successive displacements, is considered in most books treating iterative methods for solving linear algebraic equations. Additional details may be obtained by examining references such as Fox [5], Forsythe and Wasow [4], Varga [33], etc.

To illustrate the procedure, the method will be applied to the solution of the discrete representation of the Poisson equation, where the equation is defined on a square region R. However, the method may be applied to other partial differential equations.

The Poisson equation is

$$u_{xx} + u_{yy} = F(x,y) \qquad (I-1)$$

where either u or the normal derivative is specified on the boundary.

An N x N set of grid lines with lattice dimension h is superimposed on the region R. Equation (I-1) is represented by its discrete finite-difference analogue. Thus, at all mesh points

$$u(i+1,j) + u(i,j+1) + u(i-1,j)$$

$$+ u(i,j-1) - 4u(i,j) = h^2F(i,j), \qquad \text{(I-2)}$$

where on the boundary either u(i,j) or the normal derivatives are known.

If u(i,j) is known at each boundary point, then the number of points where u(i,j) is unknown is $(N - 1)^2$. However, if the normal derivatives are specified, then expressing (I-2) along with the derivative approximation permits the determination of u(i,j) on the boundary as a function of the interior points. In this latter case, the system can be solved within an arbitrary constant. In the more general case, where u(i,j) is specified at some boundary points and the normal derivative is specified at the other points, the rank of the system will be equal to the number of unknowns.

To begin the Gauss-Seidel over-relaxation procedure, an initial solution $u_o(i,j)$ is assumed. These values are recalculated during successive sweeps through the mesh. A particular cyclic order for replacing u(i,j) in any one sweep is specified.

If $u_m(i,j)$ represents the values for the m^{th} sweep, then the values $u_{m+1}(i,j)$ for the $(m+1)^{th}$ sweep are calculated by the formula,

$$u_{m+1}(i,j) = u_m(i,j) + \omega[\bar{u}_{m+1}(i,j) - u_m(i,j)], \qquad \text{(I-3)}$$

where ω is a relaxation factor and $\bar{u}_{m+1}(i,j)$ is the unextrapolated value given by Equation (I-2). Thus, $\bar{u}_{m+1}(i,j)$ depends on its nearest neighbors and on the cyclic order. If the cyclic order is such that for each i, all values of j are computed before i is increased, then $\bar{u}_{m+1}(i,j)$ is given by

$$\bar{u}_{m+1}(i,j) = [u_m(i+1,j) + u_m(i,j+1) + u_{m+1}(i-1,j) + u_{m+1}(i,j-1) - h^2F(i,j)]/4. \qquad \text{(I-4)}$$

The relaxation factor ω may take on values

$$0 < \omega < 2. \qquad \text{(I-5)}$$

If $\omega < 1$ the system is under-relaxed and if $\omega > 1$ the system is over-relaxed. For linear systems, various theorems are available for estimating the optimum ω [4], [32].

The iterations, or sweeps, are continued until some convergence criterion is satisfied. A common criterion is

$$\text{Max} \left| u_{m+1}(i,j) - u_m(i,j) \right| < \varepsilon, \qquad \text{(I-6)}$$

where the maximum is taken over all mesh points.

From the above, it appears that convergence depends on the initial $u_o(i,j)$, the relaxation factor ω, and the specified cyclic order. However, the general question of convergence depends on the properties of the system of

equations specified by (I-2). The system represented in matrix form is

$$Au = B. \tag{I-7}$$

The matrix A may be expressed as the sum

$$A = T_D - T_L - T_U, \tag{I-8}$$

where T_D is the diagonal of A such that $\left|T_D\right|^{-1} \neq 0$, T_L and T_U are respectively strictly lower and upper triangular matrices, whose entries are the negatives of the entries of A below and above the main diagonal. A necessary and sufficient condition for convergence is that all the roots of the polynomial,

$$P(\lambda) = \left|(\lambda + \omega - 1)T_D - \omega(\lambda T_L + T_U)\right| = 0, \tag{I-9}$$

have modulus less than one [33].[4]

The method may also be applied to the general quasi-linear second-order equation,

$$Au_{xx} + Bu_{xy} + Cu_{yy} + Du_x + Eu_y + F = 0, \tag{I-10}$$

where A, B, C, D, E, and F are functions of u, u_x, u_y, x, and y. In this latter example, the $(m+1)^{th}$ sweep considers the equation

$$A_m u_{xx} + B_m u_{xy} + C_m u_{yy} + D_m u_x + E_m u_y + F_m = 0, \tag{I-11}$$

---

[4]Condition follows from Varga [33], Section 3.4, page 75. Presented in this form by C. S. Duris, class notes, Math 852, Winter Term, 1965.

where the subscript m denotes that these coefficients are evaluated at each iteration as functions of u_m, x, and y. The above method is applied with this additional consideration that as $m \rightarrow \infty$, the solution to (I-11) converges to the solution to (I-10). At the present time, general theorems giving the conditions for convergence are not available.

APPENDIX II

NEWTON-RAPHSON ITERATIVE METHOD FOR SOLVING A NON-LINEAR EQUATION

The general problem is to find the solution or zeros of the equation

$$f(x) = 0. \qquad \text{(II-1)}$$

In general f(x) is a non-linear function, and the problem reduces to that of finding the zeros of (II-1) through some iterative sequence. The Newton-Raphson iterative method is a procedure for determining a single root ξ if an initial estimate of the root is near enough to ξ.

The technique may be applied to either real or complex roots. However, in the following the interest is only in determining a single real root. In this case, the method corresponds to using the tangent to the curve f(x), at the last determined point $[x_i, f(x_i)]$ to evaluate a new approximation x_{i+1}. From Figure 16, it is observed that the new approximation to x_{i+1}, according to the tangent approximation, is

$$x_{i+1} = x_i - \frac{f(x_i)}{f'(x_i)}. \qquad \text{(II-2)}$$

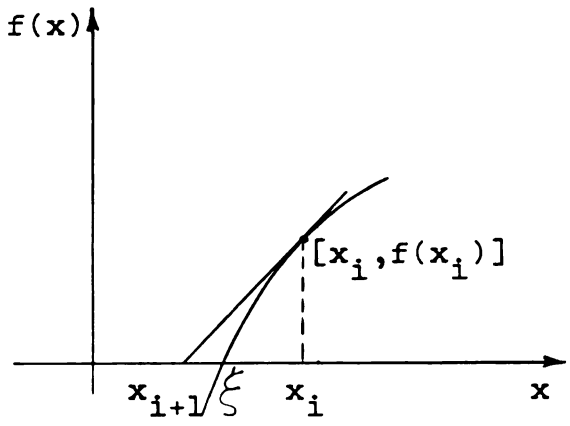

Figure 16. Estimation of new approximation by tangent

A more detailed discussion of the properties of (II-2) and the iterative method may be obtained from Todd [32] and Hildebrand [10]. However, the convergence is dependent on the error of the initial approximation. Figure 16 illustrates that if this approximation is near enough to the root ξ, then the method will always converge.

If the method converges to ξ, and k is taken sufficiently large, then the error at the k + 1 iteration is [10]

$$(\xi - x_{k+1}) \approx -\frac{1}{2}\frac{f''(\xi)}{f'(\xi)}(\xi - x_k)^2. \qquad \text{(II-3)}$$

Thus, the error in x_{k+1} is proportional to the square of the error in x_k. Iterative methods having this property are called second-order processes and should provide reasonable convergence rates.

APPENDIX III

BASIC FLOW CHART PATTERNS

The basic flow pattern for each program is shown in the following flow charts. The details of the calculations may be obtained by examining the equations listed on each flow chart. Additional information on the specific equation of each program is contained in the program listings of Appendix IV.

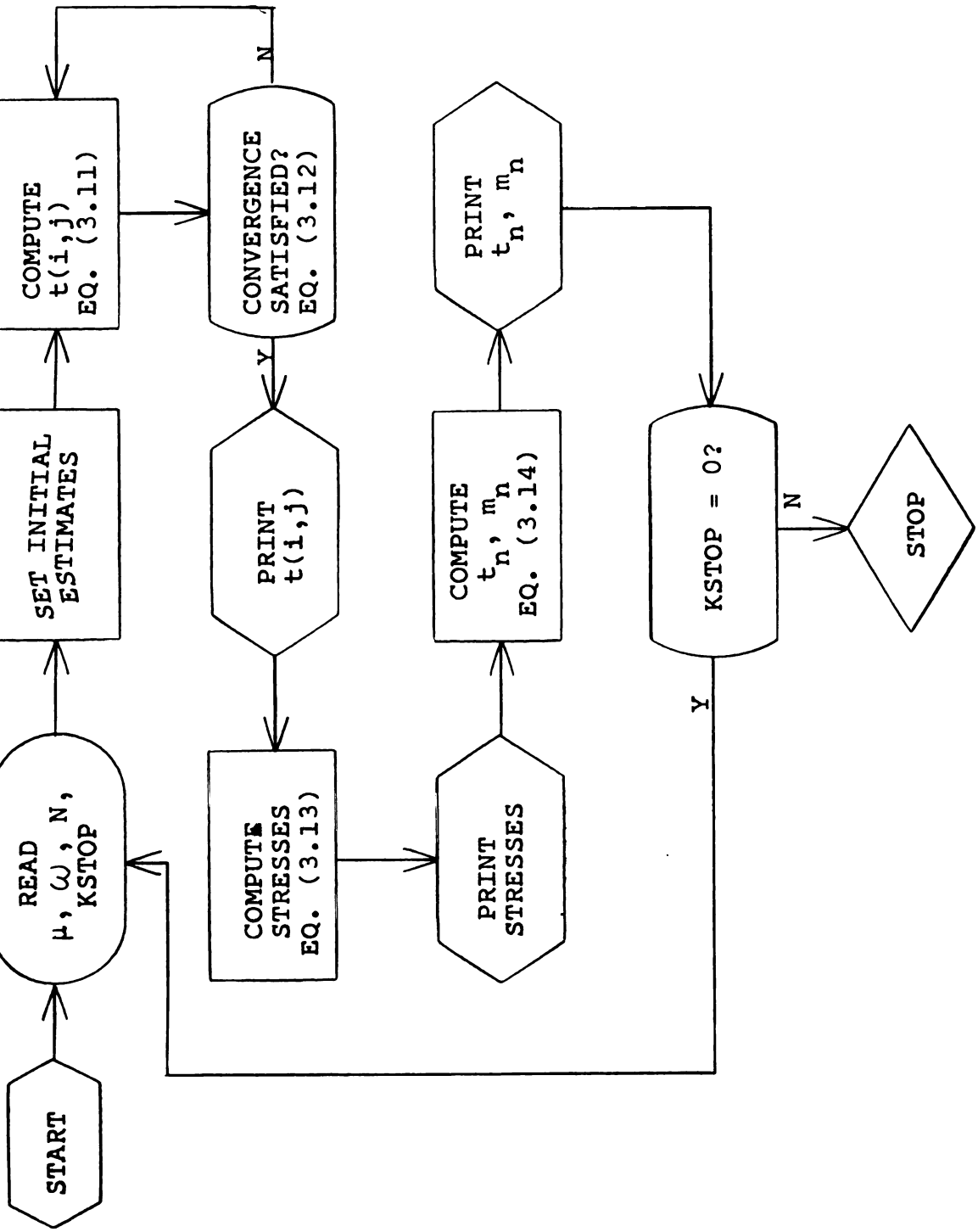

Figure 17. Basic flow chart pattern for program WARPI

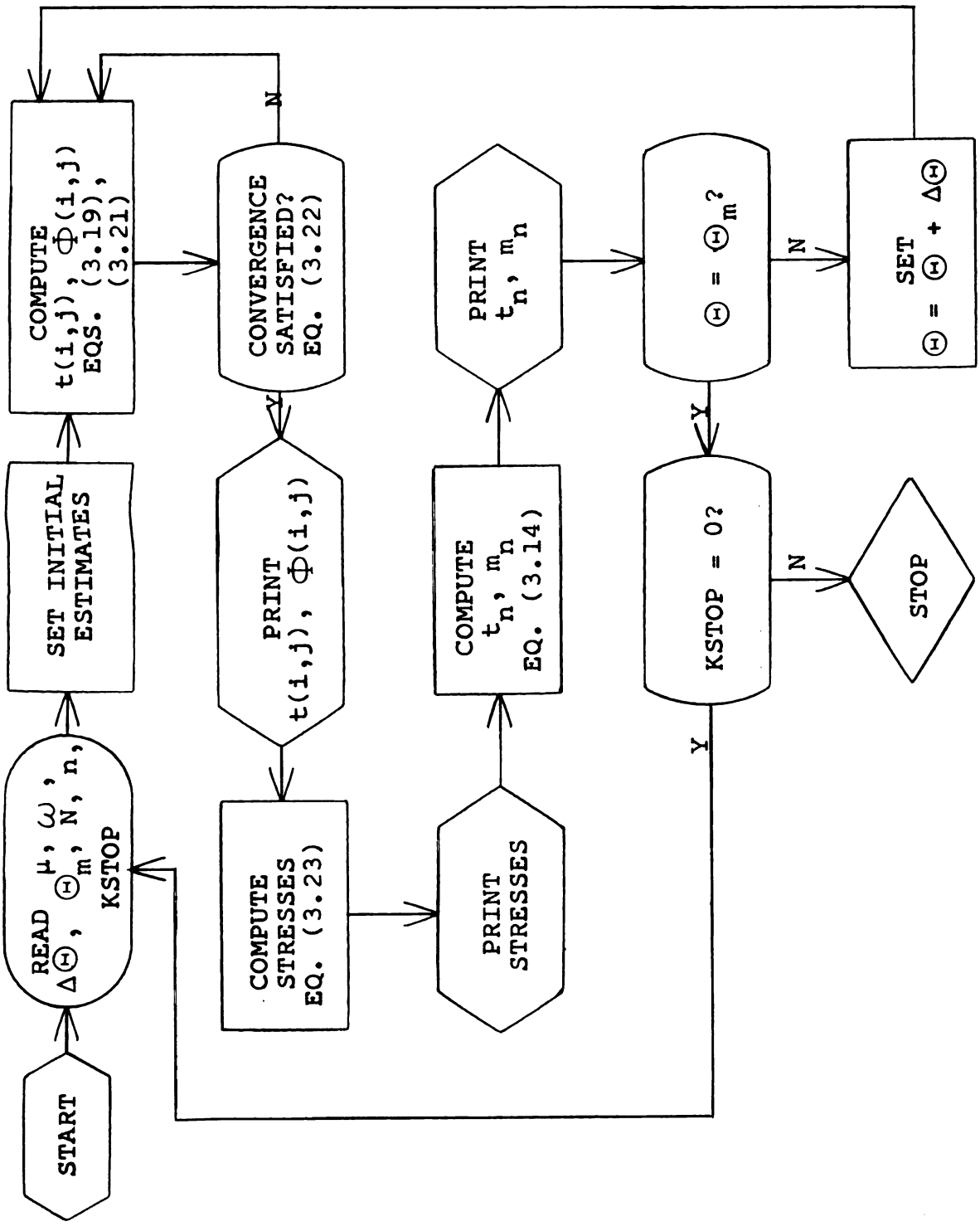

Figure 18. Basic flow chart pattern for program WARPO

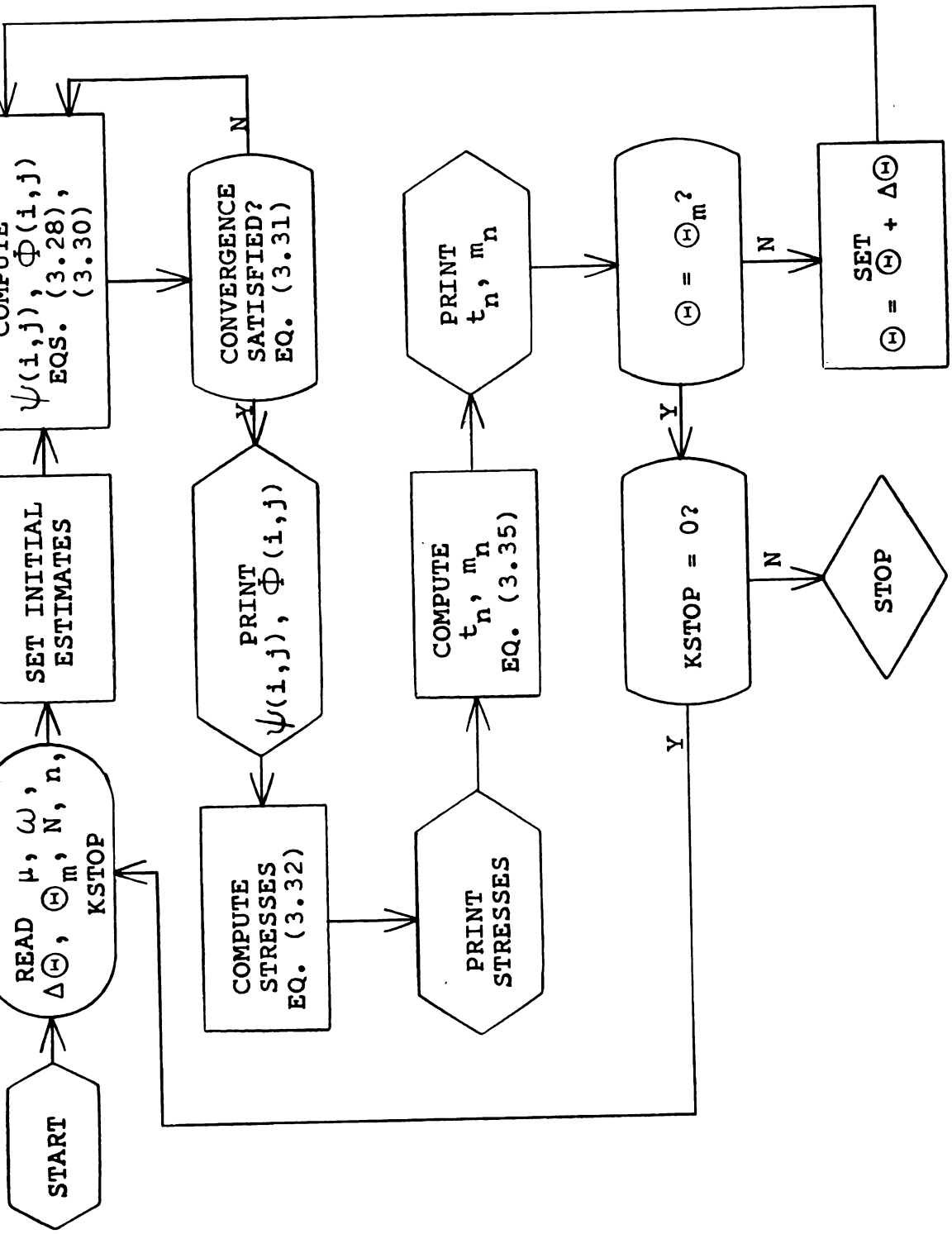

Figure 19. Basic flow chart pattern for program STRO

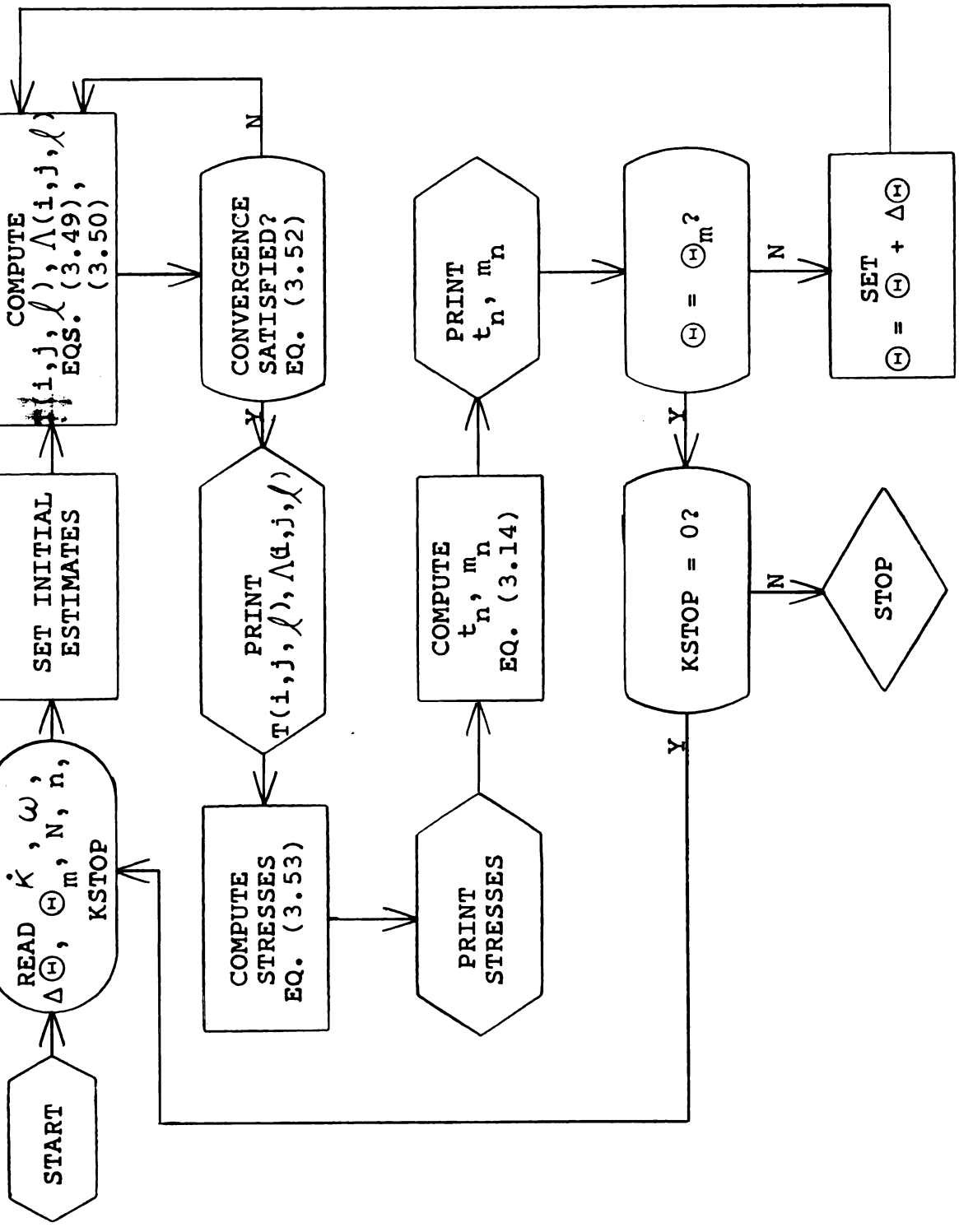

Figure 20. Basic flow pattern for program WARPLV

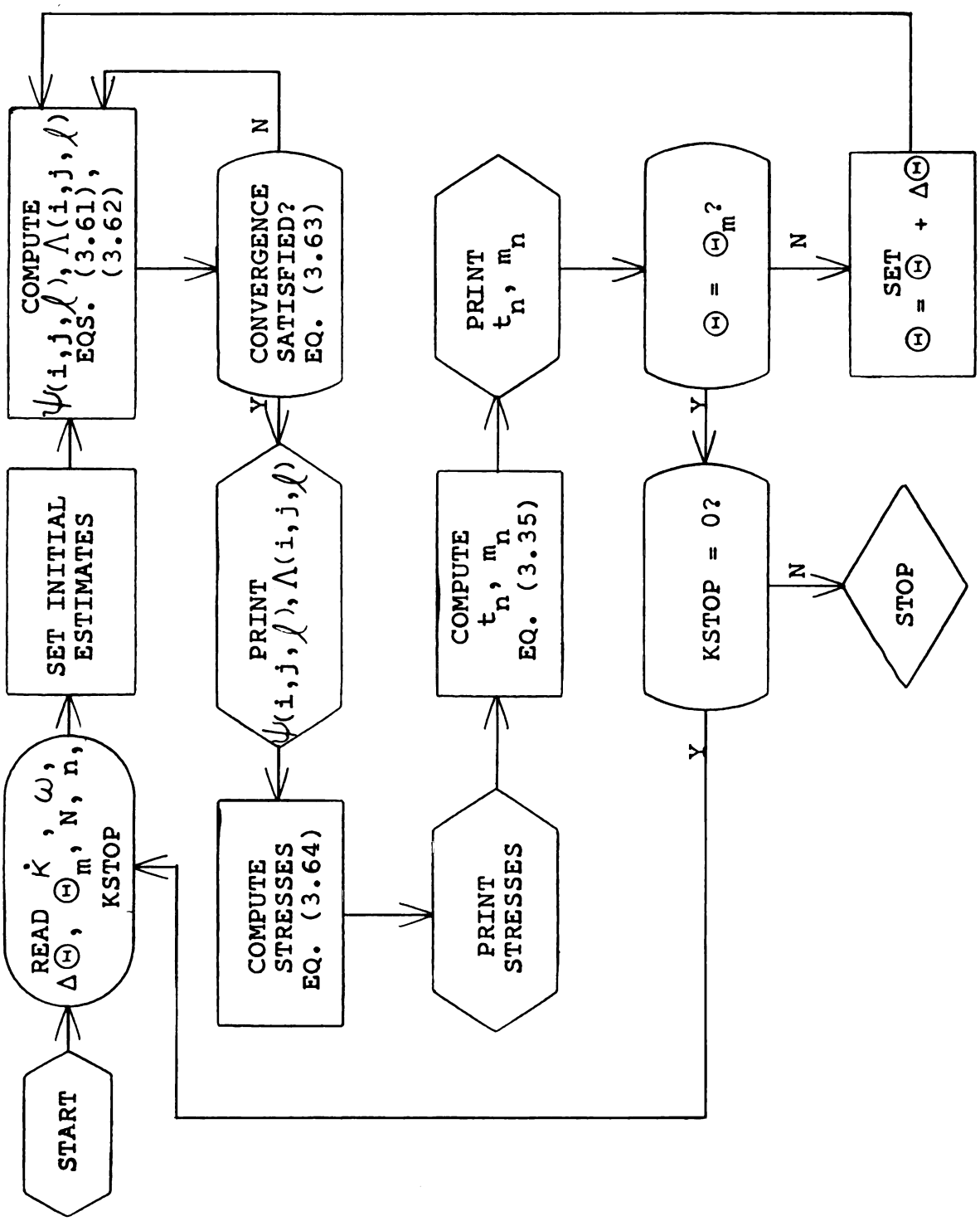

Figure 21. Basic flow chart pattern for program STPLDT

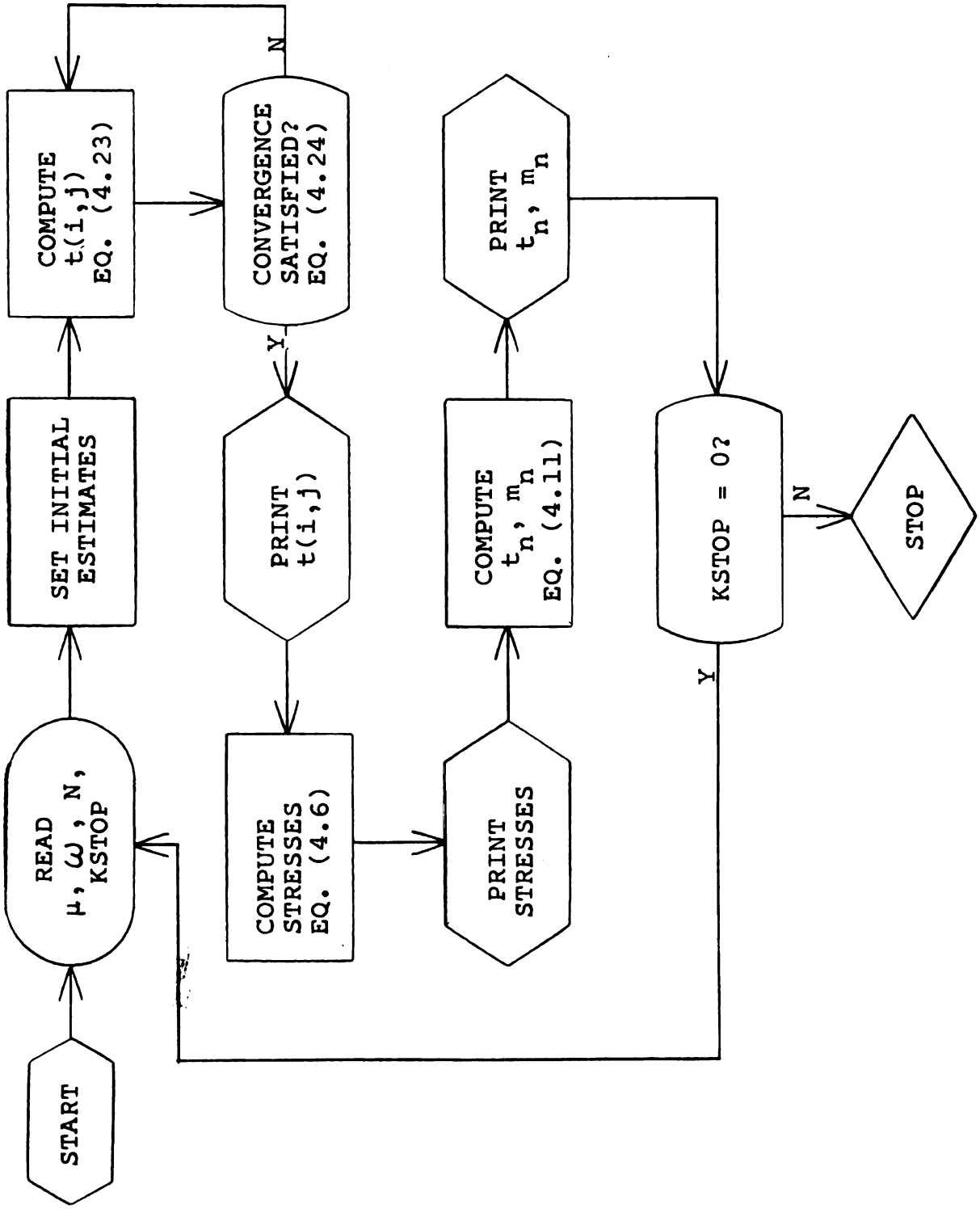

Figure 22. Basic flow chart pattern for program POLARR

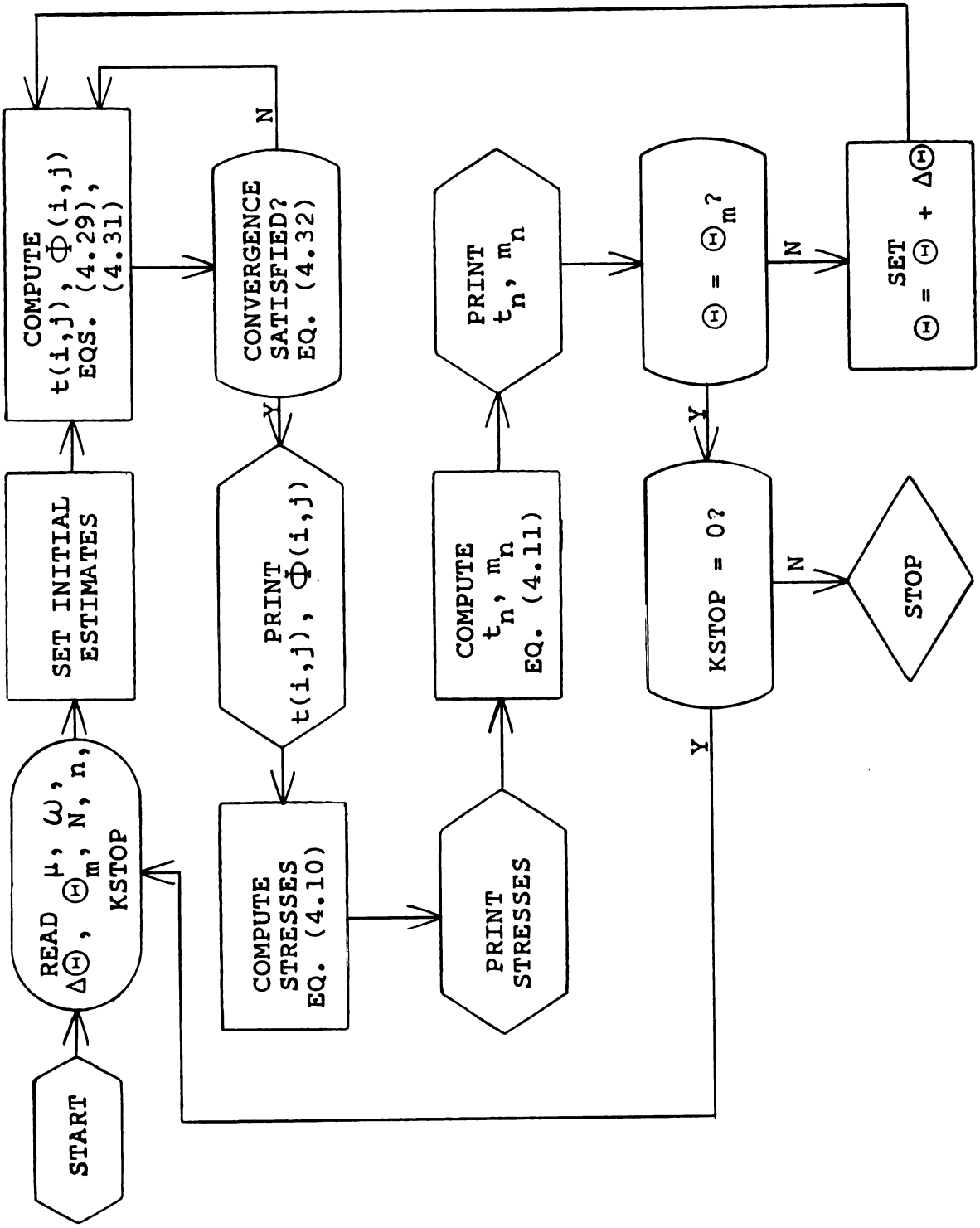

Figure 23. Basic flow chart pattern for program POLARO

APPENDIX IV

FORTRAN PROGRAMS

The listings for all FORTRAN programs are provided in this appendix. The purpose of each program and the page listings are as follows. WARPI (pages 148-50) solves the Piechnik equation for a unit square section. WARPO (pages 151-54) solves the warping-function deformation-theory equations for a unit square cross section. STRO (pages 155-58) solves the stress-function deformation-theory equations for a unit square cross section. WAPPLV (pages 159-63) solves the warping-function deformation-theory equations for a unit square cross section. STPLDT (pages 164-67) solves the stress-function deformation-theory equations for a unit square cross section. POLARR (pages 168-70) solves the Piechnik equation for a unit radial cross section. POLARO (pages 171-72) solves the warping-function deformation-theory equation for a unit radial cross section.

All programs follow the coordinate representation of Piechnik [24] while the theory follows Hill [12]. Program variable names generally agree with those of the theory. Major exceptions are T for ψ, LAMDA for Φ, and TAU for the shear stresses.

```
      PROGRAM WARPI
      TYPE REAL  LAMDA
      DIMENSION T(25,25),T1(25,25),T2(25,25),SIGMAZ(25,25),TAUYZ(25,25),
     $ TAUXZ(25,25)
    1 READ 3,PHI,BETA,N,ITER,KSTOP
    3 FORMAT(2F10.5,3I5)
      H = 0.5 / (N-1.)   $   IT = 1   $   E1 = 1.E-6   $   PHI = PHI**2
      DO 5 I=1,N    $   DO 5 J=1,N
      SIGMAZ(I,J) = 0.0   $   TAUYZ(I,J) = 0.0    $   TAUXZ(I,J) = 0.0
      T1(I,J) = 0.0   $   T2(I,J) = 0.0
    5 T(I,J) = 0.0
    6 DO 99 I =1,N          $    DO 99 J=1,N
      CHI = (I-1)*H   $   ETA = (J-1)*H
      IF(I-1)17,99,17
   17 IF(I-N)21,19,21
   19 IF(J-N)25,23,25
CASE   I=N   J=N
   23 T(I,J) = (T(I-1,J)+T(I,J-1))/2.       $   GO TO 99
   25 IF(J-1)35,99,35
CASE   I=N   J NOT =1 OR N
   35 SX = (3*T(I,J)-4*T(I-1,J)+T(I-2,J))/(2*H)
      SY = (T(I,J+1)-T(I,J-1))/(2*H)
      A = 3*PHI*ETA**2
      B = 0.0
      C = 3*PHI*ETA**2 + (SY-CHI)**2
      D = -3*PHI*ETA*H/2   $   E = 3*PHI*ETA*CHI*H**2
      T(I,J)= (2*C*(T(I-1,J)-H*ETA)+(A+D)*T(I,J+1)+(A-D)*T(I,J-1)-B+E)/
     $   (2*(A+C))
      GO TO 99
   21 IF(J-1)29,99,29
   29 IF(J-N)31,33,31
CASE   I NOT = 1 OR N   J=N
   33 SX = (T(I+1,J)+T(I-1,J))/(2*H)
      SY = (3*T(I,J)-4*T(I,J-1)+T(I,J-2))/(2*H)
      A = 3*PHI*ETA**2 + (SX+ETA)**2        $   B = 0.0
      C = 3*PHI*ETA**2
      D = -3*PHI*ETA*H/2   $   E = 3*PHI*ETA*CHI*H**2
      T(I,J) = (C*(T(I+1,J)+T(I-1,J))+(A+D)*(2*H*CHI+T(I,J-1))
     $ +(A-D)*T(I,J-1)+B+E)/(2*(A+C))
      GO TO 99
CASE I NOT = 1 OR N   J NOT = 1 OR N
   31 SX = (T(I+1,J)-T(I-1,J))/(2*H)
      SY = (T(I,J+1)-T(I,J-1))/(2*H)
      A = 3*PHI*ETA**2 + (SX+ETA)**2
      B = -(SX+ETA)*(SY-CHI)/2.
      C = 3*PHI*ETA**2 + (SY-CHI)**2
      D = -3*PHI*ETA*H/2   $   E = 3*PHI*ETA*CHI*H**2
      T(I,J) = (C*(T(I+1,J)+T(I-1,J))+(A+D)*T(I,J+1)+(A-D)*T(I,J-1)+
     $  B*(T(I+1,J+1)-T(I+1,J-1)-T(I-1,J+1)+T(I-1,J-1))+E)/(2*(A+C))
   99 CONTINUE        $   X = 0.0
      DO 301 I=1,N          $    DO 301 J=1,N
      A1 = ABSF(ABSF(T(I,J))-ABSF(T2(I,J)))
      IF(A1-X)301,305,305
```

```
  305 X=A1
  301 CONTINUE
      IF(X-E1)200,51,51
   51 DO 53 I=1,N        $   DO 53 J=1,N
      T2(I,J) = T(I,J)
      T1(I,J) = T1(I,J) + BETA*(T(I,J)-T1(I,J))
   53 T(I,J) = T1(I,J)
      IT = IT + 1  $  IF(IT-ITER)6,400,400
  200 PRINT 201,IT,BETA,PHI,((T(I,J),I=1,N),J=1,N)
  201 FORMAT (1H1,*  T(I,J) VALUES FOR ITERATION * , I10,//* RELAXATION
     $FACTOR  *,F10.5,*  PHI VALUE *,F10.5,//(7E17.8 ))
      GO TO 112
  400 PRINT 401,IT,BETA,PHI
  401 FORMAT(1H1,*  FAILED TO CONVERGE AFTER * ,I10,*ITERATIONS*
     $ ///*    BETA EQUAL*,F10.5,*  PHI EQUAL*,F10.5)
      GO TO 105
  112 DO 199 I=1,N       $  DO 199 J=1,N
      CHI = (I-1)*H  $  ETA = (J-1)*H
      IF(I-1)117,107,117
  107 IF(J-1)109,199,109
C   CASE I=1   J=1
  110 SX = T(I+1,J)/H
      SY = T(I,J+1)/H     $   GO TO 151
  109 IF(J-N)111,113,111
C   CASE I=1  J NOT = 1 OR N
  111 SX = T(I+1,J)/H
      SY  =  (T(I,J+1)-T(I,J-1))/(2*H)      $   GO TO 151
C   CASE I=1  J=N
  113 SX = T(I+1,J)/H
      SY = CHI
      GO TO 151
  117 IF(I-N)121,119,121
  119 IF(J-N)125,123,125
C   CASE   I =N  J=N
  123 SX = - ETA
      SY = CHI
      GO TO 151
  125 IF(J-1)135,137,135
C   CASE  I=N  J=1
  137 SX = - ETA
      SY = T(I,J+1)/H
      GO TO 151
C   CASE  I=N  J NOT = 1 OR N
  135 SX = - ETA
      SY = (  T(I,J+1)-  T(I,J-1))/(2*H)
      GO TO 151
  121 IF(J-1)129,127,129
C   CASE I NOT = 1 OR N  J=1
  127 SX = (  T(I+1,J)-  T(I-1,J))/(2*H)
      SY = T(I,J+1)/H
      GO TO 151
  129 IF(J-N)131,133,131
C    CASE  I NOT = 1 OR N   J=N
```

```
133 SX = (  T(I+1,J)-  T(I-1,J))/(2*H)
    SY = CHI
    GO TO 151
:   CASE  I NOT = 1 OR N   J NOT = 1 OR N
131 SX = (  T(I+1,J)-  T(I-1,J))/(2*H)
    SY = (  T(I,J+1)-  T(I,J-1))/(2*H)
151 LAMDA = SQRTF( 2.25*PHI*ETA**2 + 0.75*(SY**2-2*CHI*SY+CHI**2 +
   $ SX**2 + 2*ETA*SX + ETA**2))
    SIGMAZ(I,J) = 1.5*SQRTF(PHI)*ETA/LAMDA
    TAUXZ(I,J) =(0.5*(SX+ETA)/LAMDA)*SQRTF(3.)
    TAUYZ(I,J) =(0.5*(SY-CHI)/LAMDA)*SQRTF(3.)
199 CONTINUE
    PRINT 411,((SIGMAZ(I,J),I=1,N),J=1,N)
411 FORMAT(1H0,*   SIGMA Z STRESSES*//(7E17.8))
    PRINT 413,((TAUXZ(I,J),I=1,N),J=1,N)
413 FORMAT(1H0,*   TAU  XZ STRESSES* // (7E17.8))
    PRINT 415,((TAUYZ(I,J),I=1,N),J=1,N)
415 FORMAT(1H0,*   TAU  YZ STRESSES* //(7E17.8))
900 DO 911 I=1,N
    DO 911 J=1,N
    CHI = (I-1)*H  $   ETA = (J-1)*H
    T1(I,J) = ETA*SIGMAZ(I,J)
911 T(I,J) = ETA*TAUXZ(I,J) - CHI*TAUYZ(I,J)
    TORQ = 0.0   $  BEMO = 0.0
    DO 901 I=2,N,2
    DO 901 J=2,N,2
    TORQ = TORQ + T(I-1,J-1)+T(I+1,J-1)+T(I-1,J+1) + 4.*(T(I,J-1)+
   $ T(I+1,J)+T(I,J+1)+T(I-1,J)) + 16.*T(I,J)  +T(I+1,J+1)
901 BEMO = BEMO + T1(I-1,J-1)+T1(I+1,J-1)+T1(I+1,J+1)+T1(I-1,J+1)
   $ + 4.*(T1(I,J-1)+T1(I+1,J)+T1(I,J+1)+T1(I-1,J)) + 16.*T1(I,J)
    HSQ = (H**2)/9.
    TORQ = 12*TORQ*HSQ
    BEMO = 16.*HSQ*BEMO
    PRINT 903,TORQ,BEMO
903 FORMAT(1H0,*   TORQUE EQUALS  *,F10.8,*   BENDING MOMENT EQUALS  *
   $ ,F10.8)
105 IF(KSTOP)215, 1 ,215
215 STOP  $ END
```

```
      PROGRAM WARPO
      TYPE REAL LAMDA,J2,LAMDAX,LAMDAY
      DIMENSION T(25,25),LAMDA(25,25),T1(25,25),J2(25,25)
     $ ,SIGMAZ(25,25),TAUXZ(25,25),TAUYZ(25,25)
     $ ,BEN(25,25),TOR(25,25)
    1 READ 3,PHI, BETA,DTHETA,THETAM,N,NE,ITER,KSTOP
    3 FORMAT (4F10.5,4I5)
      PRINT 4,NE,N,BETA,PHI
    4 FORMAT(1H1,*  DEFORMATION THEORY OUTPUT FOR NE EQUAL*,I5,*  N EQUA
     $L*,I5,* BETA EQUAL*,F6.3,*  MU EQUAL*,F6.3,/  ,
     $*  IT  THETA     TORQ     MOMENT   SIGMA 1  TAUXZ 1  TAUYZ 1  SIGMA
     $ 2  TAUXZ 2  TAUYZ 2  SIGMA 3  TAUXZ 3  TAUYZ 3*)
      M = N-1  $  H = 0.5/M   $  IT = 1  $  KP = 5  $  E1 = 1.E-7
      NE2 = 2*NE  $  NE2N1=   NE2 - 1 $  THETA = DTHETA
      PHI = PHI**2
      DO 5 I=1,N
      DO 5 J=1,N
      STN(I,J) = 0.0  $  STX(I,J) = 0.0  $  STY(I,J) = 0.0
      T(I,J) = 0.0  $  T1(I,J) = 0.0
      SIGMAZ(I,J) = 0.0   $  TAUXZ(I,J) = 0.0   $   TAUYZ(I,J) = 0.0
      J2(I,J) = 0.0
    5 LAMDA(I,J) = 1.0
  112 DO 199 I=1,N
      DO 199 J=1,N
      X = (I-1)*H  $  Y = (J-1)*H
      IF(I-1)117,107,117
  107 IF(J-1)109,199,109
  109 IF(J-N)111,113,111
C   CASE I=1  J NOT = 1 OR N
  111 SX = T(I+1,J)/H
      SY  =  (T(I,J+1)-T(I,J-1))/(2*H)
      J2(I,J) = (THETA**2)*(3.*PHI*Y**2 + (SX+Y)**2 + (SY-X)**2)
      LAMDA(I,J) = LAMDA(I,J) - (LAMDA(I,J)**NE2*(LAMDA(I,J)-1.) -
     $  J2(I,J)**NE) / (LAMDA(I,J)**NE2N1 *((2*NE+1)*LAMDA(I,J) - 2*NE))
      GO TO 199
C   CASE I=1  J=N
  113 SX = T(I+1,J)/H
      SY = X
      J2(I,J) = (THETA**2)*(3.*PHI*Y**2 + (SX+Y)**2 + (SY-X)**2)
      LAMDA(I,J) = LAMDA(I,J) - (LAMDA(I,J)**NE2*(LAMDA(I,J)-1.) -
     $  J2(I,J)**NE) / (LAMDA(I,J)**NE2N1 *((2*NE+1)*LAMDA(I,J) - 2*NE))
      GO TO 199
  117 IF(I-N)121,119,121
  119 IF(J-N)125,123,125
C   CASE  I=N   J=N
  123  TBAR  = (T(I-1,J)+T(I,J-1))/2.
      T(I,J) = T(I,J) + BETA*(TBAR - T(I,J))
      J2(I,J) = (THETA**2)*(3.*PHI*Y**2)
      LAMDA(I,J) = LAMDA(I,J) - (LAMDA(I,J)**NE2*(LAMDA(I,J)-1.) -
     $  J2(I,J)**NE) / (LAMDA(I,J)**NE2N1 *((2*NE+1)*LAMDA(I,J) - 2*NE))
      GO TO 199
  125 IF(J-1)135,137,135
C   CASE  I=N  J=1
  137 SX = -Y
```

```
      SY = T(I,J+1)/H
      J2(I,J) = (THETA**2)*(3.*PHI*Y**2 + (SX+Y)**2 + (SY-X)**2)
      LAMDA(I,J) = LAMDA(I,J) - (LAMDA(I,J)**NE2*(LAMDA(I,J)-1.) -
     $  J2(I,J)**NE) / (LAMDA(I,J)**NE2N1 *((2*NE+1)*LAMDA(I,J) - 2*NE))
      GO TO 199
C    CASE  I=N  J NOT = 1 OR N
  135 SY=(T(I,J+1)-T(I,J-1))/(2*H)
      LAMDAY = (LAMDA(I,J+1) - LAMDA(I,J-1))/(2*H)
      E = LAMDAY*(SY-X)*(H**2)
       TBAR  = (LAMDA(I,J)*(2*(T(I-1,J)-H*Y)+ T(I,J+1)+ T(I,J-1)) -E)
     $ /(4*LAMDA(I,J))
      T(I,J) = T(I,J) + BETA*(TBAR - T(I,J))
      J2(I,J) = (THETA**2)*(3.*PHI*Y**2 + (SY-X)**2)
      LAMDA(I,J) = LAMDA(I,J) - (LAMDA(I,J)**NE2*(LAMDA(I,J)-1.) -
     $  J2(I,J)**NE) / (LAMDA(I,J)**NE2N1 *((2*NE+1)*LAMDA(I,J) - 2*NE))
      GO TO 199
  121 IF(J-1)129,127,129
C   CASE I NOT = 1 OR N  J=1
  127 SX = (  T(I+1,J)-  T(I-1,J))/(2*H)
      SY = T(I,J+1)/H
      J2(I,J) = (THETA**2)*(3.*PHI*Y**2 + (SX+Y)**2 + (SY-X)**2)
      LAMDA(I,J) = LAMDA(I,J) - (LAMDA(I,J)**NE2*(LAMDA(I,J)-1.) -
     $  J2(I,J)**NE) / (LAMDA(I,J)**NE2N1 *((2*NE+1)*LAMDA(I,J) - 2*NE))
      GO TO 199
  129 IF(J-N)131,133,131
C   CASE   I NOT = 1 OR N     J=N
  133 SX = (T(I+1,J)-T(I-1,J))/(2*H)
      LAMDAX = (LAMDA(I+1,J) - LAMDA(I-1,J))/(2*H)
      E = LAMDAX*(SX+Y)*(H**2)
       TBAR  = (LAMDA(I,J)*(2*(T(I,J-1)+H*X)+T(I+1,J)+T(I-1,J))-E)
     $ /(4*LAMDA(I,J))
      T(I,J) = T(I,J) + BETA*(TBAR - T(I,J))
      J2(I,J) = (THETA**2)*(3.*PHI*Y**2 + (SX+Y)**2)
      LAMDA(I,J) = LAMDA(I,J) - (LAMDA(I,J)**NE2*(LAMDA(I,J)-1.) -
     $  J2(I,J)**NE) / (LAMDA(I,J)**NE2N1 *((2*NE+1)*LAMDA(I,J) - 2*NE))
      GO TO 199
C   CASE  I NOT = 1 OR N   J NOT = 1 OR N
  131 SX = (T(I+1,J)-T(I-1,J))/(2*H)
      SY = (T(I,J+1)-T(I,J-1))/(2*H)
      LAMDAX = (LAMDA(I+1,J) - LAMDA(I-1,J))/(2*H)
      LAMDAY = (LAMDA(I,J+1) - LAMDA(I,J-1))/(2*H)
      E =(LAMDAX*(SX+Y) + LAMDAY*(SY-X))*(H**2)
       TBAR  = (LAMDA(I,J)*(T(I+1,J)+ T(I,J+1)+ T(I-1,J)+ T(I,J-1)) -E)
     $ /(4*LAMDA(I,J))
      T(I,J) = T(I,J) + BETA*(TBAR - T(I,J))
      J2(I,J) = (THETA**2)*(3.*PHI*Y**2 + (SX+Y)**2 + (SY-X)**2)
      LAMDA(I,J) = LAMDA(I,J) - (LAMDA(I,J)**NE2*(LAMDA(I,J)-1.) -
     $  J2(I,J)**NE) / (LAMDA(I,J)**NE2N1 *((2*NE+1)*LAMDA(I,J) - 2*NE))
  199 CONTINUE
      IF(IT-ITER)17,17,411
   17 X = 0.0
      DO 61 I=1,N
      DO 61 J=1,N
```

```
      A1 = ABSF(ABSF( T(I,J))-ABSF(T1(I,J)))
      IF(A1-X)61,63,63
   63 X = A1
   61 CONTINUE
      IF(X-E1)400,16,16
   16 DO 51 I=1,N
      DO 51 J=1,N
   51 T1(I,J) =  T(I,J)
      IT = IT + 1    $    GO TO 112
  400 PRINT 401,IT,NE,THETA,PHI,BETA,((T(I,J),I=1,N),J=1,N)
  401 FORMAT(1H0,*   T(I,J) VALUES FOR ITERATION*,I10,*  NE EQUAL *
     $,I10,/*   THETA EQUAL *,F10.5,* PHI EQUAL *,F10.5,*  BETA EQUAL  *
     $,F10.5,/(7E17.8))
  404 PRINT 405, ((LAMDA(I,J),I=1,N),J=1,N)
  405 FORMAT(1H0,*   LAMDA VALUES* /(7E17.8))
      DO 317 I=1,N
      DO 317 J=1,N
  317 J2(I,J) = J2(I,J) / LAMDA(I,J)**2
      PRINT 407, ((J2(I,J),I=1,N),J=1,N)
  407 FORMAT(1H0,*   J2  VALUES * /(7E17.8))
C   COMPUTE NORMALIZED STRESSES
  200 DO 299 I=1,N
      DO 299 J=1,N
      X = (I-1)*H    $     Y = (J-1)*H
      IF(I-1)217,207,217
  207 IF(J-1)209,299,209
  209 IF(J-N)211,213,211
C    CASE I=1    J NOT = 1 OR N
  211 SX = T(I+1,J)/H
      SY = (T(I,J+1)-T(I,J-1))/(2*H)
      GO TO 251
C     CASE I=1    J=N
  213 SX = T(I+1,J)/H
      SY = X
      GO TO 251
  217 IF(I-N)221,219,221
  219 IF(J-N)225,223,225
C    CASE I=N    J=N
  223 SX = -Y
      SY = X
      GO TO 251
  225 IF(J-1)235,237,235
C    CASE  I=N    J=1
  237 SX = -Y
      SY = T(I,J+1)/H
      GO TO 251
C    CASE  I=N  J NOT = 1 OR N
  235 SX = -Y
      SY = (T(I,J+1)-T(I,J-1))/(2*H)
      GO TO 251
  221 IF(J-1)229,227,229
C    CASE I NOT = 1 OR N    J=1
  227 SX = (T(I+1,J)-T(I-1,J))/(2*H)
```

```
      SY = T(I,J+1)/H
      GO TO 251
  229 IF(J-N)231,233,231
C     CASE I NOT = 1 OR N    J=N
  233 SX = (T(I+1,J)-T(I-1,J))/(2*H)
      SY = X
      GO TO 251
C    CASE I NOT = 1 OR N     J NOT = 1 OR N
  231 SX = (T(I+1,J)-T(I-1,J))/(2*H)
      SY = (T(I,J+1)-T(I,J-1))/(2*H)
  251 SIGMAZ(I,J) = SQRTF(3.*PHI)*THETA*Y/LAMDA(I,J)
      TAUXZ(I,J) = THETA*(SX+Y)/LAMDA(I,J)
      TAUYZ(I,J) = THETA*(SY-X)/LAMDA(I,J)
  299 CONTINUE
 4001 PRINT 411,((SIGMAZ(I,J),I=1,N),J=1,N)
  411 FORMAT(1H0,*    SIGMA  Z STRESSES  * /(7E17.8))
      PRINT 413,((TAUXZ(I,J),I=1,N),J=1,N)
  413 FORMAT(1H0,*     TAU  XZ STRESSES  * /(7E17.8))
      PRINT 415,((TAUYZ(I,J),I=1,N),J=1,N)
  415 FORMAT(1H0,*     TAU  YZ STRESSES  */(7E17.8))
 4002 DO 911 I=1,N
      DO 911 J=1,N
      X = (I-1)*H    $    Y = (J-1)*H
      BEN(I,J) = SIGMAZ(I,J)*Y
  911 TOR(I,J) = Y*TAUXZ(I,J) - X*TAUYZ(I,J)
      TORQ = 0.0    $  BEMO = 0.0
  900 DO 901 I=2,N,2
      DO 901 J=2,N,2
      TORQ = TORQ + TOR(I-1,J-1)+TOR(I+1,J-1)+TOR(I-1,J+1)+
     $ TOR(I+1,J+1) + 4.*(TOR(I+1,J)+TOR(I,J+1)+TOR(I-1,J)
     $ +TOR(I,J-1)) + 16.*TOR(I,J)
  901 BEMO = BEMO + BEN(I-1,J-1)+BEN(I+1,J-1)+BEN(I-1,J+1)
     $ +BEN(I+1,J+1) + 4.*(BEN(I+1,J)+BEN(I,J+1)+BEN(I-1,J)
     $ + BEN(I,J-1)) + 16.*BEN(I,J)
      HSQ = H**2 /9.
      TORQ = 12.*TORQ*HSQ
      BEMO = 16.*HSQ*BEMO
      PRINT 903,TORQ,BEMO
  903 FORMAT(1H0,*     TORQUE EQUALS *,F10.8,*    BENDING MO-ENT EQUALS*,
     $ F10.8)
  500 THETA = THETA + DTHETA
      IF(THETA-THETAM)501,501,411
  501 IT = 1    $  GO TO 112
  411 IF(KSTOP)413,1,413
  413 STOP $ END
```

```
      PROGRAM STRO
      TYPE REAL LAMDA,J2,LAMDAX,LAMDAY
      DIMENSION T(25,25),LAMDA(25,25),T1(25,25),J2(25,25)
     $ ,SIGMAZ(25,25),TAUXZ(25,25),TAUYZ(25,25)
    1 READ 3,PHI, BETA,DTHETA,THETAM,N,NE,ITER,KSTOP,KODE
    3 FORMAT(4F10.5,5I5 )
      M = N-1  $  H = 0.5/M   $  IT = 1  $  KP = 5  $  E1 = 1.E-6
      NE2 = 2*NE  $  NE2N1=   NE2 - 1  $   PHI = PHI**2
      THETA = DTHETA       $   DO 5 I=1,N   $   DO 5 J=1,N
      T(I,J) = 0.0  $  T1(I,J) = 0.0
      SIGMAZ(I,J) = 0.0   $  TAUXZ(I,J) = 0.0   $   TAUYZ(I,J) = 0.0
      J2(I,J) = 0.0
    5 LAMDA(I,J) = 1.0
  112 DO 199 I=1,N        $    DO 199 J=1,N
      X = (I-1)*H  $  Y = (J-1)*H
      IF(I-1)117,107,117
  107 IF(J-1)109,1114,109
C    CASE  I=1  J=1
 1114 SX = 0.0    $   SY = 0.0
      E = (LAMDAX*SX + LAMDAY*SY + 2*THETA)*(H**2)/LAMDA(I,J)
       TBAR  = (T(I+1,J) + T(I,J+1) + T(I+1,J) + T(I,J+1) + E)/4.
      T(I,J) = T(I,J) + BETA*(TBAR - T(I,J))      $   GO TO 199
  109 IF(J-N)111,113,111
C   CASE I=1  J NOT = 1 OR N
  111 SX = 0.0
      SY  =  (T(I,J+1)-T(I,J-1))/(2*H)
      LAMDAX = 0.0
      LAMDAY = (LAMDA(I,J+1)-LAMDA(I,J-1))/(2*H)
      E = (LAMDAX*SX + LAMDAY*SY + 2*THETA)*(H**2)/LAMDA(I,J)
       TBAR  = (T(I+1,J) + T(I,J+1) + T(I+1,J) + T(I,J-1) + E)/4.
      T(I,J) = T(I,J) + BETA*(TBAR - T(I,J))
      J2(I,J) = 3*PHI*(Y**2)*(THETA**2) + (LAMDA(I,J)**2)*(SX**2 +SY**2)
      LAMDA(I,J) = LAMDA(I,J) - (LAMDA(I,J)**NE2*(LAMDA(I,J)-1.) -
     $  J2(I,J)**NE) / (LAMDA(I,J)**NE2N1 *((2*NE+1)*LAMDA(I,J) - 2*NE))
      GO TO 199
C   CASE I=1  J=N
  113 SX = 0.0
      SY = (3*T(I,J)-4*T(I,J-1)+T(I,J-2))/(2*H)
      J2(I,J) = 3*PHI*(Y**2)*(THETA**2) + (LAMDA(I,J)**2)*(SX**2 +SY**2)
      LAMDA(I,J) = LAMDA(I,J) - (LAMDA(I,J)**NE2*(LAMDA(I,J)-1.) -
     $  J2(I,J)**NE) / (LAMDA(I,J)**NE2N1 *((2*NE+1)*LAMDA(I,J) - 2*NE))
      GO TO 199
  117 IF(I-N)121,119,121
  119 IF(J-N)125,123,125
C   CASE  I=N   J=N
  123 SX = 0.0       $   SY =0.0
      J2(I,J) = 3*PHI*(Y**2)*(THETA**2) + (LAMDA(I,J)**2)*(SX**2 +SY**2)
      LAMDA(I,J) = LAMDA(I,J) - (LAMDA(I,J)**NE2*(LAMDA(I,J)-1.) -
     $  J2(I,J)**NE) / (LAMDA(I,J)**NE2N1 *((2*NE+1)*LAMDA(I,J) - 2*NE))
      GO TO 199
  125 IF(J-1)135,137,135
C   CASE  I=N  J=1
  137 SX = (3*T(I,J)-4*T(I-1,J)+T(I-2,J))/(2*H)
```

```
      SY = 0.0
      J2(I,J) = 3*PHI*(Y**2)*(THETA**2) + (LAMDA(I,J)**2)*(SX**2 +SY**2)
      LAMDA(I,J) = LAMDA(I,J) - (LAMDA(I,J)**NE2*(LAMDA(I,J)-1.) -
     $  J2(I,J)**NE) / (LAMDA(I,J)**NE2N1 *((2*NE+1)*LAMDA(I,J) - 2*NE))
      GO TO 199
C     CASE   I=N  J NOT = 1 OR N
  135 SX = (3*T(I,J)-4*T(I-1,J)+T(I-2,J))/(2*H)          $   SY = 0.0
      J2(I,J) = 3*PHI*(Y**2)*(THETA**2) + (LAMDA(I,J)**2)*(SX**2 +SY**2)
      LAMDA(I,J) = LAMDA(I,J) - (LAMDA(I,J)**NE2*(LAMDA(I,J)-1.) -
     $  J2(I,J)**NE) / (LAMDA(I,J)**NE2N1 *((2*NE+1)*LAMDA(I,J) - 2*NE))
      GO TO 199
  121 IF(J-1)129,127,129
C    CASE I NOT = 1 OR N  J=1
  127 SX = (  T(I+1,J)-  T(I-1,J))/(2*H)      $  SY = 0.0
      LAMDAX = (LAMDA(I+1,J) - LAMDA(I-1,J))/(2*H)
      LAMDAY = 0.0
      E = (LAMDAX*SX + LAMDAY*SY + 2*THETA)*(H**2)/LAMDA(I,J)
       TBAR  = (T(I+1,J) + T(I,J+1) + T(I-1,J) + T(I,J+1) + E)/4.
      T(I,J) = T(I,J) + BETA*(TBAR - T(I,J))
      J2(I,J) = 3*PHI*(Y**2)*(THETA**2) + (LAMDA(I,J)**2)*(SX**2 +SY**2)
      LAMDA(I,J) = LAMDA(I,J) - (LAMDA(I,J)**NE2*(LAMDA(I,J)-1.) -
     $  J2(I,J)**NE) / (LAMDA(I,J)**NE2N1 *((2*NE+1)*LAMDA(I,J) - 2*NE))
      GO TO 199
  129 IF(J-N)131,133,131
C    CASE    I NOT = 1 OR N     J=N
  133 SX = (T(I+1,J)-T(I-1,J))/(2*H)
      SY = (3*T(I,J) -4*T(I,J-1) + T(I,J-2))/(2*H)
      J2(I,J) = 3*PHI*(Y**2)*(THETA**2) + (LAMDA(I,J)**2)*(SX**2 +SY**2)
      LAMDA(I,J) = LAMDA(I,J) - (LAMDA(I,J)**NE2*(LAMDA(I,J)-1.) -
     $  J2(I,J)**NE) / (LAMDA(I,J)**NE2N1 *((2*NE+1)*LAMDA(I,J) - 2*NE))
      GO TO 199
C    CASE  I NOT = 1 OR N    J NOT = 1 OR N
  131 SX = (T(I+1,J)-T(I-1,J))/(2*H)
      SY = (T(I,J+1)-T(I,J-1))/(2*H)
      LAMDAX = (LAMDA(I+1,J) - LAMDA(I-1,J))/(2*H)
      LAMDAY = (LAMDA(I,J+1) - LAMDA(I,J-1))/(2*H)
      E = (LAMDAX*SX + LAMDAY*SY + 2*THETA)*(H**2)/LAMDA(I,J)
       TBAR  = (T(I+1,J) + T(I,J+1) + T(I-1,J) + T(I,J-1) + E)/4.
      T(I,J) = T(I,J) + BETA*(TBAR - T(I,J))
      J2(I,J) = 3*PHI*(Y**2)*(THETA**2) + (LAMDA(I,J)**2)*(SX**2 +SY**2)
      LAMDA(I,J) = LAMDA(I,J) - (LAMDA(I,J)**NE2*(LAMDA(I,J)-1.) -
     $  J2(I,J)**NE) / (LAMDA(I,J)**NE2N1 *((2*NE+1)*LAMDA(I,J) - 2*NE))
  199 CONTINUE
      IF(IT-ITER)17,17,411
   17 X = 0.0
      DO 61 I=1,N          $  DO 61 J=1,N
      A1 = ABSF(ABSF( T(I,J))-ABSF(T1(I,J)))
      IF(A1-X)61,63,63
   63 X = A1
   61 CONTINUE
      IF(X-E1)400,16,16
   16 DO 51 I=1,N
      DO 51 J=1,N
```

```
   51 T1(I,J) =  T(I,J)
      IT = IT + 1    $    GO TO 112
  400 PRINT 401,IT,NE,THETA,PHI,BETA,((T(I,J),I=1,N),J=1,N)
  401 FORMAT(1H0,*   T(I,J) VALUES FOR ITERATION*,I10,*  NE EQUAL *
     $,I10,/*   THETA EQUAL *,F10.5,* PHI EQUAL *,F10.5, *  BETA EQUALS*
     $,F10.5,/(7E17.8))
      IF(KODE)200,404,200
  404 PRINT 405, ((LAMDA(I,J),I=1,N),J=1,N)
  405 FORMAT(1H0,*   LAMDA VALUES* /(7E17.8))
      DO 317 I=1,N          $    DO317 J=1,N
  317 J2(I,J) = J2(I,J) / LAMDA(I,J)**2
      PRINT 407, ((J2(I,J),I=1,N),J=1,N)
  407 FORMAT(1H0,*   J2  VALUES * /(7E17.8))
C   COMPUTE NORMALIZED STRESSES
  200 DO 299 I=1,N
      DO 299 J=1,N
      X = (I-1)*H    $     Y = (J-1)*H
      IF(I-1)217,207,217
  207 IF(J-1)209,299,209
  209 IF(J-N)211,213,211
C    CASE I=1    J NOT = 1 OR N
  211 SX = 0.0
      SY = (T(I,J+1)-T(I,J-1))/(2*H)
      GO TO 251
C     CASE I=1    J=N
  213 SX = 0.0
      SY = (3*T(I,J) -4*T(I,J-1) +T(I,J-2))/(2*H)
      GO TO 251
  217 IF(I-N)221,219,221
  219 IF(J-N)225,223,225
C    CASE I=N    J=N
  223 SX = 0.0  $    SY = 0.0
      GO TO 251
  225 IF(J-1)235,237,235
C    CASE  I=N    J=1
  237 SX = (3*T(I,J) -4*T(I-1,J) + T(I-2,J))/(2*H)
      SY = 0.0
      GO TO 251
C    CASE  I=N  J NOT = 1 OR N
  235 SX = (3*T(I,J) -4*T(I-1,J)+T(I-2,J))/(2*H)
      SY = 0.0
      GO TO 251
  221 IF(J-1)229,227,229
C    CASE I NOT = 1 OR N    J=1
  227 SX = (T(I+1,J)-T(I-1,J))/(2*H)
      SY = 0.0
      GO TO 251
  229 IF(J-N)231,233,231
C    CASE I NOT = 1 OR N    J=N
  233 SX = 0.0
      SY = (3*T(I,J) -4*T(I,J-1)+T(I,J-2))/(2*H)
      GO TO 251
```

```
C   CASE I NOT = 1 OR N     J NOT = 1 OR N
  231 SX = (T(I+1,J)-T(I-1,J))/(2*H)
      SY = (T(I,J+1)-T(I,J-1))/(2*H)
  251 SIGMAZ(I,J) = SQRTF(3.*PHI)*THETA*Y/LAMDA(I,J)
      TAUXZ(I,J) = -SY
      TAUYZ(I,J) =  SX
  299 CONTINUE
      IF(KODE)5000,5110,5000
 5110 PRINT 511,((SIGMAZ(I,J),I=1,N),J=1,N)
  511 FORMAT(1H0,*   SIGMA  Z STRESSES  * /(7E17.8))
      PRINT 413,((TAUXZ(I,J),I=1,N),J=1,N)
  413 FORMAT(1H0,*     TAU  XZ STRESSES  * /(7E17.8))
      PRINT 415,((TAUYZ(I,J),I=1,N),J=1,N)
  415 FORMAT(1H0,*     TAU  YZ STRESSES  */(7E17.8))
 5000 DO 911 I=1,N
      DO 911 J=1,N
      X = (I-1)*H    $    Y = (J-1)*H
      SIGMAZ(I,J) = Y*SIGMAZ(I,J)
  911 TAUXZ(I,J) = Y*TAUXZ(I,J) - X*TAUYZ(I,J)
      TORQ = 0.0    $  BEMO = 0.0
      TORQ2 = 0.0
  900 DO 901 I=2,N,2
      DO 901 J=2,N,2
      TORQ2 = TORQ2 + T(I-1,J-1)+T(I-1,J+1)+T(I+1,J-1)+T(I+1,J+1)
     $ + 4*(T(I+1,J)+T(I,J+1)+T(I-1,J)+T(I,J-1)) + 16*T(I,J)
      TORQ = TORQ + TAUXZ(I-1,J-1)+TAUXZ(I+1,J-1)+TAUXZ(I-1,J+1)+
     $ TAUXZ(I+1,J+1) + 4.*(TAUXZ(I+1,J)+TAUXZ(I,J+1)+TAUXZ(I-1,J)
     $  +TAUXZ(I,J-1)) +  16.*TAUXZ(I,J)
  901 BEMO = BEMO + SIGMAZ(I-1,J-1)+SIGMAZ(I+1,J-1)+SIGMAZ(I-1,J+1)
     $  +SIGMAZ(I+1,J+1) + 4.*(SIGMAZ(I+1,J)+SIGMAZ(I,J+1)+SIGMAZ(I-1,J)
     $ + SIGMAZ(I,J-1)) + 16.*SIGMAZ(I,J)
      HSQ = H**2 /9.
      TORQ2 = 24.*TORQ2*HSQ
      TORQ = 12.*TORQ*HSQ
      BEMO = 16.*HSQ*BEMO
      PRINT 903,TORQ,BEMO,TORQ2
  903 FORMAT(1H0,*     TORQUE EQUALS *,F10.8,*    BENDING MOMENT EQUALS*,
     $ F10.8,*  TORQ2 EQUALS  * ,F10.8)
  500 THETA = THETA + DTHETA
      IF(THETA-THETAM)501,501,411
  501 IT = 1    $  GO TO 112
  411 IF(KSTOP)413,1,413
  413 STOP $ END
```

```
      PROGRAM WARPLV
      TYPE REAL LAMDA,J2,LAMDAX,LAMDAY,J21,LAMDA1
      DIMENSION T(25,25),LAMDA(25,25),T1(25,25),J2(25,25),LAMDA1(25,25)
     $ ,SIGMAZ(25,25),TAUXZ(25,25),TAUYZ(25,25),TOR(25,25)
     $ ,J21(25,25),TAUXZ1(25,25),TAUYZ1(25,25),SIGMAZ1(25,25),BEN(25,25)
    1 READ 3,PHI, BETA,DTHETA,THETAM,N,NE,ITER,KPS,KSTOP
    3 FORMAT(4F10.5,5I5 )
      READ 4, PHI1,THETA1,DTHETA1,KPS1
    4 FORMAT (3F10.5,I5)
      M = N-1  $  H = 0.5/M   $  IT = 1  $  KP = 1  $  E1 8 1.E-8
      NE2 = 2*NE  $  NE2N1=   NE2 - 1    $  NEN1 = NE - 1
      E2 = 1.E-4   $   KODE = 0
      THETA = DTHETA  $  PHI = PHI**2  $   PHI1 = PHI1**2
      DO 5 I=1,N
      DO 5 J=1,N
      T(I,J) = 0.0  $  T1(I,J) = 0.0 $  TAUYZ1(I,J) = 0.0
      SIGMAZ1(I,J) = 0.0  $   LAMDA1(I,J) = 0.0
      SIGMAZ(I,J) = 0.0   $  TAUXZ(I,J) = 0.0   $   TAUYZ(+,J) = 0.0
      J2(I,J) = 0.0  $  J21(I,J) = 0.0  $  TAUXZ1(I,J) = 0.0
    5 LAMDA(I,J) = 1.0
      PRINT 80,NE,PHI,DTHETA
   80 FORMAT(1H1,*   WARPING FUNCTION FLOW THEORY CALCULATIONS FOR NE EQ
     $UAL *,I10,  * PHI EQUAL*,F10.5,*  DTHETA EQUAL *,F10.5)
  112 DO 199 I=1,N
      DO 199 J=1,N
      X = (I-1)*H  $  Y = (J-1)*H
      IF(I-1)117,107,117
  107 IF(J-1)109,199,109
  109 IF(J-N)111,113,111
C   CASE I=1  J NOT = 1 OR N
  111 SX = T(I+1,J)/H
      SY  =  (T(I,J+1)-T(I,J-1))/(2*H)
      GO TO 169
C   CASE I=1  J=N
  113 SX = T(I+1,J)/H
      SY = X*DTHETA
      GO TO 169
  117 IF(I-N)121,119,121
  119 IF(J-N)125,123,125
C   CASE  I=N   J=N
  123 SX = -DTHETA*Y
      SY = DTHETA*X
      DXTXZ = (3.*TAUXZ1(I,J) -4.*TAUXZ1(I-1,J) + TAUXZ1(I-2,J))/(2*H)
      DYTYZ = (3.*TAUYZ1(I,J) - 4.*TAUYZ1(I,J-1) + TAUYZ1(I,J-2))/(2*H)
      LAMDAX = (3.*LAMDA(I,J)-4.*LAMDA(I-1,J)+LAMDA(I-2,J))/(2*H)
      LAMDAY = (3.*LAMDA(I,J)-4.*LAMDA(I,J-1)+LAMDA(I,J-2))/(2*H)
      E = (DXTXZ + DYTYZ - (LAMDAX*((SX + DTHETA*Y) + TAUXZ1(I,J))
     $  + LAMDAY*((SY - DTHETA*X) + TAUYZ1(I,J)))/LAMDA(I,J))*(H**2)
       TBAR  = (2.*(T(I-1,J)-H*DTHETA*Y)+2.*(T(I,J-1)+H*DTHETA*X)+E)/4.
      T(I,J) = T(I,J) + BETA*(TBAR - T(I,J))
      GO TO 169
  125 IF(J-1)135,137,135
C   CASE  I=N  J=1
```

```
  137 SX = -Y*DTHETA
      SY = T(I,J+1)/H
      GO TO 169
C     CASE  I=N  J NOT = 1 OR N
  135 SX = -DTHETA*Y
      SY = (T(I,J+1) - T(I,J-1))/(2*H)
      DXTXZ = (3.*TAUXZ1(I,J) -4.*TAUXZ1(I-1,J) + TAUXZ1(I-2,J))/(2*H)
      DYTYZ = (TAUYZ1(I,J+1) - TAUYZ1(I,J-1))/(2*H)
      LAMDAX = (3.*LAMDA(I,J)-4.*LAMDA(I-1,J)+LAMDA(I-2,J))/(2*H)
      LAMDAY = (LAMDA(I,J+1) - LAMDA(I,J-1))/(2*H)
      E = (DXTXZ + DYTYZ - (LAMDAX*((SX + DTHETA*Y) + TAUXZ1(I,J))
     $  + LAMDAY*((SY - DTHETA*X) + TAUYZ1(I,J)))/LAMDA(I,J))*(H**2)
        TBAR  = (2.*(T(I-1,J)-H*DTHETA*Y)+T(I,J+1)+T(I,J-1)+E)/4.
      T(I,J) = T(I,J) + BETA*(TBAR - T(I,J))
      GO TO 169
  121 IF(J-1)129,127,129
C     CASE I NOT = 1 OR N  J=1
  127 SX = (  T(I+1,J)-  T(I-1,J))/(2*H)
      SY = T(I,J+1)/H
      GO TO 169
  129 IF(J-N)131,133,131
C     CASE   I NOT = 1 OR N     J=N
  133 SX = (T(I+1,J)-T(I-1,J))/(2*H)
      SY = DTHETA*X
      DXTXZ = (TAUXZ1(I+1,J) - TAUXZ1(I-1,J))/(2*H)
      DYTYZ = (3.*TAUYZ1(I,J) - 4.*TAUYZ1(I,J-1) + TAUYZ1(I,J-2))/(2*H)
      LAMDAX = (LAMDA(I+1,J) - LAMDA(I-1,J))/(2*H)
      LAMDAY = (3.*LAMDA(I,J)-4.*LAMDA(I,J-1)+LAMDA(I,J-2))/(2*H)
      E = (DXTXZ + DYTYZ - (LAMDAX*((SX + DTHETA*Y) + TAUXZ1(I,J))
     $  + LAMDAY*((SY - DTHETA*X) + TAUYZ1(I,J)))/LAMDA(I,J))*(H**2)
        TBAR  = (T(I+1,J)+T(I-1,J)+2.*(T(I,J-1)+H*DTHETA*X)+E)/4.
      T(I,J) = T(I,J) + BETA*(TBAR - T(I,J))
      GO TO 169
C     CASE  I NOT = 1 OR N   J NOT = 1 OR N
  131 SX = (T(I+1,J)-T(I-1,J))/(2*H)
      SY = (T(I,J+1) - T(I,J-1))/(2*H)
      DXTXZ = (TAUXZ1(I+1,J) - TAUXZ1(I-1,J))/(2*H)
      DYTYZ = (TAUYZ1(I,J+1) - TAUYZ1(I,J-1))/(2*H)
      LAMDAX = (LAMDA(I+1,J) - LAMDA(I-1,J))/(2*H)
      LAMDAY = (LAMDA(I,J+1) - LAMDA(I,J-1))/(2*H)
      E = (DXTXZ + DYTYZ - (LAMDAX*((SX + DTHETA*Y) + TAUXZ1(I,J))
     $  + LAMDAY*((SY - DTHETA*X) + TAUYZ1(I,J)))/LAMDA(I,J))*(H**2)
        TBAR  = (T(I+1,J) + T(I,J+1) + T(I-1,J) + T(I,J-1) + E)/4.
      T(I,J) = T(I,J) + BETA*(TBAR - T(I,J))
  169 J2(I,J) = (DTHETA*SQRTF(3.*PHI)*Y + SIGMAZ1(I,J))**2 + (SX+DTHETA*
     $ Y + TAUXZ1(I,J))**2 + (SY-DTHETA*X + TAUYZ1(I,J))**2
  170 IF(NEN1)173,171,173
  171 LAMDA(I,J) = LAMDA(I,J) - (LAMDA(I,J)**NE2*(LAMDA(I,J) - 1.) -
     $ ((NE2+1.)/2.)*(J2(I,J) - (LAMDA(I,J)**2)*J21(I,J)))
     $ / (LAMDA(I,J)**NE2N1*((2.*NE+1.)*LAMDA(I,J) - 2.*NE) + (2.*NE+1.)
     $ *J21(I,J)*LAMDA(I,J))
      GO TO 177
  173 LAMDA(I,J) = LAMDA(I,J) - (LAMDA(I,J)**NE2*(LAMDA(I,J) - 1.) -
```

```
     $ ((NE2+1.)/2.)*J2(I,J)**NEN1*(J2(I,J) - (LAMDA(I,J)**2)*J21(I,J)))
     $ / (LAMDA(I,J)**NE2N1*((2.*NE+1.)*LAMDA(I,J) - 2.*NE) + (2.*NE+1.)
     $ *(J2(I,J)**NEN1)*J21(I,J)*LAMDA(I,J))
  177 IF(ABSF(LAMDA(I,J) - LAMDA1(I,J)) - E2)199,175,175
  175 LAMDA1(I,J) = LAMDA(I,J)
      GO TO 170
  199 CONTINUE
      IF(IT-ITER)17,17,4111
   17 X = 0.0
      DO 61 I=1,N
      DO 61 J=1,N
      A1 = ABSF(ABSF( T(I,J))-ABSF(T1(I,J)))
      IF(A1-X)61,63,63
   63 X = A1
   61 CONTINUE
      IF(X-E1)400,16,16
   16 DO 51 I=1,N
      DO 51 J=1,N
   51 T1(I,J) =  T(I,J)
      IT = IT + 1    $    GO TO 112
  400 IF(KP-KPS)502,402,502
  502 DO 504 I=1,N
      DO 504 J=1,N
  504 J2(I,J) = J2(I,J)/LAMDA(I,J)**2
      GO TO 200
  402 PRINT 401,IT,NE,THETA,PHI,((T(I,J),I=1,N),J=1,N)
  401 FORMAT(1H0,*   T(I,J) VALUES FOR ITERATION*,I10,*  NE EQUAL *
     $,I10,/*    THETA EQUAL *,F10.5,* PHI EQUAL *,F10.5,/(7E17.8))
      PRINT 405, ((LAMDA(I,J),I=1,N),J=1,N)
  405 FORMAT(1H0,*   LAMBDA VALUES* /(7E17.8))
      DO 317 I=1,N
      DO 317 J=1,N
  317 J2(I,J) = J2(I,J) / LAMDA(I,J)**2
      PRINT 407, ((J2(I,J),I=1,N),J=1,N)
  407 FORMAT(1H0,*   J2  VALUES * /(7E17.8))
C    COMPUTE NORMALIZED STRESSES
  200 DO 299 I=1,N
      DO 299 J=1,N
      X = (I-1)*H    $     Y = (J-1)*H
      IF(I-1)217,207,217
  207 IF(J-1)209,299,209
  209 IF(J-N)211,213,211
C     CASE I=1    J NOT = 1 OR N
  211 SX = T(I+1,J)/H
      SY = (T(I,J+1)-T(I,J-1))/(2*H)
      GO TO 251
C       CASE I=1    J=N
  213 SX = T(I+1,J)/H
      SY = X*DTHETA
      GO TO 251
  217 IF(I-N)221,219,221
  219 IF(J-N)225,223,225
C     CASE I=N    J=N
```

```
  223 SX = -Y*DTHETA
      SY = X*DTHETA
      GO TO 251
  225 IF(J-1)235,237,235
C     CASE  I=N   J=1
  237 SX = -Y*DTHETA
      SY = T(I,J+1)/H
      GO TO 251
C     CASE  I=N  J NOT = 1 OR N
  235 SX = -Y*DTHETA
      SY = (T(I,J+1)-T(I,J-1))/(2*H)
      GO TO 251
  221 IF(J-1)229,227,229
C     CASE I NOT = 1 OR N   J=1
  227 SX = (T(I+1,J)-T(I-1,J))/(2*H)
      SY = T(I,J+1)/H
      GO TO 251
  229 IF(J-N)231,233,231
C     CASE I NOT = 1 OR N   J=N
  233 SX = (T(I+1,J)-T(I-1,J))/(2*H)
      SY = X*DTHETA
      GO TO 251
C    CASE I NOT = 1 OR N    J NOT = 1 OR N
  231 SX = (T(I+1,J)-T(I-1,J))/(2*H)
      SY = (T(I,J+1)-T(I,J-1))/(2*H)
  251 SIGMAZ(I,J) = (SQRTF(3.*PHI)*DTHETA*Y + SIGMAZ1(I,J))/LAMDA(I,J)
      TAUXZ(I,J) = (SX+DTHETA*Y + TAUXZ1(I,J))/LAMDA(I,J)
      TAUYZ(I,J) = (SY-DTHETA*X + TAUYZ1(I,J))/LAMDA(I,J)
  299 CONTINUE
      IF(KP-KPS)500,505,500
  505 PRINT 411,((SIGMAZ(I,J),I=1,N),J=1,N)
  411 FORMAT(1H0,*   SIGMA  Z STRESSES  * /(7E17.8))
      PRINT 413,((TAUXZ(I,J),I=1,N),J=1,N)
  413 FORMAT(1H0,*    TAU  XZ STRESSES  * /(7E17.8))
      PRINT 415,((TAUYZ(I,J),I=1,N),J=1,N)
  415 FORMAT(1H0,*    TAU  YZ STRESSES  */(7E17.8))
      DO 911 I=1,N
      DO 911 J=1,N
      X = (I-1)*H    $    Y = (J-1)*H
      BEN(I,J) = SIGMAZ(I,J)*Y
  911 TOR(I,J) = Y*TAUXZ(I,J) - X*TAUYZ(I,J)
      TORQ = 0.0    $  BEMO = 0.0
  900 DO 901 I=2,N,2
      DO 901 J=2,N,2
      TORQ = TORQ + TOR(I-1,J-1)+TOR(I+1,J-1)+TOR(I-1,J+1)+
     $ TOR(I+1,J+1) + 4.*(TOR(I+1,J)+TOR(I,J+1)+TOR(I-1,J)
     $ +TOR(I,J-1)) + 16.*TOR(I,J)
  901 BEMO = BEMO + BEN(I-1,J-1)+BEN(I+1,J-1)+BEN(I-1,J+1)
     $ +BEN(I+1,J+1) + 4.*(BEN(I+1,J)+BEN(I,J+1)+BEN(I-1,J)
     $ + BEN(I,J-1)) + 16.*BEN(I,J)
      HSQ = H**2 /9.
      TORQ = 12.*TORQ*HSQ
      BEMO = 16.*HSQ*BEMO
      PRINT 903,TORQ,BEMO
```

```
 903 FORMAT(1H0,*     TORQUE EQUALS *,F10.8,*    BENDING MOMENT EQUALS*,
    $ F10.8)
     KP = 0
 500 THETA = THETA + DTHETA
     IF(THETA - THETA1)501,501,5001
5001 IF(KODE)5003,5005,5003
5005 KODE = 1    $  THETA = THETA1 + DTHETA1
     KPS = KPS1    $    DTHETA = DTHETA1    $    PHI = PHI1  $  KP = 0
5003 IF(THETA-THETAM)501,501,411
 501 IT = 1 $  KP = KP +1
     DO 601 I=1,N
     DO 601 J=1,N
     TAUXZ1(I,J) = TAUXZ(I,J)
     TAUYZ1(I,J) = TAUYZ(I,J)
     SIGMAZ1(I,J) = SIGMAZ(I,J)
 601 J21(I,J) = J2(I,J)
     GO TO 112
4111 PRINT 4112,IT
4112 FORMAT(1H0,*    FAILED TO CONVERGE AFTER *,I10,*  ITERATIONS*)
 411 IF(KSTOP)413,1,413
 413 STOP $ END
```

```
      PROGRAM STPLDT
      TYPE REAL LAMDA,J2,LAMDAX,LAMDAY,J21,LAMDA1
      DIMENSION T(25,25),LAMDA(25,25),T1(25,25),J2(25,25)
     $ ,SIGMAZ(25,25),TAUXZ(25,25),TAUYZ(25,25) ,LAMDA1(25,25)
     $ ,J21(25,25),SIGMAZ1(25,25),T2(25,25),BEN(25,25)
    1 READ 3,PHI, BETA,DTHETA,THETAM,N,NE,ITER,KPS,KSTOP ,KODE
    3 FORMAT(4F10.5,6I5 )
      M = N-1  $  H = 0.5/M   $  IT = 1  $  KP = 1  $  E1 = 1.E-6
      NE2 = 2*NE  $  NE2N1=   NE2 - 1  $  NEN1 = NE - 1
      PHI = PHI**2       $   THETA = DTHETA
      DO 5 I=1,N       $  DO 5 J=1,N
      SIGMAZ1(I,J) = 0.0   $  T2(I,J) = 0.0   $  J21(I,J) = 0.0
      T(I,J) = 0.0  $  T1(I,J) = 0.0      $   J2(I,J) = 0.0
      SIGMAZ(I,J) = 0.0   $  TAUXZ(I,J) = 0.0   $   TAUYZ(I,J) = 0.0
      LAMDA1(I,J) = 1.0
    5 LAMDA(I,J) = 1.0
      PRINT 80,NE,PHI,DTHETA
   80 FORMAT(1H1,*   FLOW THEORY CALCULATIONS FOR NE EQUAL *,I10,    *
     $PHI EQUAL *,F10.5, *  DTHETA EQUAL *,F10.8)
      IF(KODE)4,112,4
    4 PRINT 6
    6 FORMAT (1H0,*  ITERATION    THETA        TORQUE       MOMENT *)
  112 DO 199 I=1,N          $   DO 199 J=1,N
      X = (I-1)*H  $  Y = (J-1)*H
      IF(I-1)117,107,117
  107 IF(J-1)109,1114,109
C     CASE  I=1  J=1
 1114 SX = 0.0    $   SY = 0.0
      STAR = T2(I+1,J) + T2(I,J+1) + T2(I+1,J) + T2(I,J+1) - 4.*T2(I,J)
      E = ((LAMDAX*SX + LAMDAY*SY + 2.*DTHETA)*(H**2) - STAR)/LAMDA(I,J)
       TBAR  = (T(I+1,J) + T(I,J+1) + T(I+1,J) + T(I,J+1) + E)/4.
      T(I,J) = T(I,J) + BETA*(TBAR - T(I,J))       $   GO TO 169
  109 IF(J-N)111,113,111
C     CASE I=1  J NOT = 1 OR N
  111 SX = 0.0
      SY  =  (T(I,J+1)-T(I,J-1))/(2*H)
      LAMDAX = 0.0
      LAMDAY = (LAMDA(I,J+1)-LAMDA(I,J-1))/(2*H)
      STAR = T2(I+1,J) + T2(I,J+1) + T2(I+1,J) + T2(I,J-1) - 4.*T2(I,J)
      E = ((LAMDAX*SX + LAMDAY*SY + 2.*DTHETA)*(H**2) - STAR)/LAMDA(I,J)
       TBAR  = (T(I+1,J) + T(I,J+1) + T(I+1,J) + T(I,J-1) + E)/4.
      T(I,J) = T(I,J) + BETA*(TBAR - T(I,J))       $   GO TO 169
C     CASE I=1  J=N
  113 SX = 0.0
      SY = (3*T(I,J)-4*T(I,J-1)+T(I,J-2))/(2*H)     $   GO TO 169
  117 IF(I-N)121,119,121
  119 IF(J-N)125,123,125
C     CASE  I=N   J=N
  123 SX = 0.0     $  SY = 0.0   $  GO TO 169
  125 IF(J-1)135,137,135
```

```
C   CASE   I=N   J=1
  137 SX = (3*T(I,J)-4*T(I-1,J)+T(I-2,J))/(2*H)
      SY = 0.0          $     GO TO 169
C    CASE   I=N   J NOT = 1 OR N
  135 SX = (3*T(I,J)-4*T(I-1,J)+T(I-2,J))/(2*H)
      SY = 0.0        $    GO TO 169
  121 IF(J-1)129,127,129
C   CASE I NOT = 1 OR N   J=1
  127 SX = (  T(I+1,J)-  T(I-1,J))/(2*H)          $   SY = 0.0
      LAMDAX = (LAMDA(I+1,J) - LAMDA(I-1,J))/(2*H)
      LAMDAY = 0.0
      STAR = T2(I+1,J) + T2(I,J+1) + T2(I-1,J) + T2(I,J+1) - 4.*T2(I,J)
      E = ((LAMDAX*SX + LAMDAY*SY + 2.*DTHETA)*(H**2) - STAR)/LAMDA(I,J)
       TBAR  = (T(I+1,J) + T(I,J+1) + T(I-1,J) + T(I,J+1) + E)/4.
      T(I,J) = T(I,J) + BETA*(TBAR - T(I,J))          $    GO TO 169
  129 IF(J-N)131,133,131
C   CASE    I NOT = 1 OR N     J=N
  133 SX = (T(I+1,J)-T(I-1,J))/(2*H)
      SY = (3*T(I,J) -4*T(I,J-1) + T(I,J-2))/(2*H)    $   GO TO 169
C   CASE   I NOT = 1 OR N    J NOT = 1 OR N
  131 SX = (T(I+1,J)-T(I-1,J))/(2*H)
      SY = (T(I,J+1)-T(I,J-1))/(2*H)
      LAMDAX = (LAMDA(I+1,J) - LAMDA(I-1,J))/(2*H)
      LAMDAY = (LAMDA(I,J+1) - LAMDA(I,J-1))/(2*H)
      STAR = T2(I+1,J) + T2(I,J+1) + T2(I-1,J) + T2(I,J-1) - 4.*T2(I,J)
      E = ((LAMDAX*SX + LAMDAY*SY + 2.*DTHETA)*(H**2) - STAR)/LAMDA(I,J)
       TBAR  = (T(I+1,J) + T(I,J+1) + T(I-1,J) + T(I,J-1) + E)/4.
      T(I,J) = T(I,J) + BETA*(TBAR - T(I,J))
  169 J2(I,J) = (DTHETA*SQRTF(3.*PHI)*Y + SIGMAZ1(I,J))**2 +
     $ (LAMDA(I,J)**2)*(SX**2 + SY**2)
  170 IF(NEN1)173,171,173
  171 LAMDA(I,J) = LAMDA(I,J) - (LAMDA(I,J)**NE2*(LAMDA(I,J) - 1.) -
     $ ((NE2+1.)/2.)*                (J2(I,J) - (LAMDA(I,J)**2)*J21(I,J)))
     $ / (LAMDA(I,J)**NE2N1*((2.*NE+1.)*LAMDA(I,J) - 2.*NE) +(2.*NE+1.)
     $ *J21(I,J)*LAMDA(I,J))       $  GO TO 177
  173 LAMDA(I,J) = LAMDA(I,J) - (LAMDA(I,J)**NE2*(LAMDA(I,J) - 1.) -
     $ ((NE2+1.)/2.)*J2(I,J)**NEN1*(J2(I,J) - (LAMDA(I,J)**2)*J21(I,J)))
     $ / (LAMDA(I,J)**NE2N1*((2.*NE+1.)*LAMDA(I,J) - 2.*NE) +(2.*NE+1.)
     $ *(J2(I,J)**NEN1)*J21(I,J)*LAMDA(I,J))
  177 IF(ABSF(LAMDA(I,J) - LAMDA1(I,J))- E1)199,175,175
  175 LAMDA1(I,J) = LAMDA(I,J)       $  GO TO 170
  199 CONTINUE
      IF(IT-ITER)17,17,4111
   17 X = 0.0
      DO 61 I=1,N           $  DO 61 J=1,N
      A1 = ABSF(ABSF( T(I,J))-ABSF(T1(I,J)))
      IF(A1-X)61,63,63
   63 X = A1
   61 CONTINUE
      IF(X-E1)400,16,16
   16 DO 51 I=1,N            $   DO 51 J=1,N
   51 T1(I,J) =  T(I,J)
```

```
      IT = IT + 1    $    GO TO 112
  400 IF(KP-KPS)502,402,502
  502 DO 504 I=1,N     $  DO 504 J=1,N  $  Y = (J-1)*H
      J2(I,J) = J2(I,J)/LAMDA(I,J)**2
  504 SIGMAZ(I,J) = (SQRTF(3.*PHI)*DTHETA*Y + SIGMAZ1(I,J))/LAMDA(I,J)
      GO TO 500
  402 KP = 0
      IF(KODE)406,4000,406
 4000 PRINT 401,IT,NE,THETA,PHI,((T(I,J),I=1,N),J=1,N)
  401 FORMAT(1H0,*   T(I,J) VALUES FOR ITERATION*,I10,*  NE EQUAL *
     $,I10,/*   THETA EQUAL *,F10.5,* PHI EQUAL *,F10.5,/(7E17.8))
      PRINT 405, ((LAMDA(I,J),I=1,N),J=1,N)
  405 FORMAT(1H0,*   LAMBDA VALUES* /(7E17.8))
  406 DO 317 I=1,N            $    DO 317 J=1,N
  317 J2(I,J) = J2(I,J) / LAMDA(I,J)**2
      IF(KODE)200,408,200
  408 PRINT 407, ((J2(I,J),I=1,N),J=1,N)
  407 FORMAT(1H0,*   J2  VALUES * /(7E17.8))
C   COMPUTE NORMALIZED STRESSES
  200 DO 299 I=1,N           $    DO 299 J=1,N
      X = (I-1)*H    $     Y = (J-1)*H
      IF(I-1)217,207,217
  207 IF(J-1)209,299,209
  209 IF(J-N)211,213,211
C    CASE I=1    J NOT = 1 OR N
  211 SY = (T(I,J+1)-T(I,J-1))/(2*H)          $    SX = 0.0
      GO TO 251
C     CASE I=1    J=N
  213 SY = (3*T(I,J) -4*T(I,J-1) +T(I,J-2))/(2*H)       $  SX = 0.0
      GO TO 251
  217 IF(I-N)221,219,221
  219 IF(J-N)225,223,225
C    CASE I=N    J=N
  223 SX = 0.0  $    SY = 0.0          $  GO TO 251
  225 IF(J-1)235,237,235
C    CASE  I=N    J=1
  237 SX = (3*T(I,J) -4*T(I-1,J) + T(I-2,J))/(2*H)       $  SY = 0.0
      GO TO 251
C    CASE  I=N  J NOT = 1 OR N
  235 SX = (3*T(I,J) -4*T(I-1,J)+T(I-2,J))/(2*H)        $  SY = 0.0
      GO TO 251
  221 IF(J-1)229,227,229
C    CASE I NOT = 1 OR N    J=1
  227 SX = (T(I+1,J)-T(I-1,J))/(2*H)         $  SY = 0.0
      GO TO 251
  229 IF(J-N)231,233,231
C    CASE I NOT = 1 OR N    J=N
  233 SY = (3*T(I,J) -4*T(I,J-1)+T(I,J-2))/(2*H)         $  SX = 0.0
      GO TO 251
C   CASE I NOT = 1 OR N    J NOT = 1 OR N
  231 SX = (T(I+1,J)-T(I-1,J))/(2*H)
      SY = (T(I,J+1)-T(I,J-1))/(2*H)
```

```
251 SIGMAZ(I,J) = (SQRTF(3.*PHI)*DTHETA*Y + SIGMAZ1(I,J))/LAMDA(I,J)
    TAUXZ(I,J) = -SY
    TAUYZ(I,J) =  SX
299 CONTINUE
    IF(KODE)300,909,300
909 PRINT 511,((SIGMAZ(I,J),I=1,N),J=1,N)
511 FORMAT(1H0,*   SIGMA  Z STRESSES  * /(7E17.8))
    PRINT 413,((TAUXZ(I,J),I=1,N),J=1,N)
413 FORMAT(1H0,*    TAU  XZ STRESSES  * /(7E17.8))
    PRINT 415,((TAUYZ(I,J),I=1,N),J=1,N)
415 FORMAT(1H0,*    TAU  YZ STRESSES  */(7E17.8))
300 DO 911 I=1,N          $  DO 911 J=1,N
    X = (I-1)*H    $    Y = (J-1)*H
    BEN(I,J) = Y*SIGMAZ(I,J)
911 TAUXZ(I,J) = Y*TAUXZ(I,J) - X*TAUYZ(I,J)
    TORQ = 0.0    $  BEMO = 0.0       $  TORQ2 = 0.0
900 DO 901 I=2,N,2
    DO 901 J=2,N,2
    TORQ2 = TORQ2 + T(I-1,J-1)+T(I-1,J+1)+T(I+1,J-1)+T(I+1,J+1)
   $ + 4*(T(I+1,J)+T(I,J+1)+T(I-1,J)+T(I,J-1)) + 16*T(I,J)
    TORQ = TORQ + TAUXZ(I-1,J-1)+TAUXZ(I+1,J-1)+TAUXZ(I-1,J+1)+
   $ TAUXZ(I+1,J+1) + 4.*(TAUXZ(I+1,J)+TAUXZ(I,J+1)+TAUXZ(I-1,J)
   $  +TAUXZ(I,J-1)) +  16.*TAUXZ(I,J)
901 BEMO = BEMO + BEN(I-1,J-1) + BEN(I+1,J-1) + BEN(I-1,J+1)
   $ + BEN(I+1,J+1) + 4.*(BEN(I+1,J) + BEN(I,J+1) + BEN(I-1,J)
   $ + BEN(I,J-1)) + 16.*BEN(I,J)
    HSQ = H**2 /9.
    TORQ2 = 24.*TORQ2*HSQ
    TORQ = 12.*TORQ*HSQ
    BEMO = 16.*HSQ*BEMO
    IF(KODE)904,902,904
902 PRINT 903,TORQ,BEMO,TORQ2
903 FORMAT(1H0,*    TORQUE EQUALS *,F10.8,*   BENDING MOMENT EQUALS*,
   $ F10.8,*  TORQ2 EQUALS  * ,F10.8)
    GO TO 500
904 PRINT 906,IT,THETA,TORQ2,BEMO ,TORQ
906 FORMAT(I12,4F12.6)
500 THETA = THETA + DTHETA
    IF(THETA-THETAM)501,501,411
501 IT = 1  $  KP = KP +1
    DO 601 I=1,N       $  DO 601 J=1,N
    SIGMAZ1(I,J) = SIGMAZ(I,J)
    T2(I,J) = T(I,J)
    J21(I,J) = J2(I,J)
601 CONTINUE        $  GO TO 112
4111 PRINT 4112,IT
4112 FORMAT(1H0,*    FAILED TO CONVERGE AFTER *,I10, *  ITERATIONS*)
411 IF(KSTOP)413,1,413
413 STOP $ END
```

```
      PROGRAM POLARR
      TYPE REAL  LAMDA
      DIMENSION T(25,25),T1(25,25)          , SIGMAZ(25,25),TAUYZ(25,25),
     $ TAUXZ(25,25)  ,TOR(25,25) , BEN(25,25),R(25) , THA(25)
    1 READ 3,PSI,BETA,N,ITER,KSTOP
    3 FORMAT(2F10.5,3I5)
      PRINT 5,PSI,BETA
    5 FORMAT(*1*,*  T(I,J) VALUES FOR CIRCULAR BAR OF UNIT RADIUS WHERE
     $PSI EQUAL*, F10.5,*    BETA EQUAL*,F10.5)
      PSI = PSI**2    $  M = N-1    $  M1 = N+1
      H = 1./M    $   DTHA = 1.5708 / M $ IT= 1 $ E1 = 1.E-6
      DO 7 I=1,N
      THA(I) = (I-1)*DTHA
    7 R(I) = (I-1)*H
      DO 9 I=1,M1  $ DO 9 J=1,N
      SIGMAZ(I,J) = 0.0  $  TAUYZ(I,J) = 0.0   $  TAUXZ(I,J) = 0.0
      T1(I,J) = 0.0
    9 T(I,J) = 0.0
   10 DO 11 I=2,N  $  DO 11 J=2,M
      A = (3.*PSI*(R(I)**5)*SINF(THA(J))**2 + R(I)*(((T(I,J+1)-T(I,J-1))
     $/(2.*DTHA)) - R(I)**2)**2) * (DTHA**2)
      B = (2.*R(I) * ((T(I+1,J)- T(I-1,J))/(2.*H))*(R(I)**2 - ((T(I,J+1)
     $ - T(I,J-1))/(2.*DTHA))))*(0.25*DTHA*H)
      C = (3.*PSI* (R(I)**3) * (SINF(THA(J))**2) + R(I) * ((T(I+1,J)
     $ - T(I-1,J)) /(2.*H))**2)*(H**2)
      D =((R(I)**2) * ((T(I+1,J) - T(I-1,J))/(2.*H))**2)*(0.5*H*DTHA**2)
      E = (-2.*((T(I+1,J) - T(I-1,J))/(2.*H))*(R(I)**2 - ((T(I,J+1) -
     $ T(I,J-1))/(2.*DTHA)))-3.*PSI*(R(I)**3)*SINF(THA(J)) *
     $ COSF(THA(J))) * (0.5*DTHA*H**2)
      F = (3.*PSI* (R(I)**5) * SINF(THA(J)) * COSF(THA(J)))
     $  *(H**2*DTHA**2)
        TBAR  = ((A+D)*T(I+1,J) + (A-D)*T(I-1,J) + (C+E)*T(I,J+1)
     $ + (C-E)*T(I,J-1) + B*(T(I+1,J+1) - T(I-1,J+1) + T(I-1,J-1)
     $ - T(I+1,J-1)) + F) / (2.*(A+C))
   11 T(I,J)  =  T(I,J) + BETA*(TBAR - T(I,J))
      DO 13 J=1,N
   13 T(M1,J) = T(M,J)   $  X = 0.0
      DO 301 I=1,N      $  DO 301 J=1,N
      A1 = ABSF(ABSF(T(I,J))-ABSF(T1(I,J)))
      IF(A1-X)301,305,305
  305 X=A1
  301 CONTINUE
      IF(X-E1)200,51,51
   51 DO 53 I=2,N          $  DO 53 J=2,N
   53 T1(I,J) = T(I,J)
      IT = IT + 1  $  IF(IT-ITER)10,400,400
  200 PRINT 201,IT,BETA,PSI,((T(I,J),I=1,N),J=1,N)
  201 FORMAT (1H0,*  T(I,J) VALUES FOR ITERATION * , I10,//* RELAXATION
     $FACTOR  *,F10.5,*  PSI VALUE *,F10.5,//(7E17.8 ))
      GO TO 112
  400 PRINT 401,IT,BETA,PSI
  401 FORMAT(1H1,*  FAILED TO CONVERGE AFTER * ,I10,*ITERATIONS*
```

```
     $ ///*    BETA EQUAL*,F10.5,*  PSI EQUAL*,F10.5)
      GO TO 1105
  112 DO 111 I=2,N       $   DO 111 J=1,N
      IF(J-1)103,101,103
C     CASE  J=1
  101 STHA = T(I,J+1)/DTHA
      SR = (T(I+1,J) - T(I-1,J))/(2.*H)    $  GO TO 109
  103 IF(J-N)105,107,105
C     CASE  J=N
  107 STHA = -T(I,J-1)/DTHA
      SR = (T(I+1,J) - T(I-1,J))/(2.*H)     $  GO TO 109
C    CASE J NOT = 1 OR N
  105 STHA = (T(I,J+1) - T(I,J-1))/(2.*DTHA)
      SR = (T(I+1,J) - T(I-1,J))/(2.*H)
  109 LAMDA = SQRTF(3.*PSI *(R(I)**2)*(SINF(THA(J))**2) + SR**2 +
     $  (STHA/R(I))**2  + R(I)**2    - 2.*STHA)
      SIGMAZ(I,J) = (SQRTF(3.*PSI)*R(I)*SINF(THA(J)))/LAMDA
      TAUXZ(I,J) = (SR*COSF(THA(J)) - STHA*SINF(THA(J))/R(9) + R(I)
     $ *SINF(THA(J)))/LAMDA
      TAUYZ(I,J) = (SR*SINF(THA(J)) + STHA*COSF(THA(J))/R(I) - R(I)
     $ * COSF(THA(J)))/LAMDA
  111 CONTINUE
      PRINT 411,((SIGMAZ(I,J),I=1,N),J=1,N)
  411 FORMAT(1H0,*   SIGMA Z STRESSES*//(7E17.8))
      PRINT 413,((TAUXZ(I,J),I=1,N),J=1,N)
  413 FORMAT(1H0,*   TAU  XZ STRESSES* // (7E17.8))
      PRINT 415,((TAUYZ(I,J),I=1,N),J=1,N)
  415 FORMAT(1H0,*   TAU  YZ STRESSES* //(7E17.8))
      DO 113 I=1,N
      DO 113 J=1,N
      BEN(I,J) = SIGMAZ(I,J)*(R(I)**2)*SINF(THA(J))
  113 TOR(I,J) =  (R(I)**2)*(SINF(THA(J))*TAUXZ(I,J) - COSF(THA(J))
     $ *TAUYZ(I,J))
      TORQ = 0.0  $ BEMO = 0.0
      DO 115 I=2,N,2
      DO 115 J=2,N,2
      TORQ = TORQ + TOR(I+1,J+1) + TOR(I-1,J+1) + TOR(I-1,J-1) +
     $ TOR(I+1,J-1) + 4.*(TOR(I+1,J) + TOR(I,J+1) + TOR(I-1,J) +
     $ TOR(I,J-1)) + 16.*TOR(I,J)
  115 BEMO = BEMO + BEN(I+1,J+1) + BEN(I-1,J+1) + BEN(I-1,J-1) +
     $ BEN(I+1,J-1) + 4.*(BEN(I+1,J) + BEN(I,J+1) + BEN(I-1,J) +
     $ BEN(I,J-1)) + 16.*BEN(I,J)
      HSQ = (DTHA*H)/9.
      TORQ = 4.*TORQ*HSQ/(2.094)
      BEMO = 3.*BEMO*HSQ
      PRINT 903,TORQ,BEMO
  903 FORMAT(1H0,*   TORQUE EQUALS  *,F10.8,*   BENDING MOMENT EQUALS  *
     $ ,F10.8)
 1105 IF(KSTOP)215, 1 ,215
  215 STOP  $ END
```

```
      PROGRAM POLARO
      TYPE REAL  LAMDA , J2
      DIMENSION T(25,25),T1(25,25),J2(25,25),SIGMAZ(25,25),TAUYZ(25,25),
     $ TAUXZ(25,25)  ,TOR(25,25) , BEN(25,25),R(25) , THA(25)
     $ , LAMDA(25,25)
    1 READ 3,PSI,BETA,DTHETA,THETAM,N,NE,ITER,KSTOP,KODE
    3 FORMAT(4F10.5,5I5)
      IF(KODE)2,4,2
    2 PRINT 6,PSI,BETA,NE       $  GO TO 8
    6 FORMAT(1H1,*  DEFORMATION THEORY - CIRCULAR BAR FOR PSI EQUAL*,
     $F10.5,* BETA EQUAL*,F10.5,* NE EQUAL*,I5,//*  ITERATION   THETA
     $ TORQUE   MOMENT*)
    4 PRINT 5,PSI,BETA,NE
    5 FORMAT(*1*,*  T(I,J) VALUES FOR CIRCULAR BAR OF UNIT RADIUS WHERE
     $PSI EQUAL*, F10.5,*    BETA EQUAL*,F10.5 ,* NE EQUALS*,I5)
    8 NE2 = 2*NE    $   NE2N1 = 2*NE - 1
      PSI = PSI**2    $  M = N-1    $  M1 = N+1
      H = 1./M    $   DTHA = 1.5708 / M
      IT = 1    $   E1 = 1.E-6  $  THETA = DTHETA
      DO 7 I=1,M1
      THA(I) = (I-1)*DTHA
    7 R(I) = (I-1)*H
      DO 9 I=1,M1           $   DO 9 J=1,N
      SIGMAZ(I,J) = 0.0  $  TAUYZ(I,J) = 0.0    $  TAUXZ(I,J) = 0.0
      T1(I,J) = 0.0  $   LAMDA(I,J) = 1.0
    9 T(I,J) = 0.0
   10 DO 11 I=2,N           $   DO 11 J=1,N
      IF(I-N)603,601,603
  601 IF(J-1)607,605,607
C     CASE  I=N   J=1
  605 SR = 0.0
      STHA = T(I,J+1)/DTHA       $   GO TO 625
  607 IF(J-N)611,609,611
C     CASE   I=N  J=N
  609 SR = 0.0
      STHA = -T(I,J-1)/DTHA        $  GO TO 625
C     CASE   I=N  J NOT = 1 OR N
  611 SR = 0.0
      STHA = (T(I,J+1) - T(I,J-1))/(2.*DTHA)
      A = (R(I)**2)*(DTHA**2)      $    C = H**2
      E = (((LAMDA(I,J+1) - LAMDA(I,J-1))/(2.*DTHA))*(STHA/(R(I)**2) -
     $ 1.0)/LAMDA(I,J))*(R(I)**2)*(H**2)*(DTHA**2)
      TBAR = (2.*A*T(I-1,J) + C*(T(I,J+1) + T(I,J-1)) - E)/(2.*(A+C))
      T(I,J) = T(I,J) + BETA*(TBAR - T(I,J))
      GO TO 625
  603 IF(J-1)615,613,615
C   CASE  I NOT = N   J=1
  613 SR = (T(I+1,J) - T(I-1,J))/(2.*H)
      STHA = T(I,J+1)/DTHA       $   GO TO 625
  615 IF(J-N)619,617,619
C   CASE  I NOT = 1 OR N   J=N
  617 SR = (T(I+1,J) - T(I-1,J))/(2.*H)
      STHA = -T(I,J-1)/DTHA        $    GO TO 625
```

```
C     CASE  I NOT = N    J NOT = 1 OR N
  619 A = (R(I)**2)*(DTHA**2)
      D = 0.5*R(I)*H*(DTHA**2)
      C = H**2
      E = ((((LAMDA(I+1,J) - LAMDA(I-1,J))/(2.*H))*((T(I+1,J) -
     $ T(I-1,J))/(2.* H  ))+((LAMDA(I,J+1) - LAMDA(I,J-1))/(2.*DTHA))*
     $ ((T(I,J+1) - T(I,J-1))/(2.*DTHA))/(R(I)**2)-(LAMDA(I,J+1) -
     $LAMDA(I,J-1))/(2.*DTHA))/LAMDA(I,J))*((R(I)**2)*(H**2)*(DTHA**2))
      TBAR = ((A+D)*T(I+1,J) + (A-D)*T(I-1,J) +C*(T(I,J+1) + T(I,J-1)) -
     $ E)/(2.*(A+C))
      T(I,J)  =  T(I,J) + BETA*(TBAR - T(I,J))
      SR = (T(I+1,J) - T(I-1,J))/(2.*H)
      STHA = (T(I,J+1) - T(I,J-1))/(2.*DTHA)
  625 J2(I,J) = (THETA**2)*(3.*PSI*R(I)**2*SINF(THA(J))**2 + (SR*COSF
     $ (THA(J)) - STHA*SINF(THA(J))/R(I) + R(I)*SINF(THA(J)))**2 + (SR*
     $ SINF(THA(J)) + STHA*COSF(THA(J))/R(I) - R(I)*COSF(THA(J)))**2)
   11 LAMDA(I,J) = LAMDA(I,J) - (LAMDA(I,J)**NE2*(LAMDA(I,J)-1.) -
     $  J2(I,J)**NE) / (LAMDA(I,J)**NE2N1 *((2*NE+1)*LAMDA(I,J) - 2*NE))
      X = 0.0
      =8 476 IM6P9
      A1 = ABSF(ABSF(T(I,J))-ABSF(T1(I,J)))
      IF(A1-X)301,305,305
  305 X=A1
  301 CONTINUE
      IF(X-E1)200,51,51
   51 DO 53 I=2,N
      DO 53 J=2,M
   53 T1(I,J) = T(I,J)
      IT = IT + 1  $  IF(IT-ITER)10,400,400
  200 IF(KODE)4005,202,4005
  202 PRINT 201,IT,BETA,PSI,THETA,((T(I,J),I=1,N),J=1,N)
  201 FORMAT (1H0,*  T(I,J) VALUES FOR ITERATION * , I10,//* RELAXATION
     $FACTOR  *,F10.5,*  PSI VALUE *,F10.5,* THETA EQUALS *,F10.5,//
     $ (7E17.8 ))
      PRINT 402,((LAMDA(I,J),I=1,N),J=1,N)
  402 FORMAT(1H0,*  LAMBDA VALUES *//(7E17.8))
 4005 DO 406 I=1,N          $   DO 406 J=1,N
  406 J2(I,J) = J2(I,J)/LAMDA(I,J)**2
      IF(KODE)112,4006,112
 4006 PRINT 404,((J2(I,J),I=1,N),J=1,N)
  404 FORMAT(*0*,*  J2 VALUES * //(7E17.8))
      GO TO 112
  400 PRINT 401,IT,BETA,PSI
  401 FORMAT(1H1,*  FAILED TO CONVERGE AFTER * ,I10,*ITERATIONS*
     $ ///*    BETA EQUAL*,F10.5,*  PSI EQUAL*,F10.5)
      GO TO 1105
  112 DO 111 I=2,N
      DO 111 J=1,N
      IF(J-1)103,101,103
C     CASE  J=1
  101 STHA = T(I,J+1)/DTHA
      SR = (T(I+1,J) - T(I-1,J))/(2.*H)
      GO TO 109
```

```
  103 IF(J-N)105,107,105
C       CASE  J=N
  107 STHA = -T(I,J-1)/DTHA
      SR = (T(I+1,J) - T(I-1,J))/(2.*H)
      GO TO 109
C     CASE J NOT = 1 OR N
  105 STHA = (T(I,J+1) - T(I,J-1))/(2.*DTHA)
      SR = (T(I+1,J) - T(I-1,J))/(2.*H)
  109 SIGMAZ(I,J) =((SQRTF(3.*PSI)*R(I)*SINF(THA(J)))/LAMDA(I,J))*THETA
      TAUXZ(I,J) =((SR*COSF(THA(J)) - STHA*SINF(THA(J))/R(I) + R(I)
     $ *SINF(THA(J)))/LAMDA(I,J))*THETA
      TAUYZ(I,J) =((SR*SINF(THA(J)) + STHA*COSF(THA(J))/R(I) - R(I)
     $ * COSF(THA(J)))/LAMDA(I,J))*THETA
  111 CONTINUE
      IF(KODE)4010,4011,4010
 4011 PRINT 411,((SIGMAZ(I,J),I=1,N),J=1,N)
  411 FORMAT(1H0,*    SIGMA Z STRESSES*//(7E17.8))
      PRINT 413,((TAUXZ(I,J),I=1,N),J=1,N)
  413 FORMAT(1H0,*    TAU  XZ STRESSES* // (7E17.8))
      PRINT 415,((TAUYZ(I,J),I=1,N),J=1,N)
  415 FORMAT(1H0,*    TAU  YZ STRESSES* //(7E17.8))
 4010 DO 113 I=1,N
      DO 113 J=1,N
      BEN(I,J) = SIGMAZ(I,J)*(R(I)**2)*SINF(THA(J))
  113 TOR(I,J) =  (R(I)**2)*(SINF(THA(J))*TAUXZ(I,J) - COSF(THA(J))
     $ *TAUYZ(I,J))
      TORQ = 0.0  $ BEMO = 0.0
      DO 115 I=2,N,2
      DO 115 J=2,N,2
      TORQ = TORQ + TOR(I+1,J+1) + TOR(I-1,J+1) + TOR(I-1,J-1) +
     $ TOR(I+1,J-1) + 4.*(TOR(I+1,J) + TOR(I,J+1) + TOR(I-1,J) +
     $ TOR(I,J-1)) + 16.*TOR(I,J)
  115 BEMO = BEMO + BEN(I+1,J+1) + BEN(I-1,J+1) + BEN(I-1,J-1) +
     $ BEN(I+1,J-1) + 4.*(BEN(I+1,J) + BEN(I,J+1) + BEN(I-1,J) +
     $ BEN(I,J-1)) + 16.*BEN(I,J)
      HSQ = (DTHA*H)/9.
      TORQ = 4.*TORQ*HSQ/(2.094)
      BEMO = 3.*BEMO*HSQ
      IF(KODE)904,902,904
  904 PRINT 908,IT,THETA,TORQ,BEMO
  908 FORMAT(2X,I10,2X,F10.6,2X,F10.6,2X,F10.6)
      GO TO 500
  902 PRINT 903,TORQ,BEMO
  903 FORMAT(1H0,*    TORQUE EQUALS  *,F10.8,*    BENDING MOMENT EQUALS  *
     $ ,F10.8)
  500 THETA = THETA + DTHETA
      IF(THETA - THETAM)501,501,1105
  501 IT = 1  $  GO TO 10
 1105 IF(KSTOP)215, 1 ,215
  215 STOP  $ END
```

APPENDIX V

TORQUE, MOMENT, AND STRESS OUTPUTS

Table 5. Effect of grid dimension on Piechnik equation warping function and stresses for $\mu = 1/\sqrt{3}$ (lower values for finer mesh)

Warping function: $t \times 10^{-2}$

i / j	1 / 1	2 / 3	3 / 5	4 / 7	5 / 9	6 / 11	7 / 13
1	0.0000	0.0000	0.0000	0.0000	0.0000	0.0000	0.0000
1	0.0000	0.0000	0.0000	0.0000	0.0000	0.0000	0.0000
2	0.0000	0.5028	0.7515	0.6005	0.2114	-0.3191	-0.9613
3	0.0000	0.5036	0.7243	0.5591	0.1647	-0.3681	-1.0111
3	0.0000	0.9032	1.4392	1.3673	0.7540	-0.2326	-1.4970
5	0.0000	0.8853	1.3786	1.2682	0.6365	-0.3565	-1.6220
4	0.0000	1.3055	2.1900	2.3449	1.7040	0.3830	-1.4691
7	0.0000	1.2702	2.0980	2.1946	1.5140	0.1777	-1.6758
5	0.0000	1.7619	3.0814	3.5996	3.1341	1.6625	-0.7165
9	0.0000	1.7139	2.9621	3.4021	2.8740	1.3722	-1.0060
6	0.0000	2.3023	4.1675	5.2016	5.1393	3.7911	0.9913
11	0.0000	2.2485	4.0263	4.9563	4.8026	3.4076	0.6383
7	0.0000	2.9435	5.4874	7.2137	7.8358	7.0955	4.0434
13	0.0000	2.8951	5.3334	6.9167	7.3898	6.5419	3.7365

Normal stress: $\sigma_{zz}/\sqrt{3}\ k$

i / j	1 / 1	2 / 3	3 / 5	4 / 7	5 / 9	6 / 11	7 / 13
1	0.0000	0.0000	0.0000	0.0000	0.0000	0.0000	0.0000
1	0.0000	0.0000	0.0000	0.0000	0.0000	0.0000	0.0000
2	0.5016	0.5353	0.5702	0.4287	0.2765	0.1898	0.1398
3	0.4914	0.5242	0.5656	0.4167	0.2687	0.1856	0.1374
3	0.5180	0.5462	0.6206	0.6552	0.5487	0.4052	0.2996
5	0.5126	0.5430	0.6238	0.6515	0.5362	0.3954	0.2937
4	0.5235	0.5467	0.6158	0.7077	0.7329	0.6291	0.4828
7	0.5209	0.5460	0.6198	0.7114	0.7256	0.6150	0.4726
5	0.5217	0.5404	0.5983	0.6941	0.7980	0.8165	0.6870
9	0.5207	0.5409	0.6024	0.6998	0.7981	0.8037	0.6732
6	0.5151	0.5297	0.5760	0.6584	0.7783	0.9092	0.8890
11	0.5147	0.5307	0.5805	0.6550	0.7819	0.8999	0.8792
7	0.5054	0.5162	0.5513	0.6148	0.7112	0.8746	0.9943
13	0.5052	0.5171	0.5565	0.6235	0.7202	0.8527	0.9988

Table 5 (continued)

Shear stress: $|\sigma_{xz}/k|$

i	1	2	3	4	5	6	7
j	1	3	5	7	9	11	13
1	0.0000	0.0000	0.0000	0.0000	0.0000	0.0000	0.0000
1	0.0000	0.0000	0.0000	0.0000	0.0000	0.0000	0.0000
2	0.8651	0.8242	0.6105	0.2621	0.0935	0.0296	0.0000
3	0.8709	0.8256	0.5771	0.2381	0.0871	0.0280	0.0000
3	0.8553	0.8296	0.7247	0.4939	0.2328	0.0769	0.0000
5	0.8586	0.8303	0.7126	0.4676	0.2163	0.0721	0.0000
4	0.8520	0.8344	0.7698	0.6254	0.3880	0.1501	0.0000
7	0.8536	0.8344	0.7638	0.6093	0.3677	0.1403	0.0000
5	0.8531	0.8405	0.7966	0.7010	0.5200	0.2507	0.0000
9	0.8538	0.8401	0.7927	0.6915	0.5046	0.2382	0.0000
6	0.8571	0.8480	0.8169	0.7509	0.6205	0.3663	0.0000
11	0.8574	0.8474	0.8135	0.7441	0.6118	0.3641	0.0000
7	0.8629	0.8565	0.8343	0.7884	0.7050	0.4768	0.0000
13	0.8630	0.8559	0.8308	0.7817	0.6932	0.5199	0.0000

Shear stress: $|\sigma_{yz}/k|$

i	1	2	3	4	5	6	7
j	1	3	5	7	9	11	13
1	0.0000	1.0000	1.0000	1.0000	1.0000	1.0000	1.0000
1	0.0000	1.0000	1.0000	1.0000	1.0000	1.0000	1.0000
2	0.0000	0.1870	0.5498	0.8646	0.9564	0.9814	0.9902
3	0.0000	0.2088	0.5891	0.8773	0.9593	0.9822	0.9905
3	0.0000	0.1153	0.2994	0.5716	0.8030	0.9110	0.9541
5	0.0000	0.1254	0.3210	0.5974	0.8159	0.9157	0.9559
4	0.0000	0.0696	0.1679	0.3287	0.5588	0.7627	0.8757
7	0.0000	0.0748	0.1801	0.3501	0.5816	0.7759	0.8813
5	0.0000	0.0382	0.0862	0.1637	0.3047	0.5200	0.7266
9	0.0000	0.0406	0.0935	0.1791	0.3291	0.5453	0.7395
6	0.0000	0.0158	0.0308	0.0524	0.0957	0.1980	0.4577
11	0.0000	0.0162	0.0348	0.0638	0.1195	0.2399	0.4765
7	0.0000	0.0000	0.0000	0.0000	0.0000	0.0000	0.0000
13	0.0000	0.0000	0.0000	0.0000	0.0000	0.0000	0.0000

Table 6. Comparison between stresses computed from Piechnik equation and Hill-Handelman equation for $\mu = 1/\sqrt{3}$ (lower values due to Steele)

Normal stress: $\sigma_{zz}/\sqrt{3}\,k$

i	2	4	6	8	10
j	1	2	3	4	5
2	0.497	0.496	0.246	0.137	0.091
1	0.348	0.452	0.277	0.139	0.077
4	0.526	0.622	0.629	0.444	0.296
2	0.507	0.626	0.612	0.455	0.628
6	0.531	0.612	0.738	0.729	0.543
3	0.554	0.633	0.727	0.712	0.487
8	0.524	0.586	0.712	0.865	0.819
4	0.540	0.601	0.735	0.844	0.815
10	0.510	0.554	0.648	0.802	1.000
5	0.530	0.571	0.668	0.837	1.000

Shear stress: $|\sigma_{xz}/k|$

i	2	4	6	8	10
j	1	2	3	4	5
2	0.856	0.492	0.110	0.027	0.000
1	0.907	0.553	0.097	0.027	0.000
4	0.847	0.718	0.385	0.112	0.000
2	0.849	0.664	0.339	0.116	0.000
6	0.846	0.778	0.583	0.252	0.000
3	0.829	0.746	0.532	0.229	0.000
8	0.852	0.809	0.693	0.424	0.000
4	0.841	0.788	0.651	0.381	0.000
10	0.860	0.832	0.761	0.598	0.000
5	0.848	0.821	0.744	0.548	0.000

Shear stress: $|\sigma_{yz}/k|$

i	2	4	6	8	10
j	1	2	3	4	5
2	0.137	0.715	0.963	0.990	0.996
1	0.238	0.700	0.956	0.990	0.997
4	0.076	0.311	0.675	0.889	0.955
2	0.103	0.370	0.687	0.881	0.963
6	0.039	0.142	0.339	0.636	0.840
3	0.053	0.190	0.407	0.651	0.873
8	0.015	0.050	0.113	0.269	0.574
4	0.020	0.073	0.170	0.349	0.580
10	0.000	0.000	0.000	0.000	0.000
5	0.000	0.000	0.000	0.000	0.000

Table 7a. Normalized torques for warping-function deformation-theory analysis of a square section with $\mu = 0.00$

$\frac{G\theta}{k}$	n = 1 t_n	n = 2 t_n	n = 9 t_n	n = 12 t_n
0.00	0.0000	0.0000	0.0000	0.0000
0.25			0.1041	0.1041
0.50	0.1990	0.2075	0.2082	0.2082
0.75			0.3123	0.3123
1.00	0.3627	0.3995	0.4163	0.4163
1.25			0.5190	0.5199
1.50	0.4933	0.5515	0.6136	0.6167
1.75			0.6922	0.6990
2.00	0.6006	0.6652	0.7529	0.7609
2.25			0.8003	0.8090
2.50	0.6915	0.7526	0.8375	0.8456
2.75			0.8683	0.8753
3.00	0.7707	0.8224	0.8940	0.9005
3.25			0.9150	0.9208
3.50	0.8409	0.8801	0.9326	0.9373
3.75			0.9476	0.9512
4.00	0.9042	0.9291	0.9608	0.9633
4.25			0.9727	0.9740
4.50	0.9620	0.9718	0.9833	0.9836
4.75			0.9930	0.9923
5.00	1.0152	1.0094	1.0018	1.0002
5.25			1.0098	1.0074
5.50	1.0646	1.0432	1.0173	1.0141
5.75			1.0242	1.0202
6.00	1.1107	1.0738	1.0307	1.0260
6.25			1.0368	1.0314
6.50	1.1542	1.1018	1.0426	1.0366
6.75			1.0481	1.0414
7.00	1.1952	1.1277	1.0532	1.0461
7.25			1.0581	1.0505
7.50	1.2341	1.1516	1.0627	1.0547
7.75			1.0671	1.0587
8.00	1.2711	1.1740	1.0712	1.0625

Table 7b. Normalized torques and bending moments for warping-function deformation-theory analysis of a square section with $\mu = 0.50$

$\frac{G\theta}{k}$	n = 1		n = 6		n = 9	
	t_n	m_n	t_n	m_n	t_n	m_n
0.0000	0.0000	0.0000	0.0000	0.0000	0.0000	0.0000
0.1875					0.0781	0.0541
0.3750	0.1507	0.1045	0.1561	0.1082	0.1561	0.1082
0.5625					0.2342	0.1624
0.7500	0.2786	0.1934	0.3122	0.2165	0.3123	0.2165
0.9375					0.3902	0.2706
1.1250	0.3831	0.2661	0.4635	0.3217	0.4665	0.3235
1.3125					0.5371	0.3731
1.5000	0.4700	0.3265	0.5063	0.4088	0.5974	0.4161
1.6875					0.6468	0.4522
1.8750	0.5440	0.3780	0.6699	0.4701	0.6857	0.4817
2.0625					0.7167	0.5052
2.2500	0.6087	0.4229	0.7260	0.5107	0.7418	0.5236
2.4375					0.7621	0.5380
2.6250	0.6662	0.4627	0.7653	0.5379	0.7787	0.5494
2.8125					0.7926	0.5586
3.0000	0.7180	0.4987	0.7944	0.5573	0.8047	0.5662
3.1875					0.8151	0.5728
3.3750	0.7653	0.5315	0.8169	0.5721	0.8242	0.5784
3.5625					0.8321	0.5833
3.7500	0.8089	0.5617	0.8350	0.5838	0.8391	0.5876
3.9375					0.8453	0.5915
4.1250	0.8494	0.5897	0.8500	0.5936	0.8510	0.5949
4.3125					0.8561	0.5981
4.5000	0.8872	0.6159	0.8628	0.6019	0.8609	0.6011
4.6875					0.8653	0.6038
4.8750	0.9227	0.6406	0.8741	0.6092	0.8695	0.6064
5.0625					0.8734	0.6089
5.2500	0.9563	0.6638	0.8840	0.6157	0.8771	0.6111
5.4375					0.8805	0.6133
5.6250	0.9882	0.6859	0.8929	0.6215	0.8838	0.6154
5.8125					0.8869	0.6173
6.0000	1.0185	0.7068	0.9009	0.6268	0.8898	0.6192

Table 7c. Normalized torques and bending moments for warping-function deformation-theory analysis of a square section with $\mu = 1.00$

$\frac{G\theta}{k}$	n = 1		n = 2		n = 6		n = 9		n = 12	
	t_n	m_n	t_n	m_n	t_n	m_n	t_n	m_n	t_n	m_n
0.000	0.0000	0.0000	0.0000	0.0000	0.0000	0.0000	0.0000	0.0000	0.0000	0.0000
0.125							0.0520	0.0722	0.0520	0.0722
0.250	0.1011	0.1394	0.1039	0.1441	0.1041	0.1443	0.1041	0.1443	0.1041	0.1443
0.375							0.1561	0.2165	0.1561	0.2165
0.500	0.1894	0.2581	0.2044	0.2819	0.2082	0.2886	0.2082	0.2887	0.2082	0.2887
0.625							0.2602	0.3608	0.2602	0.3608
0.750	0.2635	0.3550	0.2926	0.3981	0.3106	0.4301	0.3118	0.4323	0.3121	0.4328
0.875							0.3611	0.5000	0.3623	0.5021
1.000	0.3261	0.4354	0.3645	0.4880	0.4003	0.5473	0.4059	0.5588	0.4085	0.5641
1.125							0.4448	0.6054	0.4485	0.6131
1.250	0.3803	0.5039	0.4224	0.5573	0.4691	0.6253	0.4781	0.6413	0.4827	0.6502
1.375							0.5066	0.6696	0.5117	0.6784
1.500	0.4279	0.5636	0.4697	0.6124	0.5201	0.6764	0.5311	0.6923	0.5366	0.7008
1.625							0.5517	0.7104	0.5577	0.7188
1.750	0.4704	0.6166	0.5092	0.6575	0.5573	0.7108	0.5689	0.7245	0.5752	0.7324
1.875							0.5833	0.7360	0.5894	0.7428
2.000	0.5090	0.6643	0.5429	0.6956	0.5852	0.7355	0.5956	0.7456	0.6013	0.7512
2.125							0.6063	0.7539	0.6116	0.7584
2.250	0.5442	0.7079	0.5722	0.7285	0.6071	0.7545	0.6156	0.7611	0.6205	0.7648
2.375							0.6240	0.7675	0.6282	0.7703
2.500	0.5767	0.7480	0.5980	0.7574	0.6248	0.7698	0.6314	0.7731	0.6352	0.7750
2.625							0.6382	0.7781	0.6413	0.7792
2.750	0.6070	0.7852	0.6210	0.7833	0.6396	0.7825	0.6442	0.7827	0.6468	0.7829
2.875							0.6498	0.7869	0.6518	0.7863
3.000	0.6353	0.8200	0.6418	0.8066	0.6522	0.7947	0.6549	0.7908	0.6564	0.7894
3.125							0.6597	0.7945	0.6607	0.7924
3.250	0.6619	0.8527	0.6608	0.8280	0.6632	0.8031	0.6641	0.7979	0.6646	0.7952
3.375							0.6683	0.8012	0.6684	0.7978
3.500	0.6871	0.8836	0.6783	0.8476	0.6728	0.8117	0.6721	0.8043	0.6718	0.8004
3.625							0.6757	0.8073	0.6750	0.8028
3.750	0.7109	0.9129	0.6944	0.8657	0.6812	0.8195	0.6790	0.8101	0.6780	0.8051
3.875							0.6822	0.8127	0.6808	0.8072
4.000	0.7337	0.9407	0.7094	0.8827	0.6888	0.8265	0.6852	0.8153	0.6834	0.8093

Table 7d. Normalized torques and bending moments for warping-function deformation-theory analysis of a square section with $\mu = 2.00$

	n = 1		n = 6		n = 9	
$\frac{G\theta}{k}$	t_n	m_n	t_n	m_n	t_n	m_n
0.0000	0.0000	0.0000	0.0000	0.0000	0.0000	0.0000
0.0625					0.0260	0.0722
0.1250	0.0509	0.1403	0.0520	0.1443	0.0520	0.1443
0.1875					0.0781	0.2165
0.2500	0.0971	0.2629	0.1041	0.2887	0.1041	0.2887
0.3125					0.1301	0.3608
0.3750	0.1374	0.3654	0.1559	0.4322	0.1561	0.4329
0.4375					0.1818	0.5040
0.5000	0.1726	0.4519	0.2046	0.5622	0.2065	0.5705
0.5625					0.2290	0.6279
0.6250	0.2026	0.5263	0.2451	0.6576	0.2489	0.6737
0.6875					0.2666	0.7107
0.7500	0.2314	0.5915	0.2781	0.7240	0.2825	0.7411
0.8125					0.2970	0.7669
0.8750	0.2565	0.6497	0.3050	0.7720	0.3100	0.7888
0.9375					0.3217	0.8070
1.0000	0.2794	0.7023	0.3269	0.8071	0.3320	0.8220
1.0625					0.3412	0.8346
1.1250	0.3006	0.7504	0.3450	0.8339	0.3497	0.8456
1.1875					0.3574	0.8553
1.2500	0.3201	0.7948	0.3608	0.8554	0.3644	0.8639
1.3125					0.3710	0.8717
1.3750	0.3384	0.8360	0.3734	0.8731	0.3769	0.8786
1.4375					0.3825	0.8849
1.5000	0.3556	0.8745	0.3848	0.8880	0.3876	0.8906
1.5625					0.3924	0.8959
1.6250	0.3717	0.9107	0.3948	0.9010	0.3969	0.9007
1.6875					0.4011	0.9053
1.7500	0.3870	0.9449	0.4036	0.9121	0.4051	0.9096
1.8125					0.4088	0.9137
1.8750	0.4016	0.9774	0.4114	0.9229	0.4123	0.9176
1.9375					0.4156	0.9213
2.0000	0.4154	1.0083	0.4184	0.9324	0.4187	0.9248

Table 8. Typical stress output for warping-function deformation-theory with n = 2, μ = 1.00, and Θ = 3.00

Second invariant of stress: J_2

i / j	1	2	3	4	5	6	7
1	0.000	0.030	0.132	0.314	0.528	0.733	0.923
2	0.259	0.274	0.327	0.433	0.585	0.760	0.936
3	0.618	0.617	0.621	0.646	0.712	0.824	0.968
4	0.868	0.863	0.850	0.840	0.851	0.905	1.008
5	1.064	1.057	1.037	1.011	0.989	0.993	1.052
6	1.231	1.224	1.202	1.168	1.127	1.093	1.101
7	1.383	1.376	1.355	1.320	1.273	1.218	1.180

Normal stress: $\sigma_{zz}/\sqrt{3}\,k$

i / j	1	2	3	4	5	6	7
1	0.000	0.000	0.000	0.000	0.000	0.000	0.000
2	0.406	0.403	0.391	0.365	0.322	0.275	0.231
3	0.627	0.627	0.625	0.611	0.575	0.516	0.447
4	0.741	0.744	0.754	0.761	0.753	0.714	0.644
5	0.812	0.818	0.834	0.856	0.876	0.872	0.822
6	0.860	0.867	0.885	0.915	0.953	0.986	0.978
7	0.892	0.898	0.916	0.947	0.991	1.046	1.086

Shear stress: $\left|\sigma_{xz}/k\right|$

i / j	1	2	3	4	5	6	7
1	0.000	0.000	0.000	0.000	0.000	0.000	0.000
2	0.307	0.293	0.251	0.185	0.111	0.047	0.000
3	0.474	0.457	0.405	0.317	0.205	0.093	0.000
4	0.566	0.549	0.498	0.410	0.285	0.139	0.000
5	0.636	0.621	0.574	0.489	0.361	0.191	0.000
6	0.701	0.687	0.645	0.568	0.443	0.256	0.000
7	0.766	0.754	0.718	0.651	0.540	0.352	0.000

Shear stress: $\left|\sigma_{yz}/k\right|$

i / j	1	2	3	4	5	6	7
1	0.000	0.172	0.363	0.560	0.726	0.856	0.961
2	0.000	0.160	0.333	0.515	0.685	0.826	0.940
3	0.000	0.122	0.258	0.414	0.583	0.741	0.877
4	0.000	0.086	0.184	0.304	0.450	0.612	0.770
5	0.000	0.054	0.116	0.195	0.302	0.443	0.612
6	0.000	0.025	0.054	0.092	0.148	0.236	0.379
7	0.000	0.000	0.000	0.000	0.000	0.000	0.000

Table 9a. Normalized torques for stress-function deformation-theory analysis of a square section with $\mu = 0.00$

$\frac{G\theta}{k}$	n = 1 t_n	n = 2 t_n	n = 9 t_n
0.00	0.0000	0.0000	0.0000
0.25			0.1048
0.50	0.2015	0.2102	0.2095
0.75			0.3143
1.00	0.3668	0.4042	0.4191
1.25			0.5224
1.50	0.4982	0.5562	0.6146
1.75			0.6916
2.00	0.6060	0.6694	0.7541
2.25			0.8025
2.50	0.6974	0.7560	0.8397
2.75			0.8687
3.00	0.7769	0.8250	0.8920
3.25			0.9111
3.50	0.8474	0.8820	0.9272
3.75			0.9408
4.00	0.9110	0.9304	0.9526
4.25			0.9630
4.50	0.9690	0.9725	0.9723
4.75			0.9806
5.00	1.0224	1.0097	0.9881
5.25			0.9950
5.50	1.0721	1.0430	1.0013
5.75			1.0072
6.00	1.1185	1.0732	1.0126
6.25			1.0176
6.50	1.1621	1.1009	1.0223
6.75			1.0267
7.00	1.2033	1.1264	1.0308
7.25			1.0347
7.50	1.2424	1.1502	1.0384
7.75			1.0419
8.00	1.2797	1.1723	1.0453

Table 9b. Normalized torques and bending moments for stress-function deformation-theory analysis of a square section with $\mu = 1.00$

$\frac{G\theta}{k}$	n = 2		n = 6	
	t_n	m_n	t_n	m_n
0.000	0.0000	0.0000	0.0000	0.0000
0.125				
0.250	0.1046	0.1441	0.1047	0.1443
0.375				
0.500	0.2057	0.2818	0.2090	0.2886
0.625				
0.750	0.2947	0.3979	0.3126	0.4301
0.875				
1.000	0.3674	0.4875	0.4027	0.5471
1.125				
1.250	0.4250	0.5565	0.4722	0.6246
1.375				
1.500	0.4739	0.6112	0.5230	0.6752
1.625				
1.750	0.5141	0.6560	0.5606	0.7093
1.875				
2.000	0.5484	0.6937	0.5895	0.7335
2.125				
2.250	0.5783	0.7263	0.6124	0.7519
2.375				
2.500	0.6047	0.7550	0.6309	0.7666
2.625				
2.750	0.6283	0.7805	0.6464	0.7789
2.825				
3.000	0.6497	0.8036	0.6596	0.7894
3.125				
3.250	0.6693	0.8246	0.6711	0.7985
3.375				
3.500	0.6872	0.8439	0.6812	0.8067
3.625				
3.750	0.7039	0.8619	0.6902	0.8140
3.875				
4.000	0.7194	0.8785	0.6983	0.8207

Table 10. Typical stress output for stress-function deformation-theory with n = 2, μ = 1.00, and Θ = 3.00

Second invariant of stress: J_2

i / j	1	2	3	4	5	6	7
1	0.000	0.030	0.131	0.307	0.523	0.729	0.933
2	0.253	0.269	0.325	0.436	0.584	0.758	0.949
3	0.622	0.622	0.625	0.650	0.715	0.825	0.982
4	0.875	0.869	0.856	0.845	0.855	0.907	1.016
5	1.070	1.063	1.043	1.015	0.993	0.997	1.052
6	1.237	1.229	1.207	1.173	1.131	1.097	1.098
7	1.387	1.380	1.359	1.323	1.275	1.218	1.180

Normal stress: $\sigma_{zz}/\sqrt{3}\,k$

i / j	1	2	3	4	5	6	7
1	0.000	0.000	0.000	0.000	0.000	0.000	0.000
2	0.407	0.404	0.392	0.365	0.323	0.275	0.228
3	0.624	0.624	0.622	0.609	0.573	0.515	0.441
4	0.736	0.740	0.750	0.758	0.750	0.712	0.639
5	0.808	0.813	0.830	0.853	0.872	0.868	0.822
6	0.856	0.862	0.881	0.912	0.950	0.982	0.981
7	0.888	0.894	0.913	0.944	0.990	1.047	1.086

Shear stress: $|\sigma_{xz}/k|$

i / j	1	2	3	4	5	6	7
1	0.000	0.000	0.000	0.000	0.000	0.000	0.000
2	0.295	0.283	0.246	0.184	0.112	0.048	0.000
3	0.483	0.465	0.410	0.321	0.208	0.094	0.000
4	0.578	0.561	0.508	0.417	0.290	0.141	0.000
5	0.646	0.631	0.583	0.498	0.368	0.195	0.000
6	0.710	0.696	0.654	0.577	0.453	0.266	0.000
7	0.773	0.762	0.725	0.657	0.543	0.350	0.000

Shear stress: $|\sigma_{yz}/k|$

i / j	1	2	3	4	5	6	7
1	0.000	0.174	0.362	0.554	0.723	0.854	0.966
2	0.000	0.161	0.334	0.514	0.684	0.824	0.947
3	0.000	0.125	0.264	0.420	0.586	0.742	0.887
4	0.000	0.089	0.190	0.311	0.457	0.617	0.779
5	0.000	0.056	0.120	0.201	0.310	0.453	0.612
6	0.000	0.026	0.056	0.096	0.154	0.249	0.367
7	0.000	0.000	0.000	0.000	0.000	0.000	0.000

Table 11a. Normalized torques for warping-function deformation-theory analysis of a circular section with $\mu = 0.00$

$\frac{G\theta}{k}$	n = 1 t_n	n = 9 t_n
0.00	0.0000	0.0000
0.25		0.1875
0.50	0.3329	0.3751
0.75		0.5619
1.00	0.5579	0.7226
1.25		0.8183
1.50	0.7196	0.8761
1.75		0.9149
2.00	0.8469	0.9408
2.25		0.9599
2.50	0.9524	0.9749
2.75		0.9871
3.00	1.0433	0.9971
3.25		1.0057
3.50	1.1236	1.0133
3.75		1.0202
4.00	1.1957	1.0264
4.25		1.0322
4.50	1.2614	1.0375
4.75		1.0424
5.00	1.3219	1.0470
5.25		1.0511
5.50	1.3781	1.0550
5.75		1.0586
6.00	1.4307	1.0620
6.25		1.0651
6.50	1.4801	1.0681
6.75		1.0710
7.00	1.5269	1.0737
7.25		1.0762
7.50	1.5713	1.0787
7.75		1.0811
8.00	1.6135	1.0834

Table 11b. Normalized torques and bending moments for warping-function deformation-theory analysis of a circular section with $\mu = 1.00$

$\frac{G\theta}{k}$	n = 1		n = 6		n = 9		n = 15	
	t_n	m_n	t_n	m_n	t_n	m_n	t_n	m_n
0.000	0.0000	0.0000	0.0000	0.0000	0.0000	0.0000	0.0000	0.0000
0.125							0.0938	0.1275
0.250	0.1730	0.2305	0.1875	0.2551	0.1875	0.2551	0.1875	0.2551
0.375							0.2813	0.3826
0.500	0.3024	0.3928	0.3668	0.4912	0.3708	0.4999	0.3732	0.5053
0.625							0.4504	0.5952
0.750	0.4003	0.5114	0.4899	0.6207	0.4997	0.6355	0.5075	0.6486
0.875							0.5502	0.6823
1.000	0.4788	0.6049	0.5626	0.6830	0.5731	0.6939	0.5814	0.7034
1.125							0.6051	0.7177
1.250	0.5448	0.6827	0.6074	0.7187	0.6159	0.7239	0.6226	0.7279
1.375							0.6360	0.7355
1.500	0.6018	0.7497	0.6377	0.7426	0.6429	0.7424	0.6466	0.7415
1.625							0.6552	0.7464
1.750	0.6523	0.8089	0.6599	0.7605	0.6617	0.7557	0.6621	0.7506
1.875							0.6681	0.7542
2.000	0.6977	0.8620	0.6772	0.7748	0.6760	0.7662	0.6735	0.7575
2.125							0.6783	0.7606
2.250	0.7392	0.9104	0.6911	0.7867	0.6871	0.7748	0.6825	0.7634
2.375							0.6862	0.7659
2.500	0.7773	0.9550	0.7027	0.7969	0.6961	0.7820	0.6894	0.7682
2.625							0.6922	0.7702
2.750	0.8128	0.9964	0.7126	0.8057	0.7036	0.7882	0.6947	0.7721
2.875							0.6970	0.7738
3.000	0.8459	1.0350	0.7212	0.8135	0.7100	0.7936	0.6991	0.7755
3.125							0.7011	0.7770
3.250	0.8771	1.0714	0.7287	0.8205	0.7157	0.7983	0.7029	0.7784
3.375							0.7046	0.7797
3.500	0.9065	1.1058	0.7355	0.8268	0.7206	0.8026	0.7063	0.7810
3.625							0.7078	0.7822
3.750	0.9345	1.1384	0.7416	0.8326	0.7250	0.8065	0.7093	0.7834
3.825							0.7106	0.7845
4.000	0.9611	1.1695	0.7472	0.8380	0.7289	0.8101	0.7119	0.7855

Table 12a. Normalized torques for warping-function flow-theory analysis of a square section with $\mu = 0.00$

$\frac{G\theta}{k}$	n = 1 t_n	n = 2 t_n	n = 9 t_n	n = 12 t_n
0.00	0.0000	0.0000	0.0000	0.0000
0.25	0.1022	0.1040	0.1041	0.1041
0.50	0.1969	0.2071	0.2084	0.2084
0.75	0.2820	0.3055	0.3128	0.3128
1.00	0.3578	0.3952	0.4171	0.4172
1.25	0.4257	0.4743	0.5186	0.5202
1.50	0.4869	0.5431	0.6106	0.6150
1.75	0.5426	0.6028	0.6863	0.6940
2.00	0.5935	0.6548	0.7465	0.7558
2.25	0.6405	0.7006	0.7938	0.8039
2.50	0.6841	0.7412	0.8314	0.8411
2.75	0.7248	0.7775	0.8621	0.8711
3.00	0.7631	0.8103	0.8868	0.8954
3.25	0.7991	0.8402	0.9068	0.9144
3.50	0.8332	0.8675	0.9234	0.9297
3.75	0.8656	0.8927	0.9374	0.9424
4.00	0.8964	0.9161	0.9495	0.9533
4.25	0.9259	0.9378	0.9601	0.9627
4.50	0.9541	0.9582	0.9695	0.9710
4.75	0.9812	0.9774	0.9779	0.9784
5.00	1.0072	0.9954	0.9854	0.9849
5.25	1.0323	1.0126	0.9921	0.9907
5.50	1.0566	1.0288	0.9982	0.9958
5.75	1.0800	1.0442	1.0034	1.0005
6.00	1.1027	1.0590	1.0089	1.0047
6.25	1.1247	1.0731	1.0136	1.0086
6.50	1.1461	1.0866	1.0181	1.0122
6.75	1.1668	1.0996	1.0222	1.0155
7.00	1.1870	1.1120	1.0261	1.0187
7.25	1.2067	1.1240	1.0298	1.0216
7.50	1.2258	1.1356	1.0333	1.0244
7.75	1.2445	1.1468	1.0366	1.0270
8.00	1.2628	1.1576	1.0398	1.0295

Table 12b. Normalized torques and bending moments for warping-function flow-theory analysis of a square section with $\mu = 0.50$

$\frac{G\theta}{k}$	n = 1		n = 6		n = 9	
	t_n	m_n	t_n	m_n	t_n	m_n
0.0000	0.0000	0.0000	0.0000	0.0000	0.0000	0.0000
0.1875	0.0769	0.0534	0.0781	0.0541	0.0781	0.0541
0.3750	0.1494	0.1035	0.1563	0.1082	0.1563	0.1082
0.5625	0.2156	0.1493	0.2364	0.1624	0.2346	0.1624
0.7500	0.2754	0.1908	0.3128	0.2164	0.3129	0.2165
0.9375	0.3296	0.2283	0.3897	0.2696	0.3909	0.2704
1.1250	0.3787	0.2624	0.4621	0.3200	0.4663	0.3227
1.3125	0.4237	0.2935	0.5264	0.3653	0.5350	0.3709
1.5000	0.4650	0.3221	0.5810	0.4014	0.5937	0.4125
1.6875	0.5033	0.3486	0.6261	0.4366	0.6418	0.4475
1.8750	0.5387	0.3732	0.6631	0.4631	0.6802	0.4758
2.0625	0.5722	0.3962	0.6936	0.4848	0.7111	0.4983
2.2500	0.6035	0.4179	0.7189	0.5025	0.7361	0.5160
2.4375	0.6330	0.4383	0.7401	0.5172	0.7563	0.5301
2.6250	0.6610	0.4576	0.7582	0.5296	0.7729	0.5414
2.8125	0.6875	0.4760	0.7739	0.5402	0.7870	0.5507
3.0000	0.7129	0.4935	0.7875	0.5494	0.7990	0.5587
3.1875	0.7371	0.5103	0.7995	0.5575	0.8094	0.5656
3.3750	0.7603	0.5263	0.8102	0.5647	0.8185	0.5716
3.5625	0.7826	0.5417	0.8198	0.5712	0.8265	0.5768
3.7500	0.8040	0.5565	0.8285	0.5771	0.8335	0.5815
3.9375	0.8246	0.5708	0.8364	0.5824	0.8398	0.5857
4.1250	0.8446	0.5846	0.8438	0.5874	0.8455	0.5895
4.3125	0.8638	0.5979	0.8505	0.5919	0.8507	0.5930
4.5000	0.8825	0.6108	0.8568	0.5962	0.8556	0.5962
4.6875	0.9006	0.6233	0.8627	0.6001	0.8601	0.5991
4.8750	0.9182	0.6355	0.8682	0.6039	0.8643	0.6019
5.0625	0.9353	0.6473	0.8733	0.6074	0.8682	0.6045
5.2500	0.9519	0.6588	0.8782	0.6107	0.8719	0.6070
5.4375	0.9681	0.6699	0.8828	0.6139	0.8753	0.6093
5.6250	0.9838	0.6809	0.8872	0.6169	0.8786	0.6116
5.8125	0.9992	0.6915	0.8913	0.6198	0.8817	0.6136
6.0000	1.0142	0.7019	0.8952	0.6225	0.8846	0.6157

Table 12c. Normalized torques and bending moments for warping-function flow-theory analysis of a square section with $\mu = 1.00$

$\frac{G\theta}{k}$	n = 1		n = 2		n = 6		n = 9		n = 12	
	t_n	m_n	t_n	m_n	t_n	m_n	t_n	m_n	t_n	m_n
0.000	0.0000	0.0000	0.0000	0.0000	0.0000	0.0000	0.0000	0.0000	0.0000	0.0000
0.125	0.0514	0.0712	0.0520	0.0721	0.0502	0.0722	0.0520	0.0722	0.0520	0.0722
0.250	0.1004	0.1381	0.1039	0.1439	0.1042	0.1443	0.1042	0.1443	0.1042	0.1443
0.375	0.1459	0.1993	0.1548	0.2137	0.1564	0.2165	0.1564	0.2165	0.1564	0.2165
0.500	0.1876	0.2546	0.2034	0.2793	0.2086	0.2886	0.2086	0.2887	0.2086	0.2887
0.625	0.2258	0.3046	0.2485	0.3390	0.2603	0.3600	0.2607	0.3607	0.2608	0.3608
0.750	0.2609	0.3500	0.2898	0.3921	0.3103	0.4282	0.3120	0.4315	0.3126	0.4324
0.875	0.2933	0.3915	0.3270	0.4387	0.3564	0.4891	0.3606	0.4972	0.3622	0.5003
1.000	0.3233	0.4295	0.3605	0.4797	0.3978	0.5403	0.4042	0.5531	0.4073	0.5595
1.125	0.3513	0.4648	0.3907	0.5159	0.4340	0.5821	0.4423	0.5978	0.4465	0.6063
1.250	0.3775	0.4975	0.4180	0.5479	0.4656	0.6161	0.4754	0.6330	0.4804	0.6425
1.375	0.4020	0.5281	0.4428	0.5766	0.4929	0.6438	0.5039	0.6611	0.5095	0.6707
1.500	0.4252	0.5568	0.4655	0.6025	0.5164	0.6664	0.5283	0.6835	0.5346	0.6931
1.625	0.4471	0.5840	0.4862	0.6260	0.5366	0.6851	0.5490	0.7012	0.5558	0.7107
1.750	0.4680	0.6096	0.5053	0.6474	0.5542	0.7007	0.5665	0.7153	0.5734	0.7239
1.875	0.4878	0.6340	0.5230	0.6672	0.5695	0.7140	0.5814	0.7268	0.5881	0.7343
2.000	0.5067	0.6572	0.5395	0.6855	0.5831	0.7255	0.5943	0.7365	0.6006	0.7428
2.125	0.5249	0.6794	0.5548	0.7025	0.5952	0.7357	0.6056	0.7448	0.6115	0.7501
2.250	0.5423	0.7007	0.5692	0.7184	0.6060	0.7446	0.6155	0.7521	0.6210	0.7564
2.375	0.5590	0.7211	0.5828	0.7333	0.6158	0.7527	0.6244	0.7584	0.6293	0.7619
2.500	0.5750	0.7408	0.5955	0.7474	0.6246	0.7600	0.6323	0.7640	0.6367	0.7666
2.625	0.5906	0.7597	0.6076	0.7670	0.6327	0.7667	0.6394	0.7691	0.6433	0.7707
2.750	0.6056	0.7779	0.6190	0.7733	0.6402	0.7728	0.6459	0.7737	0.6493	0.7744
2.875	0.6201	0.7956	0.6299	0.7853	0.6470	0.7786	0.6519	0.7779	0.6547	0.7778
3.000	0.6341	0.8123	0.6402	0.7968	0.6534	0.7839	0.6573	0.7818	0.6596	0.7809
3.125	0.6477	0.8293	0.6501	0.8077	0.6592	0.7890	0.6623	0.7856	0.6641	0.7839
3.250	0.6610	0.8454	0.6596	0.8182	0.6647	0.7937	0.6670	0.7891	0.6683	0.7867
3.375	0.6738	0.8610	0.6686	0.8283	0.6698	0.7982	0.6712	0.7924	0.6722	0.7894
3.500	0.6863	0.8762	0.6773	0.8379	0.6746	0.8025	0.6752	0.7956	0.6757	0.7919
3.625	0.6985	0.8911	0.6857	0.8472	0.6791	0.8066	0.6789	0.7986	0.6790	0.7944
3.750	0.7104	0.9055	0.6937	0.8562	0.6833	0.8105	0.6823	0.8015	0.6820	0.7967
3.875	0.7220	0.9196	0.7015	0.8649	0.6872	0.8141	0.6855	0.8042	0.6848	0.7990
4.000	0.7333	0.9334	0.7089	0.8733	0.6910	0.8177	0.6884	0.8068	0.6873	0.8012

Table 12d. Normalized torques and bending moments for warping-function flow-theory analysis of a square section with $\mu = 2.00$

$\frac{G\theta}{k}$	n = 1		n = 6		n = 9	
	t_n	m_n	t_n	m_n	t_n	m_n
0.0000	0.0000	0.0000	0.0000	0.0000	0.0000	0.0000
0.0625	0.0258	0.0714	0.0260	0.0722	0.0260	0.0722
0.1250	0.0508	0.1392	0.0521	0.1443	0.0521	0.1443
0.1875	0.0744	0.2021	0.0782	0.2165	0.0782	0.2165
0.2500	0.0965	0.2598	0.1043	0.2887	0.1043	0.2887
0.3125	0.1172	0.3126	0.1304	0.3606	0.1304	0.3608
0.3750	0.1365	0.3609	0.1561	0.4314	0.1564	0.4328
0.4375	0.1546	0.4054	0.1809	0.4980	0.1820	0.5028
0.5000	0.1716	0.4465	0.2039	0.5571	0.2062	0.5672
0.5625	0.1876	0.4847	0.2248	0.6072	0.2282	0.6217
0.6250	0.2030	0.5203	0.2438	0.6493	0.2477	0.6662
0.6875	0.2170	0.5538	0.2611	0.6849	0.2654	0.7027
0.7500	0.2306	0.5853	0.2769	0.7151	0.2816	0.7332
0.8125	0.2436	0.6150	0.2912	0.7409	0.2963	0.7590
0.8750	0.2559	0.6433	0.3042	0.7629	0.3096	0.7807
0.9375	0.2678	0.6701	0.3161	0.7817	0.3216	0.7988
1.0000	0.2791	0.6957	0.3269	0.7981	0.3323	0.8139
1.0625	0.2900	0.7203	0.3369	0.8125	0.3421	0.8267
1.1250	0.3005	0.7438	0.3460	0.8253	0.3511	0.8379
1.1875	0.3106	0.7663	0.3545	0.8367	0.3594	0.8478
1.2500	0.3203	0.7881	0.3623	0.8470	0.3607	0.8566
1.3125	0.3297	0.8090	0.3696	0.8564	0.3741	0.8644
1.3750	0.3388	0.8292	0.3764	0.8649	0.3806	0.8715
1.4375	0.3477	0.8488	0.3827	0.8728	0.3866	0.8778
1.5000	0.3562	0.8677	0.3885	0.8801	0.3922	0.8836
1.5625	0.3646	0.8861	0.3941	0.8868	0.3974	0.8889
1.6250	0.3726	0.9040	0.3992	0.8932	0.4023	0.8939
1.6875	0.3805	0.9213	0.4040	0.8992	0.4069	0.8984
1.7500	0.3881	0.9382	0.4086	0.9048	0.4111	0.9028
1.8125	0.3956	0.9546	0.4128	0.9102	0.4151	0.9069
1.8750	0.4029	0.9707	0.4168	0.9153	0.4189	0.9108
1.9375	0.4100	0.9863	0.4206	0.9201	0.4223	0.9145
2.0000	0.4169	1.0016	0.4242	0.9248	0.4256	0.9180

Table 13. Typical stress output for warping-function flow-theory with n = 2, μ = 1.00, and Θ = 3.00

Second invariant of stress: J_2

i / j	1	2	3	4	5	6	7
1	0.000	0.030	0.130	0.307	0.516	0.717	0.904
2	0.257	0.272	0.324	0.427	0.575	0.745	0.919
3	0.608	0.608	0.613	0.638	0.702	0.811	0.953
4	0.852	0.847	0.836	0.828	0.839	0.891	0.993
5	1.043	1.036	1.018	0.994	0.973	0.977	1.032
6	1.206	1.199	1.178	1.146	1.107	1.076	1.080
7	1.354	1.347	1.327	1.294	1.248	1.196	1.158

Normal stress: $\sigma_{zz}/\sqrt{3}\,k$

i / j	1	2	3	4	5	6	7
1	0.000	0.000	0.000	0.000	0.000	0.000	0.000
2	0.404	0.401	0.390	0.364	0.324	0.276	0.232
3	0.617	0.619	0.618	0.606	0.571	0.514	0.446
4	0.730	0.733	0.743	0.752	0.745	0.708	0.638
5	0.800	0.805	0.822	0.845	0.865	0.863	0.816
6	0.847	0.853	0.872	0.903	0.942	0.974	0.970
7	0.878	0.884	0.903	0.934	0.981	1.034	1.076

Shear stress: $|\sigma_{xz}/k|$

i / j	1	2	3	4	5	6	7
1	0.000	0.000	0.000	0.000	0.000	0.000	0.000
2	0.306	0.293	0.254	0.189	0.113	0.048	0.000
3	0.475	0.458	0.406	0.318	0.207	0.093	0.000
4	0.565	0.549	0.499	0.411	0.287	0.138	0.000
5	0.635	0.620	0.574	0.490	0.363	0.190	0.000
6	0.699	0.685	0.644	0.567	0.444	0.261	0.000
7	0.764	0.752	0.716	0.649	0.535	0.355	0.000

Shear stress: $|\sigma_{yz}/k|$

i / j	1	2	3	4	5	6	7
1	0.000	0.172	0.361	0.554	0.718	0.847	0.951
2	0.000	0.158	0.329	0.508	0.677	0.816	0.930
3	0.000	0.120	0.256	0.411	0.577	0.733	0.869
4	0.000	0.087	0.186	0.306	0.449	0.608	0.765
5	0.000	0.055	0.118	0.199	0.305	0.444	0.605
6	0.000	0.026	0.055	0.095	0.150	0.243	0.374
7	0.000	0.000	0.000	0.000	0.000	0.000	0.000

Table 14a. Normalized torques for stress-function flow-theory analysis of a square section with $\mu = 0.00$

$\frac{G\theta}{k}$	n = 1 t_n	n = 6 t_n	n = 9 t_n
0.00	0.0000	0.0000	0.0000
0.25	0.1026	0.1045	0.1045
0.50	0.1976	0.2077	0.2090
0.75	0.2830	0.3062	0.3136
1.00	0.3594	0.3960	0.4180
1.25	0.4280	0.4753	0.5191
1.50	0.4893	0.5447	0.6079
1.75	0.5450	0.6044	0.6831
2.00	0.5960	0.6563	0.7437
2.25	0.6430	0.7019	0.7912
2.50	0.6864	0.7428	0.8282
2.75	0.7276	0.7795	0.8579
3.00	0.7663	0.8128	0.8821
3.25	0.8028	0.8430	0.9021
3.50	0.8373	0.8708	0.9190
3.75	0.8702	0.8960	0.9335
4.00	0.9016	0.9193	0.9460
4.25	0.9316	0.9413	0.9570
4.50	0.9597	0.9617	0.9667
4.75	0.9868	0.9809	0.9755
5.00	1.0129	0.9990	0.9835
5.25	1.0380	1.0168	0.9908
5.50	1.0622	1.0334	0.9975
5.75	1.0855	1.0493	1.0036
6.00	1.1082	1.0645	1.0093
6.25	1.1301	1.0790	1.0146
6.50	1.1513	1.0930	1.0195
6.75	1.1727	1.1064	1.0241
7.00	1.1933	1.1185	1.0276
7.25	1.2134	1.1315	1.0324
7.50	1.2331	1.1428	1.0354
7.75	1.2522	1.1541	1.0400
8.00	1.2710	1.1647	1.0425

Table 14b. Normalized torques and bending moments for stress-function flow-theory analysis of a square section with $\mu = 1.00$

$\frac{G\theta}{k}$	n = 2		n = 6	
	t_n	m_n	t_n	m_n
0.000	0.0000	0.0000	0.0000	0.0000
0.125	0.0521	0.0721	0.0521	0.0722
0.250	0.1040	0.1439	0.1043	0.1443
0.375	0.1548	0.2136	0.1564	0.2165
0.500	0.2034	0.2793	0.2085	0.2886
0.625	0.2486	0.3389	0.2602	0.3600
0.750	0.2900	0.3919	0.3099	0.4281
0.875	0.3275	0.4384	0.3562	0.4890
1.000	0.3613	0.4793	0.3977	0.5400
1.125	0.3919	0.5153	0.4343	0.5815
1.250	0.4196	0.5472	0.4661	0.6152
1.375	0.4448	0.5758	0.4936	0.6426
1.500	0.4679	0.6015	0.5173	0.6651
1.625	0.4891	0.6248	0.5380	0.6836
1.750	0.5087	0.6461	0.5562	0.6990
1.875	0.5268	0.6656	0.5723	0.7120
2.000	0.5438	0.6837	0.5867	0.7233
2.125	0.5597	0.7005	0.5995	0.7331
2.250	0.5746	0.7162	0.6110	0.7418
2.375	0.5886	0.7310	0.6214	0.7495
2.500	0.6018	0.7449	0.6309	0.7566
2.625	0.6144	0.7580	0.6395	0.7630
2.750	0.6263	0.7704	0.6475	0.7688
2.875	0.6376	0.7822	0.6549	0.7743
3.000	0.6484	0.7934	0.6617	0.7794
3.125	0.6587	0.8042	0.6681	0.7841
3.250	0.6686	0.8144	0.6740	0.7886
3.375	0.6781	0.8244	0.6796	0.7928
3.500	0.6872	0.8338	0.6848	0.7968
3.625	0.6959	0.8430	0.6897	0.8006
3.750	0.7044	0.8518	0.6943	0.8042
3.875	0.7125	0.8603	0.6987	0.8077
4.000	0.7204	0.8685	0.7028	0.8110

Table 15. Typical stress output for stress-function flow-theory with n = 2, μ = 1.00, and Θ = 3.00

Second invariant of stress: J_2

i / j	1	2	3	4	5	6	7
1	0.000	0.031	0.132	0.307	0.520	0.721	0.919
2	0.251	0.268	0.324	0.430	0.581	0.750	0.935
3	0.612	0.611	0.616	0.642	0.707	0.816	0.967
4	0.857	0.852	0.840	0.831	0.842	0.894	0.999
5	0.105	1.041	1.022	0.996	0.975	0.980	1.033
6	1.211	1.204	1.183	1.149	1.110	1.077	1.078
7	1.358	1.351	1.331	1.297	1.250	1.194	1.158

Normal stress: $\sigma_{zz}/\sqrt{3}\,k$

i / j	1	2	3	4	5	6	7
1	0.000	0.000	0.000	0.000	0.000	0.000	0.000
2	0.405	0.402	0.390	0.363	0.322	0.275	0.228
3	0.616	0.617	0.616	0.603	0.568	0.512	0.438
4	0.725	0.729	0.740	0.749	0.743	0.706	0.633
5	0.795	0.801	0.818	0.842	0.863	0.860	0.814
6	0.842	0.849	0.868	0.900	0.940	0.973	0.972
7	0.874	0.880	0.899	0.932	0.979	1.036	1.076

Shear stress: $|\sigma_{xz}/k|$

i / j	1	2	3	4	5	6	7
1	0.000	0.000	0.000	0.000	0.000	0.000	0.000
2	0.294	0.282	0.245	0.183	0.111	0.047	0.000
3	0.482	0.464	0.409	0.319	0.206	0.093	0.000
4	0.576	0.559	0.506	0.415	0.288	0.140	0.000
5	0.645	0.630	0.582	0.496	0.366	0.194	0.000
6	0.708	0.695	0.652	0.574	0.450	0.265	0.000
7	0.771	0.759	0.723	0.654	0.540	0.348	0.000

Shear stress: $|\sigma_{yz}/k|$

i / j	1	2	3	4	5	6	7
1	0.000	0.175	0.363	0.554	0.721	0.849	0.959
2	0.000	0.162	0.335	0.514	0.682	0.820	0.940
3	0.000	0.126	0.265	0.420	0.585	0.738	0.881
4	0.000	0.090	0.190	0.311	0.456	0.614	0.774
5	0.000	0.056	0.120	0.202	0.310	0.450	0.608
6	0.000	0.026	0.056	0.096	0.154	0.248	0.365
7	0.000	0.000	0.000	0.000	0.000	0.000	0.000

APPENDIX VI

GRAPHICAL REPRESENTATION OF TORQUES AND MOMENTS

Since all work-hardening formulations provide essentially the same numerical results when $\frac{K}{\theta}$ = constant, the results are shown graphically for only the deformation-theory warping-function formulation. These figures include both the unit square and unit radial solutions.

In all graphs, values of n were chosen so that the general effect of the work-hardening on the torques and moments is illustrated. More specific information on the exact values of the torques and moments may be obtained from Appendix V.

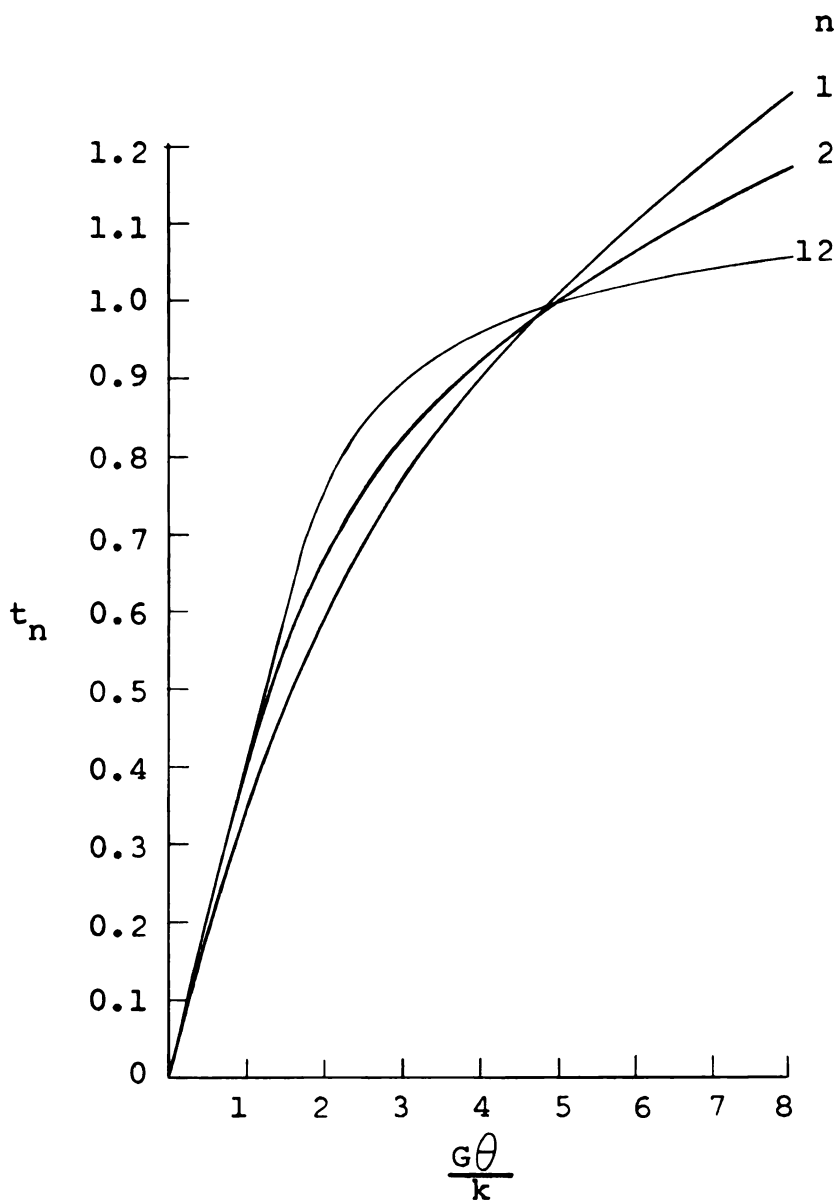

Figure 24a. Torque vs. unit angle of twist for warping-function deformation-theory solution of a square section with $\mu = 0.00$

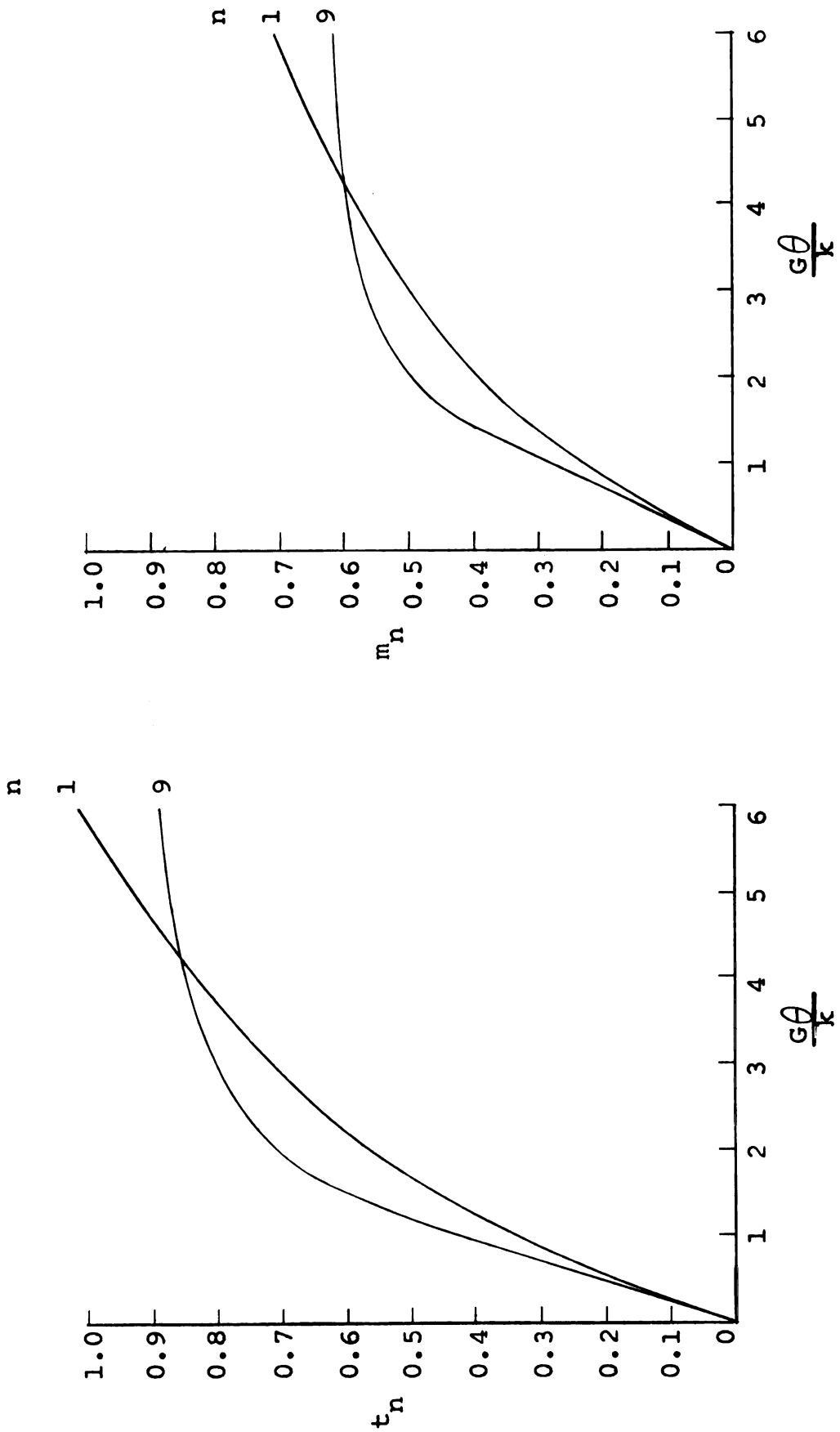

Figure 24b. Torque-moment vs. unit angle of twist for warping-function deformation-theory solution of a square section with $\mu = 0.50$

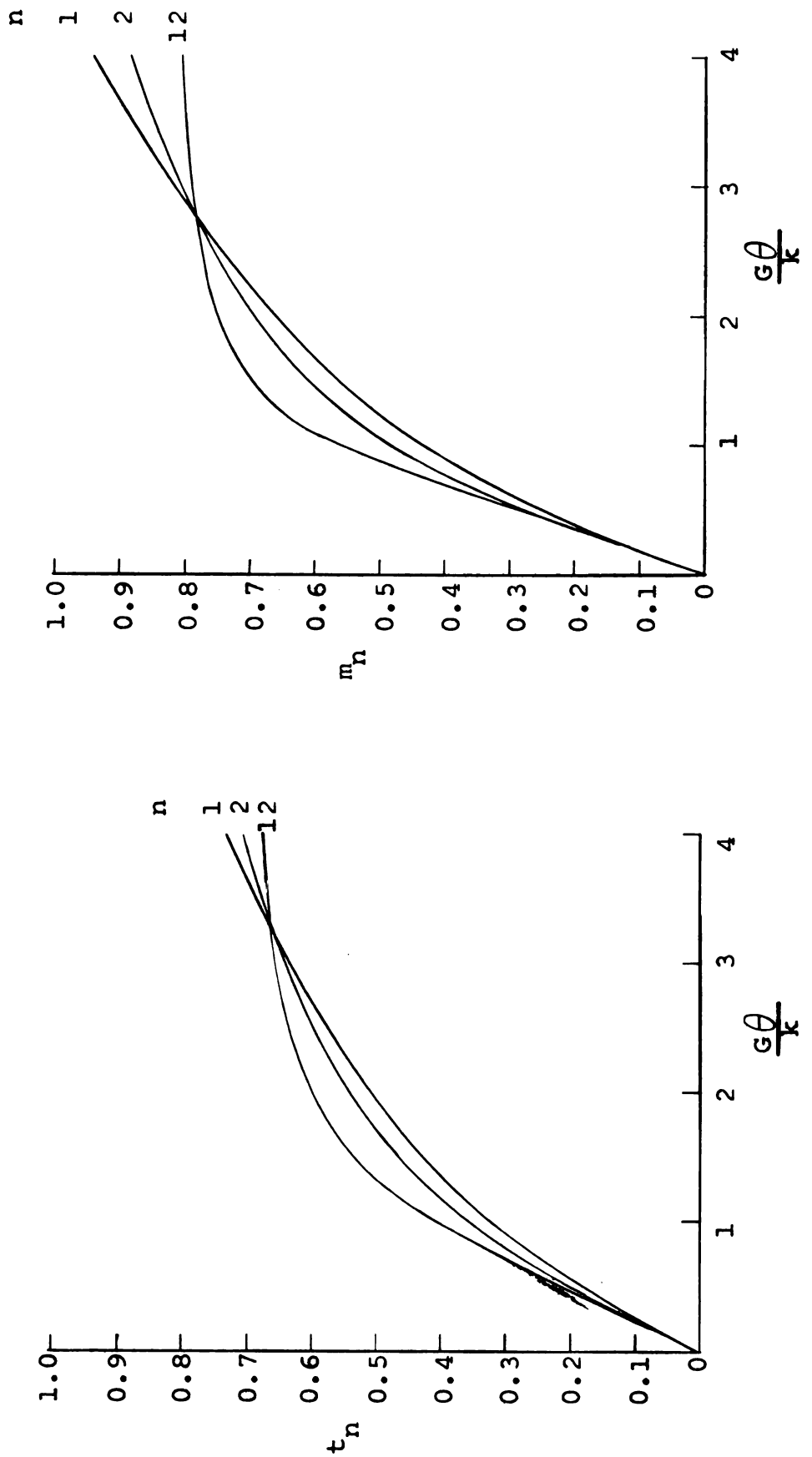

Figure 24c. Torque-moment vs. unit angle of twist for warping-function deformation-theory solution of a square section with $\mu = 1.00$

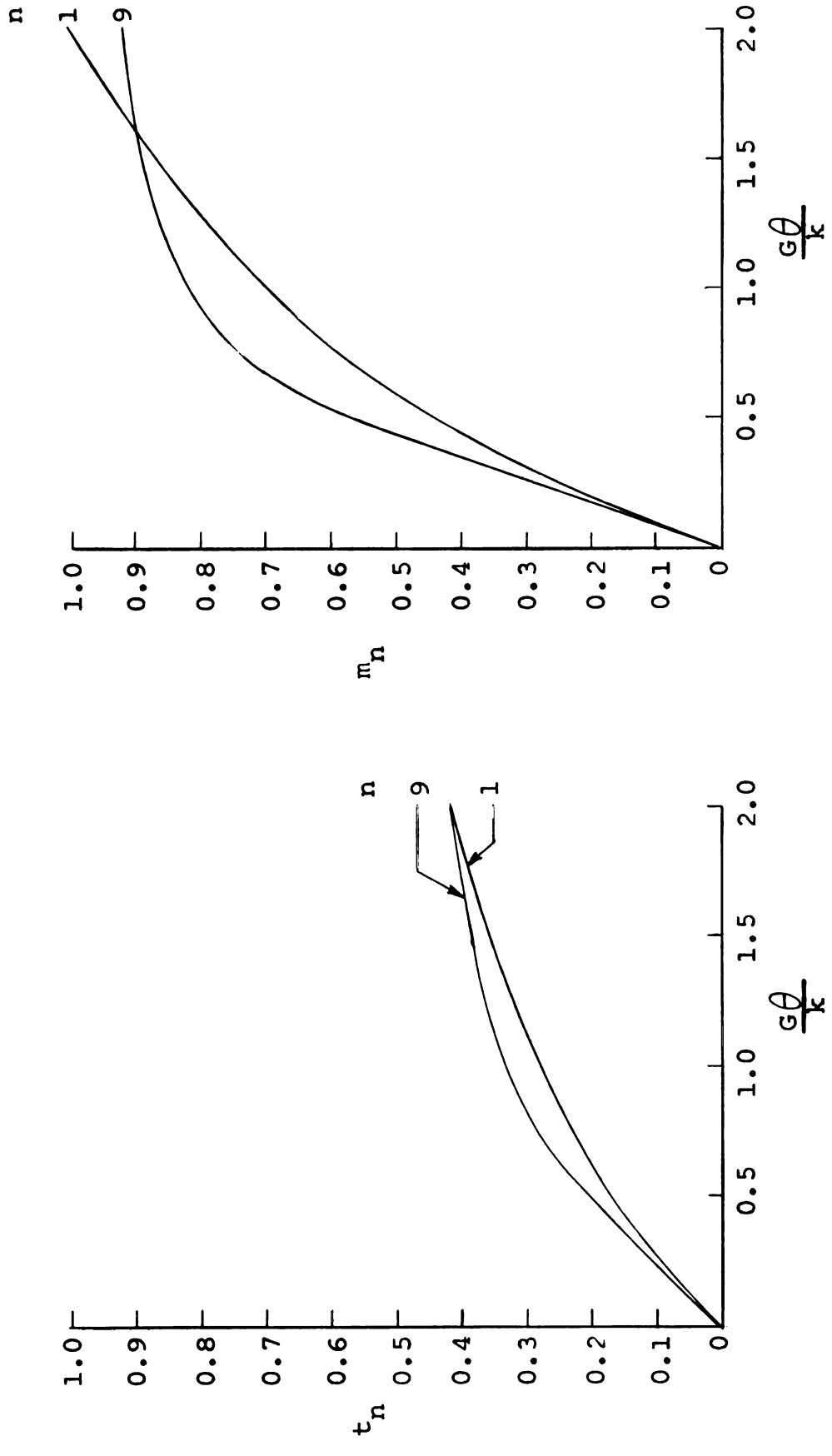

Figure 24d. Torque-moment vs. unit angle of twist for warping-function deformation-theory solution of a square section with $\mu = 2.00$

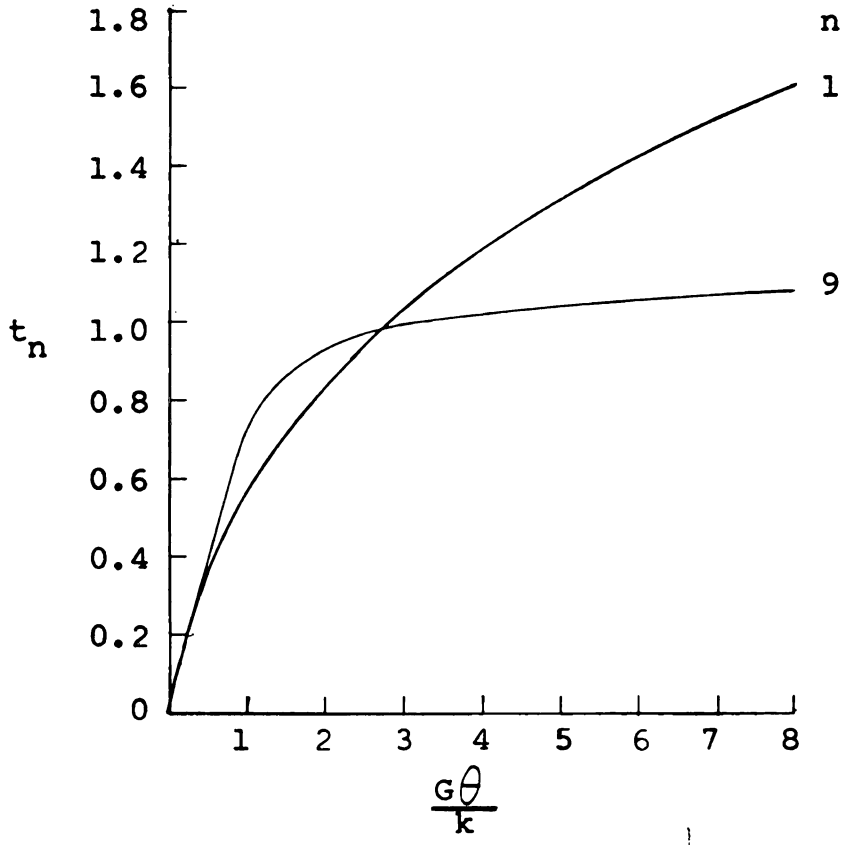

Figure 25a. Torque vs. unit angle of twist for warping-function deformation-theory solution of a circular section with $\mu = 0.00$

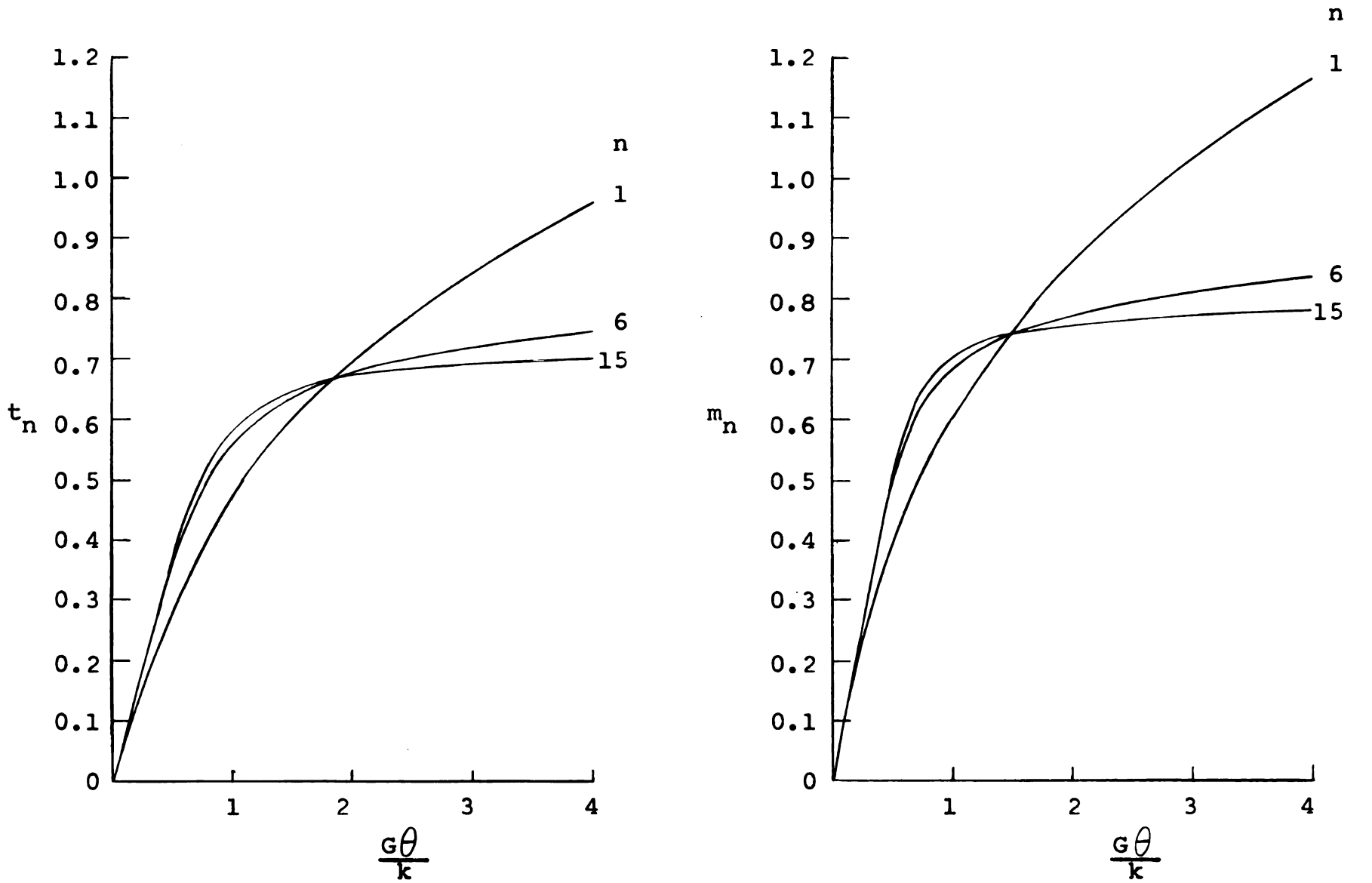

Figure 25b. Torque-moment vs. unit angle of twist for warping-function deformation-theory solution of a circular section with $\mu = 1.00$

BIBLIOGRAPHY

1. Budiansky, B., "A Reassessment of Deformation Theories of Plasticity," J. Appl. Mech., Vol. 29, Trans ASME, 1959, pp. 259-64.

2. Budiansky, B., and Mangasarian, O. L., "Plastic Stress Concentration at a Circular Hole in an Infinite Sheet Subjected to Equal Biaxial Tension," J. Appl. Mech., Vol. 27, Trans ASME, 1960, pp. 59-64.

3. Drucker, D. C., "A More Fundamental Approach to Plastic Stress-Strain Relations," Proceedings of the First U.S. National Congress of Applied Mechanics, ASME, 1951, pp. 414-27.

4. Forsythe, G. E., and Wasow, W. R., Finite Difference Methods for Partial Differential Equations, John Wiley and Sons, Inc., New York, N.Y., 1960.

5. Fox, L., Numerical Solution of Ordinary and Partial Differential Equations, Addison-Wesley Publishing Co., Inc., Reading, Mass., 1963.

6. Greenberg, H. J., Dorn, W. S., and Wetherell, E. H., "A Comparison of Flow and Deformation Theories in Plastic Torsion of a Square Cylinder," PLASTICITY, Proceedings of the Second Symposium on Naval Structural Mechanics, Edited by E. H. Lee and P. S. Symonds, Pergamon Press, Inc., 1960, pp. 279-96.

7. Handelman, G. H., "A Variational Principle for a State of Combined Plastic Stress," Quart. Appl. Math., Vol. 4, 1944, pp. 351-53.

8. Handelman, G. H., Lin, C. C., and Prager, W., "On the Mechanical Behavior of Metals in the Strain-Hardening Range," Quart. Appl. Math., Vol. 4, 1947, pp. 397-407.

9. Hencky, H., "Zur Theorie plastischer Deformationen und der hierdurch im Material hervorgerufenen Nachspannungen," Z. angew. Math. Mechanik, Vol. 4, 1924, pp. 323-34.

10. Hildebrand, F. B., Introduction to Numerical Analysis, McGraw-Hill Book Company, Inc., New York, N.Y., 1956.

11. Hill, R., "A Variational Principle of Maximum Plastic Work in Classical Plasticity," Quart. J. Mech. Appl. Math., Vol. 1, 1948, pp. 18-28

12. Hill, R., The Mathematical Theory of Plasticity, Clarendon Press, Oxford, 1950.

13. Hill, R., and Siebel, M. P. L., "On the Plastic Distortion of Solid Bars by Combined Bending and Twisting," J. Mech. Phys. Solid, Vol. 1, 1953, pp. 207-14.

14. Hodge, P. G., "On Torsion of Plastic Bars," J. Appl. Mech., Vol. 16, Trans ASME, 1949, pp. 399-405.

15. Imegwu, E. O., "Plastic Flexure and Torsion," J. Mech. Phys. Solids, Vol. 8, 1960, pp. 141-46.

16. Imegwu, E. O., "Combined Plastic Bending and Torsion," J. Mech. Phys. Solids, Vol. 10, 1962, pp. 277-82.

17. Lubahn, J. D., and Felgar, R. P., Plasticity and Creep of Metals, John Wiley and Sons, Inc., New York, N.Y., 1961.

18. Mangasarian, O. L., "Stresses in the Plastic Range Around a Normally Loaded Circular Hole in an Infinite Sheet," J. Appl. Mech., Vol. 27, Trans ASME, 1960, pp. 65-73.

19. von Mises, R., "Mechanik der festen Körper im plastisch deformablen Zustand," Göttinger Nachrichten, math.-phys. Klasse, 1913, pp. 582-92.

20. Onat, E. T., and Prager, W., "Limit Analysis of Arches," J. Mech. Phys. Solids, Vol. 1, 1953, pp. 77-89.

21. Osgood, W. R., "Stress-Strain Formulas," J. Aero. Science, Vol. 13, 1946, pp. 45-48.

22. Parter, S. V., "Mildly Nonlinear Elliptic Partial Differential Equations and their Numerical Solution. I," Numerische Math., Vol. 7, 1965, pp. 113-28.

23. Parter, S. V., and Greenspan, D., "Mildly Nonlinear Partial Differential Equations and their Numerical Solutions. II," Numerische Math., Vol. 7, 1965, pp. 129-46.

24. Piechnik, S., "The Influence of Bending on the Limit State of a Circular Bar Subjected to Torsion," Arch. Mech. Stos., Vol. 13, 1961, pp. 77-106.

25. Piechnik, S., and Zyczkowski, M., "On the Plastic Interaction-Curve for Bending and Torsion of a Circular Bar," Arch. Mech. Stos., Vol. 13, 1961, pp. 669-92.

26. Prager, W., "An Introduction to the Mathematical Theory of Plasticity," J. Appl. Phys., Vol. 18, 1947, pp. 375-83.

27. Ramberg, W., and Osgood, W., "Description of Stress-Strain Curves by Three Parameters, NACA TN No. 902, July, 1943.

28. Salvadori, M. G., and Baron, M. L., Numerical Methods in Engineering, Prentice-Hall, Inc., Englewood Cliffs, N.J., 1961.

29. Southwell, R. V., Relaxation Methods in Theoretical Physics, Clarendon Press, Oxford, 1946.

30. Steele, M. C., "The Plastic Bending and Twisting of Square Section Members," J. Mech. Phys. Solids, Vol. 3, 1954, pp. 156-66.

31. Timoshenko, S., and Goodier, J. N., Theory of Elasticity, McGraw-Hill Book Company, Inc., New York, N.Y., 1951.

32. Todd, J. (Editor), Survey of Numerical Analysis, McGraw-Hill Book Company, Inc., New York, N.Y., 1962.

33. Varga, R. S., Matrix Iterative Analysis, Prentice-Hall, Inc., Englewood Cliffs, N.J., 1962.

34. Wang, C. T., Applied Elasticity, McGraw-Hill Book Company, Inc., New York, N.Y., 1953.